PERFORMANCE ANALYSIS AND HARDWARE IMPLEMENTATION OF FrFT/FFT -BASED OFDM SYSTEM

A

Thesis Report

Submitted to

The Department di Elettronica, Informazione e Bioingegneria

POLITECNICO DI MILANO, MILANO, ITALY

In partial fulfilment for the award of degree of

MASTER OF SCIENCE

IN

ELECTRONICS ENGINEERING

Supervisor:

Prof. Maurizio Magarini

Co-Supervisor:

Ing. Stefano Olivieri

Submitted By:

Atul Kumar **10450012**

Department di Elettronica, Informazione e Bioingegneria
Politecnico di Milano, P.zza L. da Vinci, 32, 20133 Milano, Italy

SEPTEMBER 2015

POLITECNICO DI MILANO
P.zza L. da Vinci, 32, 20133 Milano, Italy
Phone: 800.02.2399 Fax: +39.02.2399.2206
Website: www.polimi.it

CERTIFICATE

This is to certify that "Atul Kumar 816323 (10450012)" students of **Electronics Engineering** from "POLITECNICO DI MILANO, ITALY" has done their Thesis at "**Politecnico di Milano, Milano, ITALY**" in the partial fulfilment for the award of degree of "**Master of Science**" under the guidance of "**Prof. Maurizio Magarini**" and "**Ing. Stefano Olivieri**"

The project work entitled as **"PERFORMANCE ANALYSIS AND HARDWARE IMPLEMENTATION OF FrFT/FFT -BASED OFDM SYSTEM"** embodies the original work done for Thesis. This work has not been submitted partially or wholly to any other university or institute for the award of this or any other degree.

Prof. Maurizio Magarini
The Department di Elettronica, Informazione e Bioingegneria.

Ing. Stefano Olivieri
Application Engineering
Mathwork

ACKNOWLEDGEMENT

I would like to thank all those who gave us the possibility to complete this Thesis. I want to thank the Department di Elettronica, Informazione e Bioingegneria of "**POLITECNICO DI MILANO"** for giving us such a golden opportunity to commence this Thesis in first instance. I express our deepest gratitude to "**Prof. Maurizio Magarini"** who encouraged me to go ahead with Thesis. It is a matter of pride and privilege for us to complete our dissertation under his close supervision. Whatever is said in the praise of **Prof. Maurizio Magarini** is not enough, his soul touching humility, his straight forward attitude, his methodological approach, his eagerness to share his wisdom, his aim for perfection and his never ending encouragement and patience are but a few of his noble qualities. It is certainly good karma to have **Prof. Maurizio Magarini** for supervising our work as his advice, his words of wisdom and valuable guidance have allowed the completion of our work without any hassle.

We are also very grateful to **Stefano Olivieri**, from Mathwork for the facilities and cooperation, he provided me guidance in the completion of Thesis work. I also express our deepest gratitude to "**Stefano Olivieri"**. Our special appreciation goes to teachers, who has inspired and guided us during two years in this institution by their brilliant and expert teaching. We gratefully acknowledge the help and cooperation extended by the library staff of the faculty as well as university. Our heart gratitude goes to our parents and all friends for their invaluable inspiration extended in the pursuit of this work.

……

Atul Kumar

List of Abbreviations

S.No.	Abbreviation	Description
1	1G	First Generation
2	2 G	Second Generation
3	2.5 G	Third Generation
4	3GPP	3G Partnership Project
5	4G	Fourth Generation
6	5GNOW	5th Generation Non-Orthogonal Waveforms for Asynchronous Signalling
7	ADC	Analog-to-digital converter
8	ADSL	Asymmetric Digital subscriber lines
9	AMPS	Advanced Mobile Phone System
10	AMTS	Advanced Mobile Telephone System
12	AWGN	Additive White Gaussian Noise
12	BER	Bit Error Rate
13	BW	Band Width
14	CCDF	Complementary Cumulative Distributive Function
15	CDMA	Code Division Multiple Access
16	CFO	Carrier Frequency Offset
17	CP	Cyclic Prefix
18	DAB	Digital Audio Broadcasting
19	DAC	Digital-to-Analog converter
20	DFTFT	Discrete Fractional Fourier Transform
21	DFT	Discrete Fourier Transform
22	FFT	Fast Fourier Transform
23	DSP	Digital Signal Processing
24	DVB-T	Terrestrial Digital Video Broadcasting
25	FDD	Frequency Division Duplex
26	FDM	Frequency Division multiplexing
27	FDMA	Frequency Division multiplexing Access

28	FEQ	Frequency Domain Equalizer
29	FFO	Fractional Frequency Offset
30	FM	Frequency Modulation
31	FrFT	Fractional Fourier Transform
32	FT	Fourier Transform
33	Gbps	Giga bit per second
34	HDSL	High Bit Rate Digital Subscriber line
35	HPA	High Power Amplifier
36	ICI	Inter Carrier Interference
37	IDFT	Inverse Discrete Fourier Transform
38	IFFT	Inverse Fast Fourier Transform
39	IFO	Integer Frequency Offset
40	Kbps	Kilobit Per Sec
41	MB-OFDM	Multiband OFDM
42	MC	Multi Carrier
43	MCM	Multi Carrier Modulation
44	MC-CDMA	Multi Carrier CDMA
45	MMSE	Minimum Mean-Square Error
46	M-PSK	M-ary Phase shift keying
47	M-QMA	M-ary Quadrature Amplitude Modulation
48	OFDM	Orthogonal Frequency Division Multiplexing
49	OFDMA	Orthogonal Frequency Division Multiplexing Access
50	PAPR	Peak to Average Power Ratio
51	SC	Single Carrier
52	SIR	Signal to interference Ratio
53	SNR	Signal to Noise Ratio
54	TDD	Time Division Duplex
55	TDM	Time Division Multiplexing
56	TDMA	Time Division Multiplexing Access
57	W-CDMA	Wideband CDMA
58	DSP	Digital Signal Processing

59	FPGA	Field Programmable Gate Array
60	SDR	Software Defined Radio
61	ZED	Zynq™ Evaluation and Development
62	EPP	Extensible Processing Platform
63	PS	Processing System
64	PL	Programmable Logic
65	ISI	Inter-Symbol Interference
66	FBMC	Filter Bank Multi-Carrier
67	GFDM	Generalized Frequency Division Multiplexing
68	UFMC	Unified Frequency Multi-Carrier
69	HST	High-speed trains
70	RTL	Register-Transfer Level
71	STO	Symbol Timing Offset
72	VHDL	VHSIC Hardware Description Language
73	BFDM	Bi-orthogonal Frequency Division Multiplexing
74	MIMO	multiple-input multiple-output
75	Fi	Fixed point representation
76	HDL	Hardware Description Language
77	LTE-A	Long Term Evolution - Advanced
78	MTC	Machine-Type-Communication
79	M2M	Machine-To-Machine
80	RF	Radio Frequency
81	ESM	Emission Spectrum Mask
82	PHY	Physical Layer
83	CoMP	Coordinated Multipoint
84	UMTS	Universal Mobile Telecommunications System
85	MAC	Medium Access Layers

List of Symbols

S. No	Symbols	Description
1	ε	Carrier-frequency offset normalized by sub-carrier spacing
2	$\Re$	Real part
3	$\Im$	Imaginary part
4	γ or ϱ	Average SNR
5	α	Angle parameter in FRFT
6	ξ	Conditional BER
7	τ_l	Propagation Delay of the l^{th} path
8	σ_l^2	Variance of each l^{th} path
9	σ_w^2	Variance of AWGN
10	σ_{ICI}^2	ICI Power of the q^{th}Sub-Carrier
11	τ_{max}	Maximum channel delay spread
12	Δf	Carrier-frequency offset (CFO)
13	$E[.]$	Expectation average
14	$f_k = k/T_u$	Sub-carrier Frequency of the k^{th} sub-carrier
15	G or CP	total Number of sub-carrier in Guard Band (CP)
16	$h(\tau, t)$	Multipath fading channel impulse response
17	$h_l(t)$	complex amplitude or tap coefficient of the l^{th} path
18	$H(k)$ or $\beta(k)$	Channel Response in frequency domain
19	L	Total number of path
20	$N_0/2$	Noise variance
21	N	Total Number of sub-carrier
22	$r(i, t)$	Received signal in time domain
23	$r(i, n)$	Received signal in frequency domain
24	$S(k - p + \varepsilon)$	ICI Coefficient
25	SIR_q	Signal to interference ratio on q^{th}sub-carrier
26	T_s	Sampling time
27	T_u	Uses full symbol duration

28	T_g	Guard band time
29	T_{sym}	Symbol time
30	T_{th}	Threshold time
31	$w(i,t)$	AWGN noise
32	$\varphi(\omega)$	Output of characteristic function
33	$P_b(\xi)$	Conditional BER
34	P_b	Unconditional BER
35	β_k	Real part of ICI term
36	δ_k	Imaginary part of ICI term
37	$\Delta\,\theta$	Symbol timing offset
38	$g(.)$	Raised cosine impulse response
39	$sgn(.)$	Signum function
40	$H(.)$	Hermitian transpose
41	$\overline{(.)}$	Complex conjugate

List of Tables

List of Figure

ABSTRACT

Performance Analysis and Hardware Implementation of Discrete Fractional Fourier Transform (DFrFT) and Fast Fourier Transform (FFT) based Orthogonal Frequency Division Multiplexing (OFDM) System in presence of Carrier Frequency Offset (CFO) and Symbol Timing Offset (STO) in terms of Symbol Error Rate (SER, performance parameter) are investigated in this Thesis. In this Thesis, the SER analysis has been done for FFT -based OFDM system in presence of CFO and STO and for FrFT -based OFDM system in presence of CFO. The expressions of SER in the presence of CFO and STO are derived for FFT -based OFDM system in additive white Gaussian noise (AWGN), flat fading Rayleigh channel and frequency selective fading Rayleigh channel for BPSK and QPSK modulation schemes. Further, the expression of SER in the presence of CFO has been derived for Fractional Fourier Transform (FrFT) -based OFDM system in AWGN, Flat fading Rayleigh channel and frequency selective fading Rayleigh channel for BPSK and QPSK modulation schemes. Enumerative results of each SER expression are given and verified by comparing them to simulated results. In this Thesis, SER expressions *in presence of CFO and STO have been derived* first time for *QPSK in AWGN, flat fading Rayleigh channel and frequency selective fading Rayleigh channel for FFT -based OFDM system*. Also the expression of *SER in the presence of CFO has been derived first time for FrFT -based OFDM system in AWGN, Flat fading Rayleigh channel and frequency selective fading Rayleigh channel for BPSK and QPSK modulation schemes*.

Second part of thesis concerns with hardware implementation using MATLAB and Simulink. First in this the real-time Simulink model of proposed FrFT -based OFDM system in presence of CFO and STO is prepared. After IFrFT/FrFT kernel is converted to *fixed point design* using the *fixed point tool* of MATLAB and then the *HDL coder tool* follow for generating the *VHDL and Verilog code* using the Zed-board (zynq-7000) and also performing logic synthesis. Finally, the *HDL verifier* tool is used for *FPGA-in-loop* both transmitter and receiver blocks respectively. In this work hardware implementation of FrFT -based OFDM in frequency selective fading channel is proposed for the first time. Our proposed FrFT -based OFDM model improves SER by large extent as compared to FFT -based OFDM system with different modulation schemes and also different channel environments.

Software used for the analytical and simulated verification is MATLAB R2014a/2015a. Using this software, all the SER expressions were plotted and analytical results were perfectly matched with simulated results. For the hardware implementation used Xilinx board Zynq®-7000 (xc7z020) with MATLAB 2015a including Xilinx support package.

In this thesis, the comparative results between FrFT -based OFDM and FFT -based OFDM systems are shown. Through the analysis of results, it is found that in AWGN, flat fading channel and frequency selective fading channel the performance (in terms of SER) of FrFT -based OFDM system has been improved than FFT -based OFDM system.

This whole Thesis consists of five chapters in which chapter 1 organised as: origin of OFDM along with Thesis Objective and Contribution are addressed, after that motivation, advantages/ disadvantages and applications. Chapter 2 is organised as: historical development of OFDM system along with literature survey on performance analysis of FFT -based OFDM system, and discussion of system model in presence of CFO and STO with mathematical formulation of transmitter, channel and receiver. The exact closed form BER and SER expressions for FFT -based OFDM systems with CFO and STO are analysed. Numerical results are given to verify the accuracy of the derivations. The chapter is concluded by giving some final remarks. Chapter 3 is organised as: literature survey on performance analysis of FrFT -based OFDM system in presence of CFO. The exact closed form BER and SER expressions for FrFT -based OFDM systems with CFO are analysed for BPSK and QPSK modulation schemes AWGN, frequency flat Rayleigh fading channel and frequency selective Rayleigh fading channel. Numerical results are given to verify the accuracy of the derivations. The chapter is concluded by giving some final remarks.

Chapter 4 is organised in three sections: first discusses about the fixed point design and historical development of cordic theory. After that, by using the “HDL coder” the HDL code is generated and also optimize the code through the HDL workflow Advisor. Finally, FPGA-in-loop co-simulation is run with the Xilinx ZYNQ SoC FPGA by using the HDL Verifier Toolbox, for Verification of HDL code by putting in FPGA-in-loop. Lastly, chapter 5 will conclude the report and tells us about further scope of this work.

ABSTRACT

In questo lavoro di tesi si considera l'analisi delle prestazioni e l'implementazione hardware di sistemi di modulazione con multiplazione di frequenza a portanti ortogonali (OFDM) basati sull'impiego della trasformata discreta frazionaria di Fourier (DFrFT) e della trasformata discreta di Fourier veloce (FFT). Nello studio si considera il tasso di errore sul simbolo (SER) e quello sul bit (BER) in presenza di scostamenti della fase di campionamento (STO) e/o della frequenza della portante (CFO). In particolare, l'analisi del tasso d'errore per l'OFDM basato su FFT è fatto per il caso in cui è presente sia CFO che STO mentre per l'OFDM basato su FrFT si considera la sola presenza di CFO. Le espressioni di SER sono state ottenute per il canale con rumore additivo gaussiano bianco (AWGN) e per canale con affievolimento di Rayleigh selettivo e non selettivo in frequenza per schemi di modulazione BPSK e QPSK. I risultati numerici ottenuti per ogni espressione di SER sono verificati mediante confronto con i risultati ottenuti per simulazione. Le espressioni in forma chiusa per il SER *in presenza di CFO e STO sono state derivate* prima volta nel caso di *QPSK per canale AWGN e di canale con affievolimento di Rayleigh sia selettivo che non selettivo in frequenza per il sistema OFDM basato su FFT*. Anche nel caso di FrFT l'espressione di *SER in presenza di CFO sono state derivate* prima volta nel caso di modulazione BPSK e *QPSK per canale AWGN e di canale con affievolimento di Rayleigh sia selettivo che non selettivo in frequenza*.

La seconda parte del lavoro di tesi riguarda l'implementazione hardware mediante l'utilizzo di MATLAB e Simulink. In tale sviluppo si considera dapprima la costruzione del modello Simulink per la simulazione in tempo reale del sistema OFDM basato su FrFT in presenza di CFO e STO. Successivamente il kernel IFrFT/FrFT è convertito in rappresentazione in virgola fissa utilizzando il *Fixed Point Tool* di MATLAB e, successivamente, *l'HDL Coder Tool* viene impiegato per generare il *codice VHDL e Verilog da trasferire sulla* scheda ZedBoard (zynq-7000) e per la sintesi di logica. Infine, viene utilizzato lo strumento HDL *Verifier* per la co-simulazione *FPGA-in-loop* sia del trasmettitore che del ricevitore. In questo ambito l'implementazione hardware del sistema FrFT-OFDM è stato affrontato per la prima volta. E' importante osservare che un sistema OFDM basato sull'impiego della FrFT migliora sensibilmente il rispetto a quello basato su FFT con schemi di modulazione diversi e anche ambienti di canale diverso.

Il software utilizzato per la verifica analitica e simulata è MATLAB R2014a/2015a. Mediante tale software tutte le espressioni di SER analitiche sono state verificate mostrando un'aderenza perfetta con risultati ottenuti dalla simulazione. Nell'implementazione si è utilizzato l'hardware Xilinx Zynq®-7000 (xc7z020) e i relativi supporti di Xilinx in MATLAB 2015a.

L'intero lavoro di tesi si compone di cinque capitoli organizzati come segue:

- Capitolo 1: origini del sistema OFDM, obiettivi del lavoro di tesi e contributi originali;
- Capitolo 2: evoluzione storica del sistema OFDM con indagine bibliografica relativa all'analisi delle prestazioni di sistemi OFDM basati su FFT e introduzione del modello del sistema in presenza di CFO e STO. Derivazione in forma chiusa delle espressioni di BER e SER per sistemi OFDM basati su FFT in presenza di CFO e STO. Presentazione di risultati numerici per verificare l'esattezza delle derivazioni matematiche.
- Capitolo 3: analisi bibliografica dei metodi impiegati per l'analisi delle prestazioni di sistemi OFDM basati su FrFT in presenza di CFO. Derivazione in forma chiusa delle espressioni matematiche per il calcolo del BER e del SER in presenza di CFO per modulazioni BPSK e QPSK su canali AWGN e soggetti ad affievolimento di Rayleigh selettivi e non selettivi in frequenza. Confronto tra risultati analitici e simulativi. Il capitolo è concluso dando alcune osservazioni finali.
- Capitolo 4, organizzato in tre sezioni: in primo luogo si discute il progetto in virgola fissa design e lo sviluppo storico della teoria CORDIC. Successivamente, utilizzando l'HDL Coder si genera e ottimizza il codice HDL. Infine, si illustra come è stata realizzata la cosimulazione FPGA-in-Loop con FPGA Xilinx ZYNQ SoC mediante il tool HDL Verifier.
- Capitolo 5: si illustreranno le conclusioni e i possibili sviluppi futuri di questo lavoro.

CONTENTS

CHAPTER-I

INTRODUCTION AND MOTIVATION

Topics:

CHAPTER-1 INTRODUCTION AND MOTIVATION

This chapter consists of: the introduction of OFDM along with Thesis objective and contribution, the research motivation along with Advantage/Disadvantage, the applications of OFDM technique and the organization of thesis.

1.1. INTRODUCTION

Orthogonal frequency division multiplexing (OFDM) is one of the multi-carrier modulation (MCM) techniques that transmit signals through multiple carriers. These carriers (sub-carriers) have different frequencies and they are orthogonal to each other. Orthogonal Frequency Division Multiplexing based on Fast Fourier Transform (FFT -based OFDM) has drawn major attention in broad band wireless communication due to its various advantages like less complex equalizer, high data rate, efficient bandwidth utilization and robustness against multi-path fading channel *etc.* [1-5]. It has been adopted by many wireless communication standards, IEEE 802.11 standard. The carrier frequency can go up to as high as 2.4 GHz or 5 GHz. Researchers tend to pursue OFDM operating at even much higher frequencies nowadays [6-10]. For example, the IEEE 802.16 standard proposes yet higher carrier frequencies ranging from 10 GHz to 60 GHz and terrestrial digital video broadcasting (DVB-T) system [11-14].

1.1.1 Origin of OFDM

It is well known that **Chang** *et al.* [15] proposed the original OFDM principles in 1966, and successfully achieved a patent in January of 1970. Later on, **Saltzberg** *et al.* [18] analysed the OFDM performance and observed that the crosstalk was the severe problem in this system. Although each subcarrier in the principal OFDM systems overlapped with the neighbourhood subcarriers, the orthogonality can still be preserved through the staggered QAM technique. However, the difficulty will emerge when a large number of subcarriers are required. In some earlier OFDM applications [6-8], the number of subcarriers can be chosen up to 34. Such 34 symbols will be appended with redundancy of a guard time interval to eliminate inter-symbol interference (ISI) [9-14]. However, more subcarriers should be required and the modulation, synchronization and coherent demodulation would induce a very complicated OFDM requiring additional hardware cost. In 1971, **Weinstein** and **Ebert** *et al*. [18] proposed a modified OFDM system in which the discrete Fourier Transform (DFT)

was applied to generate the orthogonal subcarriers waveforms. Their scheme reduced the implementation complexity significantly, by making use of the inverse DFT (IDFT) modules and the digital-to-analog converters. In their proposed model, baseband signals were modulated by the IDFT at the transmitter and then demodulated by DFT at the receiver. Therefore, all the subcarriers were overlapped with others in the frequency domain, while the DFT modulation still assures their orthogonality, as shown in Fig. 1.1.1

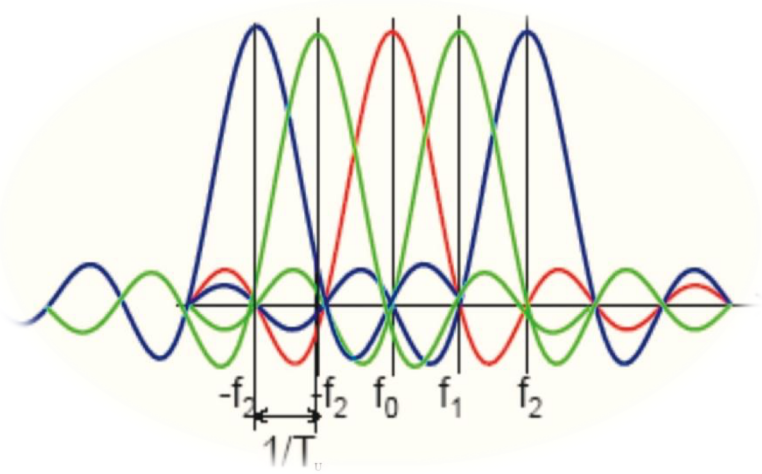

Fig. 1.1.1 Frequency spectrum of OFDM subcarrier signals

Cyclic prefix (CP) was first introduced by **Peled** and **Ruiz** *et al.* [4] for OFDM systems. In their scheme, conventional null guard interval is substituted by cyclic extension for fully-loaded OFDM modulation. As a result, the orthogonality among the subcarriers was guaranteed. With the trade-off of the transmitting energy efficiency, this new scheme can result in a phenomenal ICI reduction. In 1980, **Hirosaki** *et al*. [24] introduced an equalization algorithm to suppress both ISI and ICI. In 1985, **Cimini** *et al.* [6] introduced a pilot-based method to reduce the interference emanating from the multipath and co-channels. In 1989, **Kalet** *et al.* [5] suggested a subcarrier-selective allocating scheme. He allocated more data through transmission of "good" subcarriers near the centre of the transmission frequency band, these subcarriers will suffer less channel distortion. In the 1990s, OFDM system was exploited for high data rate communications.

1.1.2 Thesis Objective and Contribution

After the careful literature survey and study of OFDM system, the foremost research area of multicarrier system performance analysis is of my keen interest. In such a context for

my M.S. Thesis I undertook the Thesis "Performance Analysis and Hardware Implementation of FrFT/FFT based- OFDM System". The FrFT is a generalization of the ordinary FFT that allows for more flexibility in applications. I started focusing on hardware implementation of FrFT -based OFDM system and also analyse performance of FrFT/FFT -based OFDM system in presence of CFO and STO and derived SER expression for QPSK in case of frequency selective fading channel for FrFT -based OFDM system in presence of CFO. Among main contributions I extended work done in [44 and 45] for QPSK modulation scheme in the presence of CFO and STO for AWGN, flat fading and Frequency selective fading channel and also present the SER expression for FrFT -based OFDM in presence of CFO for BPSK and QPSK in AWGN, Flat fading and frequency selective fading channel.

Second part of thesis is hardware implementation of FrFT -based OFDM system, In this, first prepare real time Simulink model of proposed FrFT -based OFDM system in presence of CFO and STO. After that by converting IFrFT/FrFT kernel to fixed point design using MATLAB "Fixed point tool" we can generate fixed point code from floating point with the help of fixed point advisor, Fixed-Point Advisor uses either the design or simulation minimum and maximum from the floating-point data to propose the initial fixed-point scaling. Using the Fixed-Point Tool's scaling function, we analyse, refine, and optimize scaling for relevant blocks in the model that we initially scaled using Fixed-Point Advisor. We use the data type override feature to collect the dynamic range of signals in double precision. The Fixed-Point Tool uses this information to propose a more suitable fixed-point scaling for each block, based on the number of available bits. FPGA implementation uses fixed-point representation, and the follow the HDL coder tool, HDL Coder provides two types of linkage between the model and generated HDL code. Code-to-model and Model-to-code are hyperlinks that let user to view the blocks or subsystems from which the code was generated and generated code for any block in the model, respectively. HDL Coder also provides Embedded MATLAB Function Block which automatically generates HDL code from an m-file. Embedded MATLAB Function Block also employs fixed-point arithmetic by using the Fixed-Point Toolbox.

After the generation and optimization of HDL coder our next goal is to synthesis the HDL code through the Zed Board with Vivado® Design Suite. The Vivado® Design Suite development environment enables a rapid product development for software and hardware because after the synthesis resources requirements for the design can be found. During the synthesis several steps are performed.

After the synthesis the last step is model validation. The validation process starts in the software simulation domain by verifying the design at a high level of abstraction. This allows us to benefit from the acceleration of much of the design yielding dramatically faster simulation iterations. As each block is verified at the RTL level in the context of our full-chip design, its synthesised/gate-level equivalent can be moved over into the physical FPGA, after that use the HDL verifier tool for FPGA in loop both Transmitter and Receiver block respectively. During this work, First time proposed hardware implementation of FrFT -based OFDM in Frequency selective fading channel. Our proposed FrFT -based OFDM model improved SER by large extent as compare to FFT -based OFDM system with different modulation schemes for different channel environments. Moreover, literature survey in Generalized Frequency Division Multiplexing (GFDM) in 5th Generation Non-Orthogonal Waveforms for Asynchronous Signalling (5GNOW) based on GFDM.

In this thesis, the comparative results between FrFT -based OFDM and FFT -based OFDM systems are shown. Through the Analytical as well as simulation analysis of results, it is found that in AWGN, Flat fading channel and frequency selective fading channel the performance (in terms of BER/SER) of FrFT -based OFDM system has been improved with respect to FFT -based OFDM system.

Summary of Performance Analysis Proposed in this Thesis:

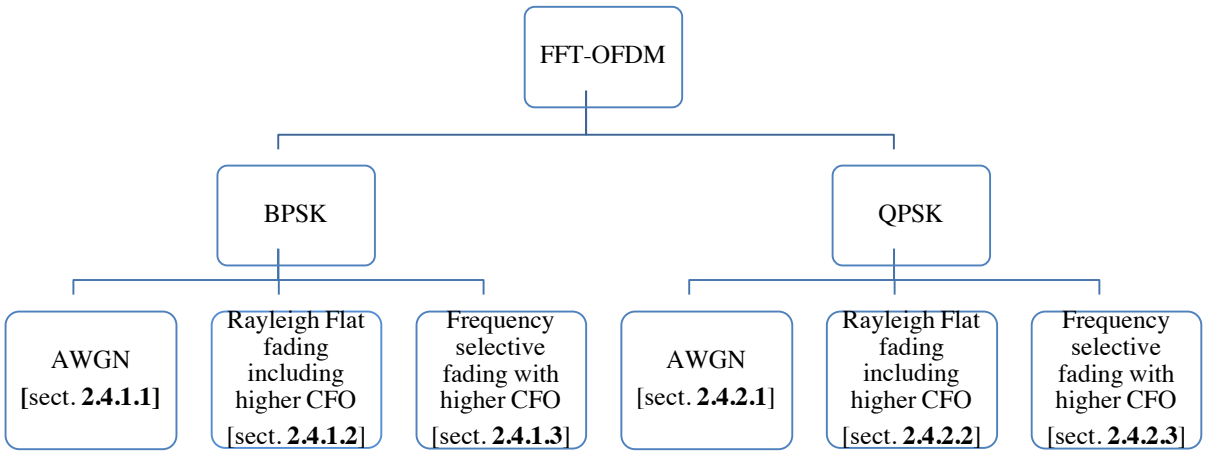

Figure- 1.1.2.1 SER Analysis for FrFT based- OFDM in presence of CFO and STO

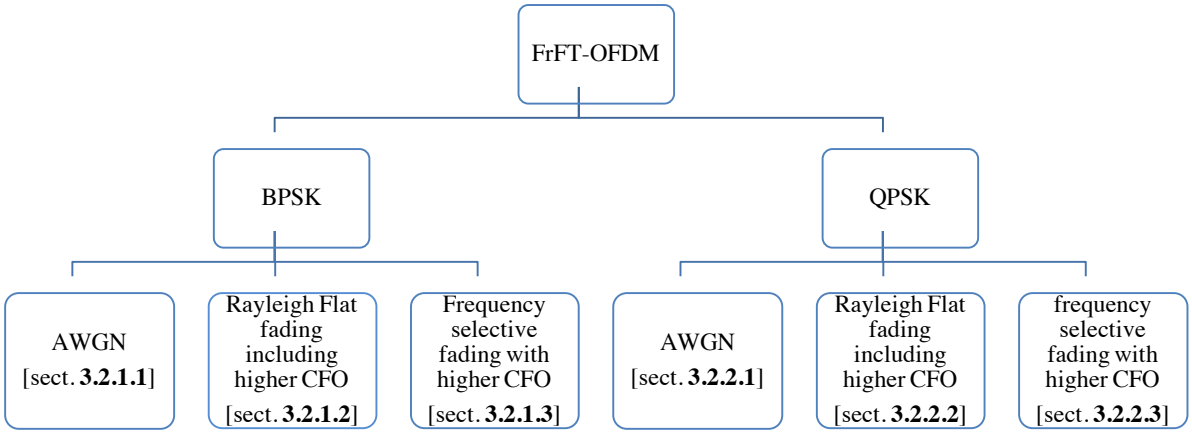

Figure- 1.1.2.2 SER Analysis for FrFT -based OFDM in presence of CFO

1.2. MOTIVATION

Before going to the discussion let's have a brief review of prior techniques.

- The main limitation of FDMA and TDMA are the capacity (the number of users, which can be accommodated without interference).
- The CDMA technique has been developed mainly for capacity reasons.
- CDMA techniques can potentially accommodate more users than either TDMA or FDMA.
- W-CDMA is a 3G wireless standard, evolved from CDMA to support the wideband services at data rate higher than 2 Mbps.
- The wide band signal like DS-CDMA (Direct Sequence CDMA) has a problem of frequency selective multipath fading.
- Frequency selective multipath fading is common in "Urban and Indoor Environment" and it is significant source of performance degradation.
- The performances degrades more if the number of users increases.
- It is observed that the narrow band signals are less sensitive to ISI and frequency selective fading.

Therefore, orthogonal multi-carrier modulation combined with CDMA has been used to solve the problem.

It is obvious that a parallel system is capable of carrying more information than a cascaded system, simply because it uses a variety of frequency bands. However, the significant advantage of OFDM is that it is robust in frequency selective channels, which results from

either multipath fading or other communication interferences. In order to deal with frequency selective fading, the transmitted OFDM signals are divided into many sub-channels so that those sub-channels can be considered frequency flat approximately as the number of the N sub-channel is large enough. Hence the OFDM signals will suffer less channel distortion than the conventional modulated signals.

Under OFDM modulation, the symbol duration becomes N times longer. For example, if the input data rate is 20Mbps, then, the symbol duration is 50 ns, however, in an OFDM system with 128 subcarriers, the symbol duration could become 6.4 us. If these two kinds of symbols are modulated and transmitted through a channel with a particular rms value say, rms = 60 ns, it is clear that the system with a longer symbol duration would perform better. In practice, the DVB-T standard suggests to use 2,048 subcarriers, or 8,192 subcarriers. In these cases, the symbol duration can be even increased by several thousand times.

During the literature survey of OFDM, the main reference of FrFT -based OFDM system was [54], where it is shown that in presence of CFO an OFDM system based on Fractional Fourier Transform (FrFT) allows a better tolerance to ICI than that based on the use of FFT. The FrFT is a generalization of the ordinary FFT that allows for more flexibility in applications. In presence of CFO and STO an OFDM system based on FrFT allows a better tolerance to ICI and also ISI than that based on the use of FFT. As it is known, synchronization is a major issue of OFDM system. So, for reducing the impact of synchronization errors, new method based on localization of chirp training signal in FrFT based- OFDM have been proposed in [46] for STO and CFO estimation. The FrFT has already been established as a superior tool for locating the chirp signal in fractional Fourier domain given in [46].

1.3. ADVANTAGES & DISADVANTAGES OF OFDM BASED ON FFT/FrFT

1.3.1 Advantages

- High spectral efficiency.
- Efficient implementation using FFT.
- Low sensitivity to time synchronization error.
- OFDM has improved quality of narrow band interference.
- Can easily adapt to severe channel conditions without complex equalization.
- Robust against ISI and multipath Fading channel.
- FrFT -based OFDM less sensitive to CFO and STO.

- FrFT -based OFDM less sensitive to Doppler frequency spreading.
- Forward error correction is employed to accurate for sub-carrier that super form deep fades.
- Use of FrFT more Robust against ISI and multipath Fading channel as compare to FFT based- OFDM.

1.3.2 Disadvantages

- Sensitive to frequency synchronization problem.
- Sensitivity to CFO at the receiver.
- Sensitivity to STO at the receiver.
- High High Peak-to-Average Power Ratio (PAPR), requiring linear transmitter circuitry, which suffers from poor power efficiency.
- FrFT -based OFDM increase the computational complexity.

1.4. APPLICATION

After the IFFT/FFT technique was introduced, the implementation of OFDM became more convenient. Generally speaking, the OFDM applications may be divided into two categories-wired and wireless technologies. In wired systems such as Asymmetric Digital Subscriber Line (ADSL) and high speed DSL, OFDM modulation may also be referred as Discrete Multitone Modulation (DMT). In addition, wireless OFDM applications may be shown in numerous standards such as IEEE 802.11 [10].

- IEEE 802.11a/g, IEEE 802.16a [10].
- Asymmetric Digital Subscriber Line (ADSL) services [10].
- Digital Audio Broadcasting (DAB) [10].
- Digital Terrestrial Television Broadcasting: DVB-T in Europe, ISDB in Japan
- 4G, IEEE 802.11n, IEEE 802.16, and IEEE 802.20 [10].
- Generalized Frequency Division Multiplexing (GFDM) in 5th Generation Non-Orthogonal Waveforms (5GNOW) based on GFDM [47].
- Aspects of timing and frequency synchronization for LTE-A system.

OFDM was also applied for the development of Digital Video Broadcasting (DVB) in Europe, which was widely used in Europe and Australia. In the DVB standards, the number of subcarriers can be more than 8,000, and the data rate could go up as high as 15Mbps. At present, many people still work to modify the IEEE 802.16 standard, which may result in an even higher data rate up to 100Mbps.

1.5. ORGANIZATION OF THESIS

Chapter 2 contains two section: section 1, contain the system model of FFT -based OFDM system in presence of CFO and STO and the mathematical formulation of transmitter, channel and receiver. It also contains the ICI coefficient of OFDM system. Section 2, contain an exact SER analysis of FFT -based OFDM system in presence of CFO and STO for BPSK and QPSK modulation in AWGN, frequency flat Rayleigh fading channels and frequency selective Rayleigh fading channels.

Chapter 3 contains 2 sections: section 1, contain the system model of FrFT -based OFDM system in presence of CFO. It also contains the ICI coefficient of FrFT -based OFDM system. Section 2 contain, SER analysis of FrFT -based OFDM system in presence of CFO has been derived for BPSK and QPSK modulation schemes are analysed for AWGN, frequency-flat Rayleigh fading channels and Frequency selective Rayleigh fading channels.

Chapter 4, contain the Hardware implementation of FrFT -based OFDM system in presence of CFO and STO. In this, first prepare real time Simulink model of FrFT -based OFDM system in presence of CFO and STO. After that converts IFrFT/FrFT kernel to fixed point design and follow the HDL coder tool and also perform logic synthesis, after that use the HDL verifier tool for FPGA-in-loop.

Finial chapter 5 is organised as: section 1, contain the project report is concluded regarding the Performance Analysis and Hardware Implementation of FrFT/FFT -based OFDM System in presence of CFO and STO. Section 2, contain the further scope of this work is decided through a literature survey based on **"*Performance Analysis and Hardware Implementation of FrFT/FFT -based OFDM System in presence of CFO and STO*".**

****

CHAPTER-II

AN EXACT SER ANALYSIS OF FFT-BASED OFDM

Topics:

2.1. Historical Development of OFDM

2.2. Literature Survey on Performance Analysis of FFT -Based OFDM System

2.3. System Model In Presence of CFO and STO

2.3.1. Transmitter Model

2.3.1.1 Cyclic Prefix or Guard Band Insertion

2.3.2. Channel Model

2.3.2.1 AWGN Channel

2.3.2.2 Frequency Selective Rayleigh Fading Channel

2.3.3. Receiver Model

2.4. BER Analysis for FFT Based- OFDM In Presence of CFO and STO

2.4.1. BPSK Modulation

2.4.1.1 AWGN Channel

2.4.1.2 Rayleigh Flat Fading Channel

2.4.1.3 Rayleigh frequency selective fading channel

2.4.2. QPSK Modulation

2.4.2.1 AWGN Channel

2.4.2.2 Rayleigh Flat Fading Channel

2.4.2.3 Rayleigh frequency selective fading channel

2.5. Discussion of Simulated Results

2.6. Summary of BER Expression for FFT -based OFDM

- Expressions of BER in presence of CFO given by **Dharmawansa** *et al.*[37]:

2.6.1. AWGN Channel

2.6.1.1 BPSK modulation

2.6.1.2 QPSK modulation

2.6.2. Flat Fading channel

2.6.2.1 BPSK modulation

2.6.2.2 QPSK modulation

2.6.3 BPSK in frequency selective fading channel

❖ Expressions of BER in presence of CFO given by **A. Chaturvedi** *et al* [39]:

2.6.4. BPSK in Rayleigh flat fading channel

2.6.5. BPSK in frequency selective fading channel

❖ Expressions of SER in presence of CFO given by ***A. Hamza*** *et al.* [53]:

2.6.6. QPSK in frequency selective fading channel

2.6.7. QPSK in Flat fading channel

❖ Expressions of BER in presence of CFO and STO given by ***A. K. Chaturvedi*** *et al.* and ***Y. Wang*** *et al.* [44 and 45]:

2.6.8. BPSK in AWGN Channel

2.6.9. BPSK in Flat fading channel

2.6.10. BPSK in frequency selective fading channel

❖ Proposed Expressions of SER in presence of CFO and STO given by ***A. Kumar*** *et al.* [section- **2.4.2.**]:

2.6.11. QPSK in AWGN Channel

2.6.12. QPSK in Flat fading channel

2.6.13. QPSK in frequency selective fading channel

CHAPTER-2 AN EXACT SER ANALYSIS OF FFT-BASED OFDM

In this chapter, historical development of OFDM system along with literature survey on performance analysis of FFT -based OFDM system, and discussion of system model in presence of CFO and STO with mathematical formulation of transmitter, channel and receiver. The exact closed form bit error rate (BER) and symbol error rate (SER) expressions for FFT -based OFDM systems with CFO and STO are analysed. Starting from BER performances of BPSK given in [44, 45], proposed SER expressions are given for QPSK modulation schemes for AWGN, flat Rayleigh fading channel and frequency selective Rayleigh fading channel. Numerical results are given to verify the accuracy of the derivations. The chapter is concluded by giving some final remarks.

2.1. HISTORICAL DEVELOPMENT OF OFDM

Taking a brief discussion about the historical development of OFDM (milestones in history). Through this initially developed OFDM, attentions of researches moved towards the performance analysis of OFDM system. So firstly, summarizing the beginning of OFDM.

Table-2.1: Summary of OFDM

1965	P. A. Bello *et al*. [13]	Initial multicarrier (MCM) system KINEPLEX [13-14]
1967	M. Zimmerman *et al.* [14]	
1968	R.W. Chang *et al.* [15]	MCM employing overlapped band limited orthogonal signals.
1967	Saltzberg *et al.* [18]	MCM system employing orthogonal time staggered QAM.
1971	S.B. Weinstein *et al.* [20]	OFDM became more popular after the use of DFT to generate the orthogonal subcarriers
1980	J.S. Chow *et al.* [21]	Suggested the use of DFT based OFDM for high speed modems
1980	Hirosiki *et al.* [24]	Suggested a system for Saltsberg O-QAM OFDM system
1985	Cimini *et al.* [25]	Analytical and simulated results on the performance of OFDM modems
1988-1995	ETSI DAB standard [41]	first OFDM based standard for digital broadcasting system

2.2. LITERATURE SURVEY ON PERFORMANCE ANALYSIS OF FFT -BASED OFDM SYSTEM

After the historical development of OFDM system moving towards the problem formulation on performance analysis of OFDM system. Two methods were available for the analysis of the resultant degradation in performance. Firstly, the statistical average of the ICI could be used as a performance measure. Secondly, the BER caused by CFO and STO could be approximated by assuming the ICI to be Gaussian. So that I have taken the performance analysis of OFDM system in presence of CFO and STO in terms of BER. The performance analysis in different channel environments (flat fading, frequency selective fading, etc.) with CFO has been done by different authors in [32-40]. Furthermore, the effect of CFO and STO combined was considered in [44-45]. Before moving towards the problem formulation, I would like to discuss the brief summary of performance analysis of FFT -based OFDM system given by many authors.

"Probability of Error Calculation of OFDM Systems with Frequency Offset" by **K. Sathananthan** and **C. Tellambura** [35], 2001. In [35], a precise numerical techniques is given for calculating the effect of the CFO on the BER in an OFDM system. The subcarriers are modulated with binary phase shift keying (BPSK) and the analysis workout as using a series due to Beaulieu. For QPSK and 16-QAM cases, they used an infinite series expression for the error function in order to express the average probability of error in terms of the two-dimensional characteristic function of the ICI. The results are derived for the average probability of error in case of BPSK, QPSK and 16-QAM modulation techniques. In same work a gaussian approximation is proposed for the approximate SNR degradation.

Later, in 2005 a "BER of OFDM Systems Impaired by Carrier Frequency Offset in Multipath Fading Channels" was given by **Luca Rugini** and **Paolo Banelli** [36]**.** This paper contains an analytical approach to evaluate the error probability of OFDM system subject to CFO in frequency selective channel, characterized by Rayleigh and Rician fading. By properly exploiting the Gaussian approximation of the ICI, it is shown that BER for an uncoded OFDM system with quadrature amplitude modulation (QAM) can be expressed by the sum of a few integrals, whose number depends on the constellation size, each integral can be evaluated numerically. In Rayleigh fading, by using a series expansion that involves generalized hyper geometric functions, each integral can be evaluated. This letter has

basically proposed the result for QAM technique by assuming different channel environments Rayleigh fading and Rician fading.

Further in 2007 a "Effects of Receiver Windowing on OFDM Performance in the Presence of Carrier Frequency Offset" discussed by **Norman C. Beaulieu** and **Peng Tan** [34] was published. The paper has a derived expression of an exact BER expression for an OFDM system with windowing reception, and it is found that performance of OFDM in terms of BER is improved using window family.

In 2009 a paper on "an Exact Error Probability Analysis of OFDM Systems with Frequency Offset" was given by **Prathapasinghe Dharmawansa, Nandana Rajatheva, and Hlaing Minn** [37]**.** The paper also comprises all the work related to performance evaluation, done till then. Characteristic functions and Beaulieu series [37] have been used to derive exact BER expressions in the presence of ICI. They have followed the procedure presented in **Sathananthan** and **Tellambura** [35] and **Rugini** and **Banelli** [36] with different mathematical insight to derive the exact closed form BER/SER expressions for OFDM with ICI over AWGN, frequency selective and flat fading channel. They have not considered the Gaussian approximation of the ICI, instead they have shown that the probability density function of ICI is a mixture of Gaussian densities with properly selected parameters. In 2010 a letter was published on Closed Form BER Expressions for BPSK OFDM Systems with Frequency Offset by **R. Uma Mahesh** and **A. K. Chaturvedi** [39]. This letter addresses the performance degradation caused by the presence of CFO in OFDM systems. In this paper they have modified the result given in [37]. The results in [37] was analysed for lower values of CFO and there was a difference between analytical and simulated results for higher values of CFO. In this paper the modification is done for higher values of CFO for flat and frequency selective Rayleigh fading channels.

Very few literatures studied on the combined effects of STO and CFO in OFDM system for BER evaluation. Some recent work shows about BER performance considering both CFO and STO are [44, 45]. Due to high sensitivity of OFDM systems to synchronization errors, they treated the ICI introducing by residual frequency and timing offsets. By Following with the result of [45], **R. Uma Mahesh** and **A. K. Chaturvedi** derived BER expression with frequency and fractional timing offsets over AWGN and flat Rayleigh fading channels [45]. This approach is convenient to analyse BER, but its the computational complexity grows exponentially. Furthermore, In [44] by exploiting CHF and Beaulieu series, evaluated BER

expressions of BPSK impaired by residual frequency and timing offsets over frequency selective Rayleigh fading channel.

Later on **A. Hamza**, *et al.* [52] gave the first time Closed Form SER Expressions for QPSK OFDM Systems CFO in Rayleigh Fading Channel. This paper considers the two dimensional PDF and CHF for deriving the SER expression.

Table 2.2: Summary of performance Analysis of FFT -based OFDM system.

1990	Cases *et al*. [27]	Gave analytical and experimental results of OFDM system
1991-1993	Hara *et al*. [29-31]	Rayleigh frequency selective fading channel Bit Error Rate Performance for Multicarrier Modulation Radio Transmission
1995	T. Pollet *et al*. [32]	BER sensitivity of OFDM to carrier frequency offset & wiener phase noise
2001	K. Sathananthan *et al*. [35]	Calculated the probability of Error of OFDM Systems with Frequency Offset [35]
2005	Luca Rugini, *et at*. [36]	Analytical approach to evaluate the error probability of OFDM systems in presence of CFO for frequency selective channels
2009	P. Dharmawansa *et al*. [37]	Gave an exact error probability analysis of OFDM systems with frequency offset
2010	A. Chaturvedi *et al*. [39]	Given closed form BER expressions for BPSK OFDM systems with frequency offset
2012	R. Mahesh *et al*. [45]	BER analysis of BPSK OFDM systems with CFO and STO in AWGN and Flat fading
2012	Y. Wang, *et al*. [44]	BER analysis of BPSK OFDM systems with CFO and STO over frequency selective fading channels
2014	A. Hamza, *et al.* [52]	Closed Form SER Expressions for QPSK OFDM Systems CFO in Rayleigh Fading Channel

2.3. SYSTEM MODEL

The basic principle of OFDM is to split a high data rate stream into a number of lower data rate streams and then to transmit these streams in parallel using several orthogonal sub-carriers. By using this parallel transmission, the symbol duration increases and the relative amount of dispersion in time caused by multipath delay spread decreases. If 1/T is the symbol rate of the input data to be transmitted then the symbol interval in the OFDM system is

increased to NT. For reducing the inter-symbol interference, a guard band is inserted between successive OFDM symbols. The block diagram representation of Fast Fourier Transform (FFT) based- OFDM system with N subcarrier is shown in Figure-2.3.1. It consists of a transmitter segment, then channel part followed by the receiver segment. The description about each segment is included below.

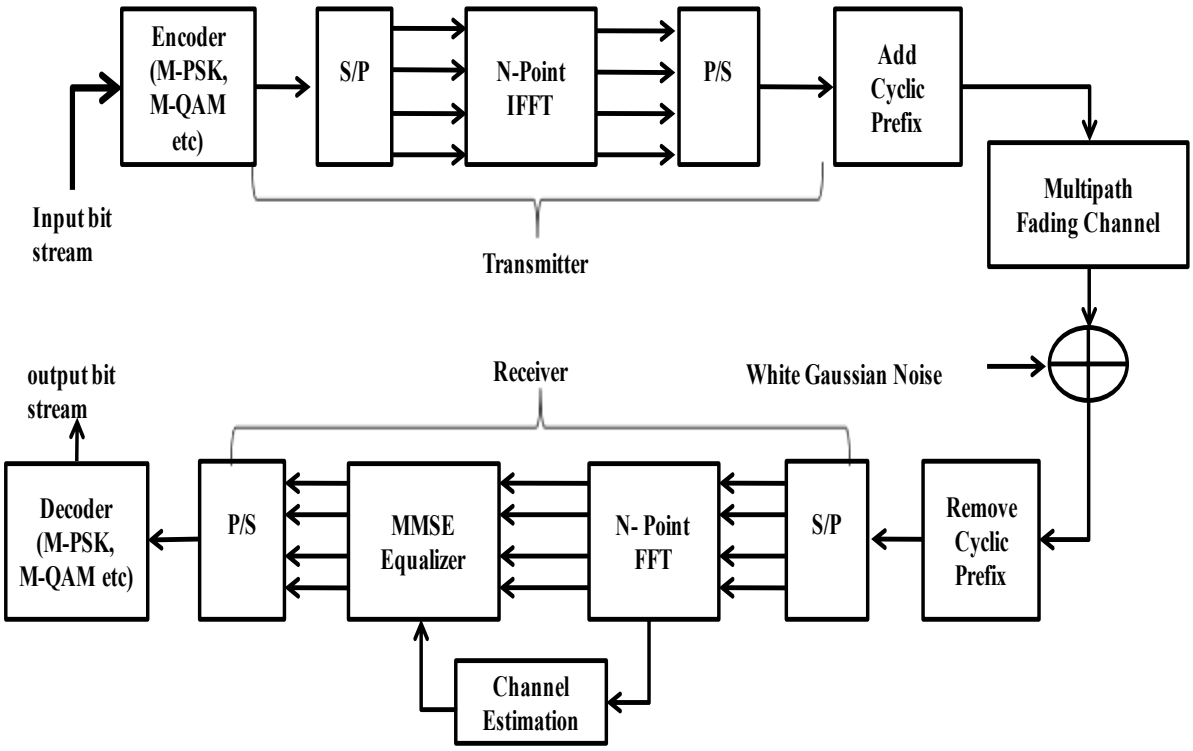

Figure-2.3.1. OFDM System Model

2.3.1. Transmitter Model

The input data stream bits are encoded into continuous signals by the encoder, which is first block of the transmitter. Data encoding can be done by using any of the digital modulation techniques viz. M-QAM, M-PSK, or M-FSK. After that N such symbols are transferred by the serial-to-parallel converter. These complex parallel data symbols $\{X(k), for\ k = 1,2, \dots, N\}$ are fed into the IFFT block. After taking N point IFFT, the last g samples are appended at the front (the cyclic prefix addition) to form $x(m)$. These complex parallel data symbols are then modulated by a group of orthogonal sub-carriers, which satisfy the following condition of orthogonality-

$$\frac{1}{T_u}\int_0^{T_u} e^{j2\pi f_k t}\, e^{j2\pi f_m t} dt = \begin{cases} 1, & k = m \\ 0, & k \neq m \end{cases}$$

(2.3.1.1)

where $f_k = k/T_u$, for $k = 0, 1, 2 \cdots, N-1$ and $1/T_u$ is the minimum sub-carrier spacing required. The baseband OFDM signal transmitted during i^{th} block can be written as –

$$x(i,t) = \frac{1}{\sqrt{N}} \sum_{k=0}^{N-1} X(i,k) e^{j2\pi f_k t}, \qquad 0 \leq t \leq T$$

(2.3.1.2)

where T_u is the useful duration of one OFDM symbol, $f_k (= k/T_u)$ is the sub-carrier frequency of the k^{th} sub-carrier $X(i,k)$ is the complex data symbol of i^{th} block modulated on k^{th} sub-carrier and N is the total number of sub-carriers. It is assumed that the complex data symbols are un-correlated.

$$E[\, X(i,k) X^*(i,k)\,] = \begin{cases} 1, & k = m \\ 0, & k \neq m \end{cases} \qquad (2.3.1.3)$$

where $x^*(.)$ represents the complex conjugate of $x(.)$. The discrete form of the baseband OFDM signal $x(i,t)$ in (2.3.1.2) can be expressed as-

$$x(i,m) = \frac{1}{\sqrt{N}} \sum_{l=0}^{N-1} X(i,k)\, e^{\frac{j2\pi\, m\, l}{N}}, m = 0, 1, 2 \ldots\ldots\ldots\ldots, N-1$$

(2.3.1.4)

It is clearly visible from (2.3.1.2.4) that the transmitted signal is the IFFT of the complex input data symbols $X(i,k)$ and hence it can be easily and efficiently generated using inverse fast Fourier transform (IFFT) as shown in Fig-2.3.1 Similarly, the FFT can be used at the receiver side for demodulation.

2.3.1.1 Cyclic Prefix or Guard Band Insertion

A guard band interval is usually inserted between successive OFDM symbols to avoid the ISI caused by the delay spread of multipath channel. If a guard band interval is inserted without any signal transmission then the ISI can be eliminated almost completely. But a sudden change in waveform contains higher spectral components, resulting into ICI. Therefore the guard interval insertion technique with cyclic prefix is generally used to avoid

ICI. In this method, the OFDM symbol is cyclically extended in the guard time. Due to cyclic prefix (CP) insertion, the transmitted signal is extended to $T_s = T_g + T$ and can be expressed as-

$$s(i,t) = \sum_{m=-N_{cp}}^{N-1} x(i,m) g_t(t - mT) \tag{2.3.1.1.1}$$

where $g_t(.)$ representing the raised cosine filter for the pulse shaping at the transmitter side, T is the sampling period and N_{cp} is the length of guard interval or cyclic prefix (CP) plays an important role in the performance of OFDM system. If the length of the guard interval (CP) is set shorter than the maximum delay of a multipath channel, the tail part of an OFDM symbol affects the head part of the next symbol, resulting in the ISI. On the other hand a long CP increases the overhead of the system.

2.3.2. Channel Model

2.3.2.1 AWGN Channel

AWGN is often used as a channel model in which the only impairment to communication is a linear addition of wideband or white noise with a constant spectral density (expressed as watts per hertz of bandwidth) and a Gaussian distribution of amplitude. The model does not account for fading, frequency selectivity, interference, nonlinearity or dispersion. However, it produces simple and tractable mathematical models which are useful for gaining insight into the underlying behaviour of a system before these other phenomena are considered.

The AWGN channel is represented by a series of outputs Y_i at discrete time event index i. Y_i is the sum of the input X_i and noise w_i , where w_i is independent and identically distributed and drawn from a zero-mean normal distribution with variance σ_s^2. The w_i are further assumed to not be correlated with the X_i

$$w_i = \mathcal{N}(0, \sigma_s^2) \tag{2.3.2.1.1}$$

2.3.2.2 Frequency selective Rayleigh Channel

Now the effects of multipath fading channel $h(\tau, t)$ (channel impulse response) have been considered here with the n^{th} sample of OFDM symbol. The L-path tap-delay line model with frequency selective fading channel has been taken as in [38].

The impulse response $h(\tau, t)$ can be expressed as-

$$h(\tau, t) = \sum_{l=0}^{l-1} h(l, t)\delta(t - \tau_l)$$

(2.3.2.2.1)

where $h(l, t)$ and τ_l are the complex amplitude (or tap coefficient) and propagation delay of the l^{th} path, respectively and $\delta(t)$ is the Dirac function. The tap coefficients $\{h(l, t), for\ l = 0, 1, 2 \cdots, L-1\}$ are modeled as zero mean complex Gaussian random variables having variances $\{\sigma_l^2\}\ with\ \sigma_0^2 + \sigma_1^2 + \cdots + \sigma_{L-1}^2 = 1$. If substitute $L = 1$ then $h(\tau, t)$ become the flat fading channel.

2.3.3. Receiver Model

After considering the effect of multipath fading channel $h(\tau, t)$, the i^{th} received signal $r(i, t)$ can be expressed as-

$$r(i, t) = \sum_{l=0}^{L-1} h(l, t)\, s(i, t - \tau_l T) + w(t)$$

(2.3.3.1)

where $w(t)$ represents the Additive White Gaussian Noise at the receiver with two sided power spectral density of $\frac{N_o}{2}$, where N_o is the noise power. If the length of CP is more than the maximum delay spread of multipath channel and if the STO and CFO are correctly estimated and compensated the received is impaired only by the channel. However, because of presence of estimation errors, time varying Doppler shift and oscillators drift, there exists residual timing and frequency offsets. Therefore, after removing the cyclic prefix, the received discrete time signal before the DFT block can be represented as-

$$r(i, n) = e^{\frac{j2\pi\, \Delta\varepsilon\, n}{N}} \sum_{l=0}^{L-1} h(l, t) \sum_{m=0}^{N-1} x(i, m) g(n - m - \tau_l - \Delta\, \theta) + w(n)$$

(2.3.3.2)

where $\Delta\, \varepsilon = \Delta\, f\, T$ is the carrier frequency offset $\Delta\, f$ normalized to sub-carrier spacing $\frac{1}{T}$, $\Delta\, \theta$ represent residual normalized timing offsets and $g(.)$ denotes the raised cosine impulse response which satisfies the Nyquist condition, and $w(n)$ is the zero-mean complex AWGN with variance N_0 . By taking the DFT of the received signal and substituting (2.3.3.2) we the received signal is given to the FFT block.

The output of FFT can be expressed as-

$$Y(l) = \frac{1}{\sqrt{N}} \sum_{n=0}^{N-1} r(i,n) e^{\frac{-j2\pi ln}{N}} \tag{2.3.3.3}$$

After the substituting the value of $r(i,n)$ from the equation (2.3.3.2) in to the equation (2.3.3.3)-

$$Y(l) = \frac{1}{\sqrt{N}} \sum_{n=0}^{N-1} \left\{ e^{\frac{j2\pi \Delta\varepsilon n}{N}} \sum_{l=0}^{L-1} h(l,t) \sum_{m=0}^{N-1} x(i,m) g(n-m-\tau_l - \Delta\theta) + w(t) \right\} e^{\frac{-j2\pi ln}{N}} \tag{2.3.3.4}$$

what is the effect on the l^{th} sub-carrier of a symbol transmitted on the k^{th} sub-carrier. If $k = l$, then signal will be orthogonal and desired signal will be received. If $k \neq l$, then signal will be non-orthogonal and interference signal will be generated. The received signal can be rewritten as-

$$Y(l) = X(k)H(k)S(l) + \sum_{\substack{l=0, \\ l \neq k}}^{N-1} X(l)H(l)S(l-k+1) + w(l) \tag{2.3.3.5}$$

where $w(n)$ is the AWGN component in time domain, $H(k)$ denotes the frequency response of the multipath fading channel at the k^{th} sub-channel is defined as-

$$H(k) = \sum_{l=0}^{L-1} h(l,t) e^{\frac{-j2\,\pi\, k\, \tau_l}{N}} \tag{2.3.3.6}$$

and $S(l-k+1)$ denotes the ICI coefficient define as- using trigonometric identity- $\sum_{n=1}^{N} e^{j\theta n} = \frac{\mathrm{Sin}(\frac{n\theta}{2})}{\mathrm{Sin}(\theta/2)} e^{j\theta^{\sim}}$ where $e^{j\theta^{\sim}}$ term doesn't affect power.
After further simplification the ICI coefficient can be written as-

$$S(k) = \frac{\mathrm{Sin}\,\pi(k+\Delta\varepsilon)}{\mathrm{N\,Sin}\left(\frac{\pi(k+\Delta\varepsilon)}{N}\right)} e^{j\pi\left(1-\frac{1}{N}\right)(k+\Delta\varepsilon)} g(\Delta\theta) \tag{2.3.3.7}$$

The equation (2.3.3.7) describes the ICI coefficient at the receiver. If non-orthogonal ($k \neq l$), the received signal (2.3.3.5) contains three terms: first term is desired signal, second term is ICI signal and third term is noise signal. By substituting $H(k) = 1$ the output of FFT -based OFDM system in fading channel will be similar to the output in AWGN channel [44] Interference term occurs only if non-orthogonal sub-carrier term ($k \neq l$) will be present.

2.4. BER ANALYSIS OF OFDM IN PRECENCE OF CFO AND STO

We assume equiprobable message symbols and consider error rates for the first subcarrier. Before starting the main analysis, an important identity is presented between product and sum of cosines as-

$$\sum_{k=1}^{M}\cos(\phi_k)=\frac{1}{2^{M-1}}\sum_{k=1}^{2^{M-1}}\cos(\boldsymbol{\phi}^T e_k)=\frac{1}{2^M}\sum_{k=1}^{2^{M-1}}e^{j\boldsymbol{\phi}^T e_k}+e^{-j\boldsymbol{\phi}^T e_k} \tag{2.4.1}$$

where $\boldsymbol{\phi}=(\phi_1,\phi_2,\phi_3\ldots\ldots\phi_M)^T$, e_k is k^{th} column of $M\times 2^{M-1}$ matrix E_M. The k^{th} column of E_M is essentially the binary representation of the number 2^M-k, where zeros are replaced by -1. The matrix E_M for the value of $M=4$ can be written as-

$$\mathrm{E}_4=\begin{pmatrix}1&1&1&1&1&1&1&1\\1&1&1&1&-1&-1&-1&-1\\1&1&-1&-1&1&1&-1&-1\\1&-1&1&-1&1&-1&1&-1\end{pmatrix}$$

The identity in (2.4.1) can be verified very easily by repeatedly applying the identity $(cosC\ cosD\equiv\frac{1}{2}\ [cos(C+D)+cos(C-D)])$ to the product of two cosine terms taken at a time, in the left side of (2.4.1).

2.4.1. BPSK Modulation

2.4.1.1 AWGN Channel

For BPSK modulation $X(k)\in\{1,-1\}$ and the first subcarrier with the transmitted symbol 1 is considered here. Since the constellation is purely real, only the real part of (2.3.3.5) will be considered. Following [37], we obtain the CHF of the real part of $Y(1)$, $\Re(Y(1))$, written as-

$$\varphi_{\Re[Y(1)]}(\omega)=E\left(e^{j\omega\Re[Y(1)]}\right) \tag{2.4.1.1.1}$$

Substituting the value of $Y(1)$ from (2.3.3.5) in to the eq. (2.4.1.1.1)-

$$\varphi_{\Re[Y(1)]}(\omega)=\left(e^{j\omega\Re[S(1)]}\right).e^{j\omega W(1)}.\prod_{\substack{l=2\\l\neq k}}^{N-1}\left(e^{j\omega\Re[S(l)]}\right) \tag{2.4.1.1.2}$$

Now, it can be simplified as-

$$\varphi_{\Re[Y(1)]}(\omega) = \left(e^{j\omega\Re[S(1)]-\frac{\omega^2\sigma_s^2}{2}}\right)\prod_{\substack{l=2\\ l\neq k}}^{N-1} cos(\omega\Re[S(l)])$$

(2.4.1.1.3)

The above equation can be further simplified by using trigonometric identity (2.4.1) as-

$$\varphi_{\Re[Y(1)]}(\omega) = \frac{1}{2^{N-1}}\sum_{k=1}^{2^{N-2}} exp\left(j\omega\theta_k - \frac{\omega^2\sigma_s^2}{2}\right) + exp\left(j\omega\beta_k - \frac{\omega^2\sigma_s^2}{2}\right)$$

(2.4.1.1.4)

where $\theta_k = \Re[S(1) + \boldsymbol{S}^T e_k]$, $\beta_k = \Re[S(1) - \boldsymbol{S}^T e_k]$ and $\boldsymbol{S} = (S(2),\ S(3),\ \ldots S(N))^T$, E_{N-1} is of dimension $(N-1)\times 2^{N-2}$. It is obvious that (2.4.1.1.4) represents the CHF of a mixture of Gaussian density function. Since the hypotheses are binary, an error occurs if $\Re[Y(1)] < 0$. Now, the bit error probability can be written as-

$$P_b(\xi) = \frac{1}{2^{N-1}}\sum_{k=1}^{2^{N-2}} \{Q(\sqrt{2\gamma}\,\theta_k) + Q(\sqrt{2\gamma}\,\beta_k)\}$$

(2.4.1.1.5)

where $\gamma = E_b/N_0$, $Q(x)$ is the Gaussian Q function. One should note that in our case of interest $E_b = 1$ and $\sigma_s^2 = N_0/2$ with N_0 being the noise power spectral density.

2.4.1.2 Rayleigh Flat Fading Channel

In the Rayleigh flat fading channel, the conditional bit error probability can be written by using (2.4.1.1.5) as-

$$P_b(\xi|H) = \frac{1}{2^{N-1}}\sum_{k=1}^{2^{N-2}} \{Q(\sqrt{2\gamma}\,\theta_k|H|) + Q(\sqrt{2\gamma}\,\beta_k|H|)\}$$

(2.4.1.2.1)

where $|H|$ denotes the absolute value of H. Now, the unconditional bit error probability is calculated as in [38, eq. 8.102]-

$$P_b(\xi) = \int_0^\infty P_b(\xi|H)P(|H|)\,d|H|$$

(2.4.1.2.2)

where $|H|$ has a Rayleigh distribution given by $P(|H|) = \frac{|H|}{\sigma_R^2} exp\left(\frac{|H|^2}{2\sigma_R^2}\right)$. After applying the following Craig's formula-

$$Q(x) = \frac{1}{\pi}\int_0^{\pi/2} \exp\left(-\frac{x^2}{2sin\psi}\right)d\psi, \qquad x > 0$$

(2.4.1.2.3)

Individually, putting Q- function from (2.4.1.2.1) into (2.4.1.2.3) and after performing some algebraic manipulations, The bit error probability written as-

$$P_b(\xi) = \frac{1}{2} - \frac{1}{2^N} \sum_{k=1}^{2^{N-2}} \left\{ \sqrt{\frac{2\sigma_R^2\theta_k^2\gamma}{1+2\sigma_R^2\theta_k^2\gamma}} + \sqrt{\frac{2\sigma_R^2\beta_k^2\gamma}{1+2\sigma_R^2\beta_k^2\gamma}} \right\}$$

(2.4.1.2.4)

However, closed form analytical BER expressions for CFO were given the first time in [37]. The BER expression derived in [37] is correct for all values of CFO for AWGN channel, the same is not true for flat and frequency selective channels. This is because the expressions have been derived assuming the argument of Q function in the expressions (7) of [37] to be positive. This is not true for higher values of CFO, leading to a mismatch between the theoretical and actual BER. The same is true also for system model based on the CFO and STO. So by considering the argument of Q function is $+$ ive as well as $-$ ive so by following the same derivation approch for $+$ ive argument of Q function as well as $-$ ive argument of Q function, After some mathematical manipulation an exact BER expression is written as-

$$P_b(\xi) = \frac{1}{2} - \frac{1}{2^N} \sum_{k=1}^{2^{N-2}} \left\{ sgn(\theta_k) \sqrt{\frac{2\sigma_R^2\theta_k^2\gamma}{1+2\sigma_R^2\theta_k^2\gamma}} + sgn(\beta_k) \sqrt{\frac{2\sigma_R^2\beta_k^2\gamma}{1+2\sigma_R^2\beta_k^2\gamma}} \right\}$$

(2.4.1.2.5)

where $sgn(.)$ denotes the signum function.

2.4.1.3 Rayleigh Frequency Selective Fading Channel

Here, L sample-spaced tap-delay-line model is assumed for the frequency selective channel. Furthermore, the channel is assumed to be quasi-static. The received k^{th} subcarrier written as-

$$Y(k) = X(k)H(k)S(k) + \sum_{\substack{l=2 \\ l \neq k}}^{N} X(l)H(l)S(l-k+1) + w(k), \quad k = 1, 2, \ldots, N$$

(2.4.1.3.1)

where $H(k)$ is the channel response in frequency domain and $\big(H(1), H(2), .., H(N)\big)^T = F_L h$ with $h = (h_1, h_2, \ldots, h_L)^T$, and F_L denotes the first L columns of the $N \times N$ discrete Fourier transform (DFT) matrix, defined by $F_L[p,q] = e^{\left(\frac{-j2\pi(p-1)(q-1)}{N}\right)}$. For BPSK modulation $X(k) = \{+1, -1\}$, the first subcarrier is considered with the transmitted symbol $X(1) = 1$.

Then (2.4.1.3.1) can be written as-

$$Y(1) = H(1)S(1) + \sum_{l=2}^{N} H(l)S(l) + w(1)$$

(2.4.1.3.2)

The decision variable can be formed as $\Re\left[\overline{H(1)}\, Y(1)\right]$, where $\overline{H(1)}$ denotes the complex conjugate of $H(1)$. Now, we can rewrite the equation (2.4.1.3.2) in terms of the decision variable written as-

$$\Re\left[\overline{H(1)}\, Y(1)\right] = |H(1)|^2\, \Re[S(1)] + \sum_{l=2}^{N} \Re\left[\overline{H(1)}\, H(1)\, S(l)\right] + \Re\left[\overline{H(1)}\, w(1)\right]$$

(2.4.1.3.3)

After following the same approach given in [37] the conditional CHF of (2.4.1.3.3) will be written as-

$$\varphi_{\Re\left[\overline{H(1)}\, Y(1)/H(1)\, \boldsymbol{H}\right]}(\omega) =..$$

$$E[\ exp(j\omega|H(1)|^2\, \Re[S(1)])].\prod_{l=2}^{N} exp\left(j\omega\Re\left[\overline{H(1)}\, H(1)\, S(l)\right]\right).exp\left(\frac{-\omega|H(1)|^2\sigma_R^2}{2}\right)$$

(2.4.1.3.4)

where $\boldsymbol{H} = (H(2)\, H(3)\, \ldots\ldots H(N))^T$. Following the same line of arguments as before, we can rewrite the conditional CHF of the random variable $\Re\left[\overline{H(1)}\, Y(1)/H(1), \boldsymbol{H}\right]$ as-

$$\varphi_{\Re\left[\overline{H(1)}\, Y(1)/H(1)\, \boldsymbol{H}\right]}(\omega) =..$$

$$E[\ exp(j\omega|H(1)|^2\, \Re[S(1)])].\prod_{l=2}^{N} cos\left(\omega\Re\left[\overline{H(1)}\, H(1)\, S(l)\right]\right).exp\left(\frac{-\omega^2|H(1)|^2\sigma_R^2}{2}\right)$$

(2.4.1.3.5)

After further simplification, by using (2.4.1) identity, it can be written as-

$$\varphi_{\Re\left[\overline{H(1)}\, Y(1)/H(1)\, \boldsymbol{H}\right]}(\omega) = [\ exp(j\omega|H(1)|^2\, \Re[S(1)])].exp\left(\frac{-\omega^2|H(1)|^2\sigma_R^2}{2}\right)..$$

$$\ldots E\left(\frac{1}{2^{N-1}}\sum_{l=2}^{2^{N-2}}\left\{\exp\left(j\omega\overline{H(1)}\, H(1)\, S(l)\right) + \exp\left(-j\omega\overline{H(1)}\, H(1)\, S(l)\right)\right\}\right)$$

(2.4.1.3.6)

After some mathematical manipulations, it can be written as-

$$\varphi_{\Re\left[\overline{H(1)}\,Y(1)/H(1)\,\boldsymbol{H}\right]}(\omega) = exp\left(\frac{-\omega^2|H(1)|^2\sigma_R^2}{2}\right)\ldots$$
$$\ldots\frac{1}{2^{N-1}}\left\{\sum_{k=1}^{2^{N-2}} exp\left(j\omega\left(|H(1)|^2\,\Re[S(1)] + \Re\left[\overline{H(1)}\,H(1)S^T e_k\right]\right)\right)\right.$$
$$\left. +exp\left(j\omega\left(|H(1)|^2\,\Re[S(1)] - \Re\left[\overline{H(1)}\,H(1)S^T e_k\right]\right)\right)\right\} \quad (2.4.1.3.7)$$

where e_k being a diagonal matrix with $diag\,(.)$ indicating as diagonal matrix and $\sigma_n^2 = |H(1)|^2\sigma_R^2$. It is obvious that (2.4.1.3.7) represents the CHF of a mixture of Gaussian densities. Now, an error occurs if $\Re\left[\overline{H(1)}\,Y(1)/H(1)\,\boldsymbol{H}\right] \leq 0$. Thus, the conditional BER can be written as-

$$P_{b_{\Re\left[\overline{H(1)}\,Y(1)/H(1)\,\boldsymbol{H}\right]}}(\omega) = \frac{1}{2^{N-1}}\sum_{k=1}^{2^{N-2}} Q\left(\frac{\left(|H(1)|^2\,\Re[S(1)] + \Re\left[\overline{H(1)}\,H(1)S^T e_k\right]\right)}{\sigma_n}\right)\ldots$$
$$+Q\left(\frac{\left(|H(1)|^2\,\Re[S(1)] - \Re\left[\overline{H(1)}\,H(1)S^T e_k\right]\right)}{\sigma_n}\right) \quad (2.4.1.3.8)$$

By following [37], the unconditional BER can be calculated as-

$$P_b(\xi) = \int\int P_b(\xi|H(1),\boldsymbol{H})\; f_{\frac{\boldsymbol{H}}{H(1)}}\left(\frac{\boldsymbol{H}}{H(1)}\right) d\boldsymbol{H}\, f_{H(1)}\big(H(1)\big)dH(1) \quad (2.4.1.3.9)$$

where the conditional density function $f_{\frac{\boldsymbol{H}}{H(1)}}\left(\frac{\boldsymbol{H}}{H(1)}\right)$ is Gaussian with mean $E\,(\boldsymbol{H}|H(1))$ and covariance $C(\boldsymbol{H}|H(1))$ is defined by [37]-

$$E\left(\boldsymbol{H}\middle|H(1)\right) = H(1)C^{-1}_{H(1)H(1)}C_{\boldsymbol{H}H(1)} \quad (2.4.1.3.10a)$$

$$C_{\boldsymbol{H}|H(1)} = C_{\boldsymbol{HH}} - C^{-1}_{(1)H(1)}C_{\boldsymbol{H}H(1)}C^H_{\boldsymbol{H}H(1)} \quad (2.4.1.3.10b)$$

with $E(\cdot)$ and $H(\cdot)$ representing as the statistical expectation and the Hermitian transpose operation respectively. The matrix $C_{\boldsymbol{HH}}$ is obtained from the frequency domain channel covariance matrix defined as- $C = E\{(H(1)\boldsymbol{H}^T)^T\left(\overline{H(1)}\,\boldsymbol{H}^H\right)$ and it can also be written as $C = F_L C_h F_L^H$ where C_h is the time domain channel covariance matrix. The integral form (2.4.1.3.9) involves multidimensional integration. So, the evaluation of the multidimensional integral in (2.4.1.3.9) is an arduous task. Hence, the following alternative formulation was proposed which avoids much of the complexity associated with (2.4.1.3.9).

Let us consider the random variable $b_k = \Re\left[\overline{H(1)} S^T \boldsymbol{H}\right]$, the conditional random variable $b_k|H(1)$ is Gaussian with mean and variance to be determined. Using (2.4.1.3.10), it can be obtained as-

$$E[\, b_k|H(1)] = |H(1)|^2 C^{-1}_{H(1)H(1)} \Re\left[S(k)^T C_{\boldsymbol{H}H(1)}\right] = |H(1)|^2 z_k \tag{2.4.1.3.11}$$

$$var(b_k|H(1)) = \frac{1}{2}|H(1)|^2\, S(k)^T C_{\boldsymbol{H}|H(1)} \overline{S(k)} = \frac{1}{2}\,|H(1)|^2 a_k \tag{2.4.1.3.12}$$

where $b_k = \Re\left[\overline{H(1)}(S_k)^T\, H\right]$, $C_{\boldsymbol{H}H(1)} = E\left[\boldsymbol{H}\,\overline{H(1)}\right]$ and $C_{\boldsymbol{H}H(1)} = \mathcal{F}_L h\, \mathcal{F}_L{}^H = C_{\boldsymbol{HH}} - C^{-1}_{H(1)H(1)} C_{\boldsymbol{H}H(1)}\, C^H_{\boldsymbol{H}H(1)} C_{\boldsymbol{HH}}$. Hence, we can say that $b_k|H(1)$ is a Gaussian random variable with mean and variance given by $|H(1)|^2 a_k$ and $\frac{|H(1)|^2 b_k}{2}$ respectively.

Now, (2.4.1.3.8) can be written as-

$$P_b(\xi|H(1), \boldsymbol{H}) = \frac{1}{2^{N-1}} \sum_{K=1}^{2^{N-2}} Q\left(\frac{|H(1)|^2\, \Re[S(1)] + z_k}{\sigma_n}\right) + Q\left(\frac{|H(1)|^2\, \Re[S(1)] - z_k}{\sigma_n}\right) \tag{2.4.1.3.13}$$

After rearranging the arguments of the Q functions, it can be written as-

$$P_b(\xi|H(1), \boldsymbol{H}) = \frac{1}{2^{N-1}} \sum_{K=1}^{2^{N-2}} Q(\mu_{+k} + \lambda_k y_k) + Q(\mu_{-k} - \lambda_k y_k) \tag{2.4.1.3.14}$$

where $\mu_{+k} = \frac{|H(1)|^2\, \Re[S(1)] + z_k}{\sigma_n}$, $\mu_{-k} = \frac{|H(1)|^2\, \Re[S(1)] - z_k}{\sigma_n}$, $\lambda_k = \sqrt{\frac{b_k}{2\sigma^2}}$ and $y_k = \sqrt{\frac{2}{b_k}}\, \frac{z_k - |H(1)|^2 H(k)}{|H(1)|}$. Furthermore, $y_k|H(1)$ is a Gaussian random variable with zero mean and unit variance. Averaging (2.4.1.3.14) with respect to the conditional Gaussian random variables $y_k|H(1)$, we can written as -

$$P_b(\xi|H(1), \boldsymbol{H}) = \frac{1}{2^{N-1}} \sum_{K=1}^{2^{N-2}} Q\left(\frac{|H(1)|(\,\Re[S(1)] + a_k)}{\sigma\sqrt{1 + \frac{b_k}{2\sigma^2}}}\right) + Q\left(\frac{|H(1)|(\,\Re[S(1)] - a_k)}{\sigma\sqrt{1 + \frac{b_k}{2\sigma^2}}}\right) \tag{2.4.1.3.15}$$

Now, averaging (2.4.1.3.15) over the Rayleigh random variable $|H(1)|$ with pdf $P(|\boldsymbol{H}|) = \frac{|\boldsymbol{H}|}{\sigma_R^2} exp\left(\frac{|\boldsymbol{H}|^2}{2\sigma_R^2}\right)$ the unconditional BER can be obtained as –

$$P_b(\xi) = \frac{1}{2} - \frac{1}{2^N}\sum_{K=1}^{2^{N-2}} \sqrt{\frac{\gamma(\Re[S(1)] + a_k)^2}{1+\gamma\{(\Re[S(1)] + a_k)^2 + b_k\}}} + \sqrt{\frac{\gamma(\Re[S(1)] - a_k)^2}{1+\gamma\{(\Re[S(1)] - a_k)^2 + b_k\}}}$$

(2.4.1.3.16)

where the modified parameters a_k and b_k are given as $a_k = \boldsymbol{S}^T C_{\boldsymbol{HH(1)}}$ and $b_k = (\boldsymbol{S}^T C_{\boldsymbol{HH}} - C_{\boldsymbol{HH(1)}})$ respectively.

However, the BER expression derived in [37] is not correct for all values of CFO for frequency selective channels. This is because the expressions have been derived assuming the argument of Q function in the expressions (34) of [37] to be positive. This is not true for higher values of CFO, leading to a mismatch between the theoretical and actual BER. The same is true also for system model in presence of CFO and STO. So for, an accurate BER considering the argument of Q function is +ive as well as – ive so by following the same derivation approch for + ive argument of Q function as well as − ive argument of Q function. After some mathematical manipulation an exact BER expression is-

$$\mathrm{P_b}(\xi) = \frac{1}{2} - \frac{1}{2^N}\sum_{K=1}^{2^{N-2}} \mathrm{F_1}\sqrt{\frac{\gamma(\Re[S(1)] + a_k)^2}{1+\gamma\{(\Re[S(1)] + a_k)^2 + b_k\}}} + \mathrm{F_2}\sqrt{\frac{\gamma(\Re[S(1)] - a_k)^2}{1+\gamma\{(\Re[S(1)] - a_k)^2 + b_k\}}}$$

(2.4.1.3.17)

where F_1 denotes the $F_1 = sgn([S(1) + a_k])$ and $F_2 = sgn([S(1) - a_k])$

2.4.2. QPSK Modulation

2.4.2.1 AWGN Channel

With loss of generality we consider the first subcarrier with the transmitted symbol $X(1) = 1 + j$ with $X(k) = \{\pm 1 \pm j\}$ and the received signal is written as-

$$Y(1) = X(1)S(1) + \sum_{l=2}^{N} S(l)X(l)$$

(2.4.2.1.1)

The probability of a correct decision is the probability that $Y(1) + W(1)$ lies inside $D1$ (the first quadrant of the complex plane) and it is written as-

$$p\big(Y(1) + w(1) \in D_1 \big| X(1) = 1 + j, Y(k)\big) = Q\left(\frac{-\Re(Y(k))}{\sigma}\right) Q\left(\frac{-\Im(Y(k))}{\sigma}\right)$$

(2.4.2.1.2)

where $\Im(z)$ is the imaginary part of z. The average correct symbol decision probability is obtained by averaging (2.4.2.1.2) over Y for which the required pdf of $Y(1)$ is derived below. Since the variable $Y(1)$ is two dimensional and $X(1) = 1 + j$, its two dimensional CHF can be written as-

$$\varphi(\omega_I, \omega_Q) = exp(j\{\omega_I \Re[S(l)] + \omega_Q \Im[S(l)]\}) \times \prod_{l=2}^{N} \left\{ \begin{matrix} cos(\omega_I \Re[S(l)] + \omega_Q \Im[S(l)]) \\ \times cos(\omega_I \Im[S(l)] - \omega_Q \Re[S(l)]) \end{matrix} \right\}$$

(2.4.2.1.3)

Now, more compact version of (2.4.2.1.3) can be written using the vector notations as-

$$\varphi(\omega_I, \omega_Q) = exp(j\sigma^T\{S_A^1 + S_B^1\}) \times \prod_{l=2}^{N} \{cos(\sigma^T (S_A)^l) \times cos(\sigma^T (S_B)^l)\}$$

(2.4.2.1.4)

where $\sigma = \begin{pmatrix} \omega_I & \omega_Q \end{pmatrix}^T$, $(S_A)^l = (\Re[S(l)] + \Im[S(l)])^T$ and $(S_B)^l = (\Re[S(l)] - \Im[S(l)])^T$ for all $l = 1, 2, \ldots, N$. Then, using (2.4.1) identity the above eq. is written as-

$$\varphi(\omega_I, \omega_Q) = exp(j\sigma^T\{S_A^1 + S_B^1\}) \times \frac{1}{2^{2(N-2)}} \sum_{n=1}^{2^{N-2}} \sum_{k=1}^{2^{N-2}} \{cos(\sigma^T S_A e_k) \times cos(\sigma^T S_B e_n)\}$$

(2.4.2.1.5)

where $S_A = \{(S_A)^2 \ (S_A)^3 \ldots (S_A)^N\}$, $S_B = \{(S_B)^2 \ (S_B)^3 \ldots (S_B)^N\}$, e_k and $\boldsymbol{e}_n$ are column vectors taken from more general matrix E_{N-1}.

By using Euler's relationship with some rearrangements of terms, eq.(2.4.2.1.5) written as-

$$\varphi(\omega_I, \omega_Q) = exp(j\sigma^T\{S_A^1 + S_B^1\}) \times \frac{1}{2^{2(N-2)}} \sum_{n=1}^{2^{N-2}} \sum_{k=1}^{2^{N-2}} \left\{ \begin{matrix} e^{-j\sigma^T S_A e_k} + e^{j\sigma^T S_A e_k} \\ + e^{-j\sigma^T S_B e_n} + e^{j\sigma^T S_B e_n} \end{matrix} \right\}$$

(2.4.2.1.6)

After further simplification the above eq. written as-

$$\varphi(\omega_I, \omega_Q) = \frac{1}{2^{2(N-2)}} \sum_{n=1}^{2^{N-2}} \sum_{k=1}^{2^{N-2}} \{e^{j\sigma^T G_1} + e^{j\sigma^T G_2} + e^{j\sigma^T G_3} + e^{j\sigma^T G_4}\}$$

(2.4.2.1.7)

where $G1 = (S_A)^1 - (S_B)^1 + S_A e_k + S_B e_n$, $G2 = (S_A)^1 - (S_B)^1 + sS_A e_k - S_B e_n$

$G3 = (S_A)^1 - (S_B)^1 - S_A e_k + S_B e_n$ and $G4 = (S_A)^1 - (S_B)^1 - S_A e_k - S_B e_n$

The Fourier transform of (2.4.2.1.7) will gives the two dimensional probability density functions written as-

$$P\big(\Re(u),\Im(u)\big)=\frac{1}{2^{2(N-2)}}\sum_{n=1}^{2^{N-2}}\sum_{k=1}^{2^{N-2}}\sum_{m=1}^{4}\{\delta(\Re[Y]-\psi_{\mathrm{kn}}[1,m])\delta(\Re[Y]-\psi_{\mathrm{kn}}[2,m])\}$$

(2.4.2.1.8)

where $\psi_{kn}[p,q]$ is the $(p,q)^{th}$ element of the 2×4 matrix Ψ defined as $\Psi=(G1\ \ G2\ \ G3\ \ G4)$ and $\delta(x)$ is the Dirac delta function.

Averaging (2.4.2.1.8) with respect to the pdf given in (2.4.2.1.2) yields the SER expression written as-

$$P_b(\xi)=1-\frac{1}{2^{2(N-1)}}\sum_{n=1}^{2^{N-2}}\sum_{k=1}^{2^{N-2}}\sum_{m=1}^{4}\{Q\big(-\sqrt{2\gamma}\,\psi_{\mathrm{kn}}[1,m]\big)Q\big(-\sqrt{2\gamma}\,\psi_{\mathrm{kn}}[2,m]\big)\}$$

(2.4.2.1.9)

where $\gamma=\frac{E_b}{N_0}=\frac{1}{2}\frac{E_s}{N_0}$, $Q(x)$ is the Gaussian Q function. One should note that in our case of interest $E_b=1$ and $\sigma_s^2=N_0/2$ with N_0 being the noise power spectral density.

2.4.2.2 Rayleigh Flat Fading Channel

The conditional symbol error rate expression written as-

$$P_b(\xi||H|)=1-\frac{1}{2^{2(N-1)}}\sum_{n=1}^{2^{N-2}}\sum_{k=1}^{2^{N-2}}\sum_{m=1}^{4}\{Q\big(-\sqrt{2\gamma}\,\psi_{\mathrm{kn}}[1,m]\,|H|\big)Q\big(-\sqrt{2\gamma}\,\psi_{\mathrm{kn}}[2,m]\big)|H|\}$$

(2.4.2.2.1)

where $|H|$ is Rayleigh distributed random variable. Now, for finding the unconditional bit error rate, the evaluation of integral will be encountered. After averaging (2.4.2.2.1), it can be solved using [38,eq. 4.8], [38,eq. 5.102] and [38,eq. 5.6] to give the SER.

$$\begin{aligned}P_b(\xi)=\frac{3}{4}-\frac{1}{2^{(N-1)}}\sum_{n=1}^{2^{N-2}}\sum_{k=1}^{2^{N-2}}\sum_{m=1}^{4}\sqrt{\frac{2\sigma_r^2\psi_{kn}^2[1,m]\,\gamma}{1+2\sigma_r^2\psi_{kn}^2[1,m]\,\gamma}}\ \cdot\cdot\\ \times\left(1-\frac{1}{\pi}arctan\left\{\frac{\psi_{\mathrm{kn}}[1,m]}{\psi_{\mathrm{kn}}[2,m]}\sqrt{1+\frac{1}{2\sigma_r^2\psi_{kn}^2[1,m]\,\gamma}}\right\}\right)\\ +\sqrt{\frac{2\sigma_r^2\psi_{kn}^2[2,m]\,\gamma}{1+2\sigma_r^2\psi_{kn}^2[2,m]\,\gamma}}\left(1-\frac{1}{\pi}arctan\left\{\frac{\psi_{\mathrm{kn}}[2,m]}{\psi_{\mathrm{kn}}[1,m]}\sqrt{1+\frac{1}{2\sigma_r^2\psi_{kn}^2[2,m]\,\gamma}}\right\}\right)\end{aligned}$$

(2.4.2.2.2)

However, the analytical SER expression given in the (2.4.2.2.2) is not correct for all value of CFO because the expressions have been derived in eq.(20) of [37] assuming the argument of Q function positive. This is not true for higher values of CFO, leading to a mismatch between the theoretical and actual SER. So for, an accurate SER expression, considering the argument of Q function is +ive as well as – ive so by following the same derivation approch for + ive argument of Q function as well as- ive argument of Q function.

After some mathematical manipulation an exact SER expression written as-

$$P_b(\xi) = \frac{3}{4} - \frac{1}{2^{(N-1)}} \sum_{n=1}^{2^{N-2}} \sum_{k=1}^{2^{N-2}} \sum_{m=1}^{4} sgn\left(\frac{\psi_{\mathrm{kn}}[1,m]}{\psi_{\mathrm{kn}}[2,m]}\right) \sqrt{\frac{2\sigma_r^2\psi_{kn}^2[1,m]\,\gamma}{1+2\sigma_r^2\psi_{kn}^2[1,m]\,\gamma}} \,..$$
$$\times\left(1-\frac{1}{\pi}arctan\left\{\frac{\psi_{\mathrm{kn}}[1,m]}{\psi_{\mathrm{kn}}[2,m]}\sqrt{1+\frac{1}{2\sigma_r^2\psi_{kn}^2[1,m]\,\gamma}}\right\}\right) + sgn\left(\frac{\psi_{\mathrm{kn}}[2,m]}{\psi_{\mathrm{kn}}[2,m]}\right)...$$
$$..\sqrt{\frac{2\sigma_r^2\psi_{kn}^2[2,m]\,\gamma}{1+2\sigma_r^2\psi_{kn}^2[2,m]\,\gamma}}\left(1-\frac{1}{\pi}arctan\left\{\frac{\psi_{\mathrm{kn}}[2,m]}{\psi_{\mathrm{kn}}[1,m]}\sqrt{1+\frac{1}{2\sigma_r^2\psi_{kn}^2[2,m]\,\gamma}}\right\}\right) \quad (2.4.2.2.3)$$

2.4.2.3 Rayleigh Frequency Selective Fading Channel

After the $\boldsymbol{N}$-point FFT at the receiver, the signal observed on the $\boldsymbol{k^{th}}$ sub-carrier in the presence of CFO and STO can be expressed as-

$$\boldsymbol{Y(k) = \underbrace{X(k)H(k)S(k) + \sum_{l=0,\ l\neq k}^{N-1} X(l)H(l)S(l-k+1))}_{R(l)} + w(k)} \quad (2.4.2.3.1)$$

where $X(k)$ is the symbol transmitted over the k^{th} sub-carrier, $S(k)$ is the inter-carrier interference (ICI) coefficient, $w(k)$ is the additive white Gaussian noise (AWGN) with variance $\sigma^2 = N_o/2$ and $H(\mathrm{k})$ is the channel frequency response for the $(k+1)^{th}$ sub-carrier. By adopting a matrix notation, let $h = [h_1, h_2 \ldots, h_L]^T$ be the $L\times1$ vector of time-domain channel coefficients, where $(\cdot)^{\mathrm{T}}$ denotes the transpose operation. The vector containing the coefficients of frequency-domain channel for all the sub-carriers can be expressed as $[H(1), H(2), \ldots, H(\mathrm{N})]^{\mathrm{T}} = \mathcal{F}_{\mathrm{L}}\mathrm{h}$, where $\mathcal{F}_{\mathrm{L}}$ is the $N\times L$ matrix obtained by taking

the first columns of $N \times N$ FFT matrix given is equation (2.3.3.7). Considering QPSK modulation, where symbols are drawn from the set $\{\pm 1 \pm j\}$, as in [37] we assume that symbol $X(1) = 1 + j$ is transmitted on the first subcarrier. The equalized signal on the first sub-carrier is-

$$\bar{H}(1)\,Y(1) = |H(1)|^2 X(1)S(1) + \sum_{l=2}^{N} \bar{H}(1)H(l)X(l)S(l) + \bar{H}(1)w(1) \tag{2.4.2.3.2}$$

where $\bar{H}(1)$ is the complex conjugate of $H(1)$, The probability of making a correct decision is given by the probability that $\bar{H}(1)\,Y(1) = \bar{H}(1)\,R(1) + \bar{H}(1)\,w(1)$ lies inside the first quadrant D_1 of the complex plan. The probability of making a correct decision conditioned to transmission of symbol $1 + j$ on the first subcarrier is given by-

$$P_c\big(\bar{H}(1)\,Y(1) \in D_1 \,|X(1) = 1 + j, \bar{H}(1)\,R(1)\big) = Q\left(-\frac{\Re[\bar{H}(1)\,R(1)]}{\sigma_H}\right) Q\left(-\frac{\Im[\bar{H}(1)\,R(1)]}{\sigma_H}\right) \tag{2.4.2.3.3}$$

where $\Re[c]$ and $\Im[c]$ denotes the real and the imaginary part of complex number c respectively, and $\sigma_H = |H(1)|\,\sigma$. The conditional probability of correct decision is obtained by averaging (2.4.2.3.3) over the probability density function (PDF) of $\bar{H}(1)R(1)$ which is obtained from the characteristic functions (CHF) as reported in what follows. Since $\bar{H}(1)R(1)$ is a complex random variable its CHF is two-dimensional (2-D) and, as shown in [53], it is given by-

$$\begin{aligned}\varphi(\omega_I, \omega_Q) = {} & e^{j|H(0)|^2\left(\omega_I(\Re[S(1)]-\Im[S(1)])+\omega_Q\,(\Im[S(1)]+\Re[S(1)])\right)} \dots \\ & \times \prod_{l=2}^{N} cos\big(\omega_I \Re[\bar{H}(1)H(1)S(l)] + \omega_Q \Im[\bar{H}(1)H(1)S(l)]\big) \\ & \times cos\big(\omega_I \Im[\bar{H}(1)H(1)S(l)] - \omega_Q \Re[\bar{H}(1)H(1)S(l)]\big)\end{aligned} \tag{2.4.2.3.4}$$

where $\boldsymbol{H} = \big(H(2), \dots, H(N)\big)^T$. Following the mathematical derivation reported in [53], the 2-D PDF resulting from the inverse Fourier transform of (2.4.2.3.4) can be written as-

$$\begin{aligned}p(\Re[\bar{H}(1)R(1)], \Im[\bar{H}(1)H(1)]) = {} & \frac{1}{2^{2N-2}} \times \\ & \sum_{k=1}^{2^{N-2}} \sum_{n=1}^{2^{N-2}} \sum_{m=1}^{4} \delta\big[\Re\big(\bar{H}(1)R(1)\big) - \big(|H(1)|^2 D_A + \gamma_{k,n}[1,m]\big)\big] \dots \\ & \times \delta\big[\Im\big(\bar{H}(1)R(1)\big) - \big(|H(1)|^2 D_B + \gamma_{k,n}[2,m]\big)\big]\end{aligned} \tag{2.4.2.3.5}$$

where $\delta[.]$ is the Dirac delta function, $D_A = \Re[S(1)] - \Im[S(1)]$, $D_B = \Re[[S(1)]] + \Im[[S(1)]]$ and $\gamma_{k,n}[p,q]$ is the (p,q) entry of the 2×4 matrix of Γ defined as $\Gamma = \left((\Gamma_A + \Gamma_B)\ (-\Gamma_A - \Gamma_B)\ (\Gamma_A - \Gamma_B)\ (-\Gamma_A + \Gamma_B)\right)$ with matrices-

$$\Gamma_A = \left[\Re[\bar{H}(1)e_k^T \Lambda\beta] \quad \Im[\bar{H}(1)e_n^T \Lambda\beta]\right]^T,$$

$$\Gamma_B = \left[\Im[\bar{H}(1)e_k^T \Lambda\beta] \quad -\Re[\bar{H}(1)e_n^T \Lambda\beta]\right]^T,$$

where $\Lambda = \mathrm{diag}\left(S(2), S(3), \ldots, S(N)\right)$ and zeros are replaced with -1s. The analytical expression of the probability of symbol error given $(H(0), \mathbf{H})$ can be obtained by subtracting (2.4.2.3.5) to 1 and averaging over (2.4.2.3.3) as-

$$P_s(\xi|H(1),\mathbf{H}) = 1 - \frac{1}{2^{2N-2}} \sum_{k=1}^{2^{N-2}} \sum_{n=1}^{2^{N-2}} \sum_{m=1}^{4} Q\left\{\frac{-\left(|H(1)|^2 S_A + \gamma_{k,n}[1,m]\right)}{\sigma_H}\right\} \ldots$$

$$\times Q\left\{\frac{-\left(|H(1)|^2 S_B + \gamma_{k,n}[2,m]\right)}{\sigma_H}\right\} \quad (2.4.2.3.6)$$

The probability of symbol error can be calculated from the integral-

$$P_s(\xi) = \int_{H(1)} P_s\left(\xi|H(1)\right) p_{H(1)}\left(H(1)\right) dH(1) \quad (2.4.2.3.7)$$

where $p_{H(1)}(H(1))$ is the probability density function of the Rayleigh distribution and

$$P_s\left(\xi|H(1)\right) = 1 - \frac{1}{2^{2N-2}} \sum_{k=1}^{2^{N-2}} \sum_{n=1}^{2^{N-2}} \sum_{m=1}^{4} Q\left\{\frac{-\left(|H(1)|\, S_A + \vartheta_{k,n}[1,m]\right)}{\sigma\sqrt{1 + \frac{v_{k,n}[m]}{2\sigma^2}}}\right\} \ldots$$

$$\times Q\left\{\frac{-\left(|H(1)|\, S_B + \vartheta_{k,n}[2,m]\right)}{\sigma\sqrt{1 + \frac{v_{k,n}[m]}{2\sigma^2}}}\right\} \quad (2.4.2.3.8)$$

By following the same approach reported in [53], the conditional probability of symbol error $P_s\left(\xi|H(1)\right)$ in (2.4.2.3.8) has been evaluated using the mean $|H(1)|^2\vartheta_{k,n}[i,m]$ and the variance $|H(1)|^2 v_{k,n}[m]/2$ of the conditional Gaussian random variable $\gamma_{k,n}[i,m]|H(1)$.

The term $\vartheta_{k,n}[i,m]$ is the entry (i,m) of the 2×4 matrix $W = \left((W_A + W_B)\ (-W_A - W_B)\ (W_A - W_B)\ (-W_A + W_B)\right)$ with

$$W_A = C^{-1}_{H(1)H(1)} \left[\Re\left[e_k^T \Lambda C_{\mathbf{H}H(1)}\right] \quad \Im\left[e_k^T \Lambda C_{\mathbf{H}H(1)}\right]\right]^T,$$

$$W_B = C^{-1}_{H(1)H(1)} \left[\Im\left[e_n^T \Lambda C_{\mathbf{H}H(1)}\right] \quad -\Re\left[e_n^T \Lambda C_{\mathbf{H}H(1)}\right]\right]^T,$$

where $\boldsymbol{C}_{\mathbf{H}H(1)}$ is the channel autocovariance matrix given in [53]. The term $v_{k,n}[m]$ is the m-th element of the 1×4 vector $\mathbf{v} = (v_1\ v_2\ v_3\ v_4)$, where $v_i = \boldsymbol{\xi}_i^T \boldsymbol{\Lambda} \boldsymbol{C}_{\mathbf{H}H(1)} \boldsymbol{\Lambda} \boldsymbol{\xi}_i$, $\boldsymbol{\xi}_1 = \mathbf{e}_k + \mathbf{e}_k$, $\boldsymbol{\xi}_2 = -\mathbf{e}_k - \mathbf{e}_k$, $\boldsymbol{\xi}_3 = \mathbf{e}_k - \mathbf{e}_k$, $\boldsymbol{\xi}_4 = -\mathbf{e}_k + \mathbf{e}_k$. The probability of symbol error for QPSK resulting from computation of (2.4.2.3.7) is-

$$P_s(\xi) = \frac{3}{4} - \frac{1}{2^{2N-1}} \sum_{k=1}^{2^{N-2}} \sum_{n=1}^{2^{N-2}} \sum_{m=1}^{4} \sqrt{\frac{C_{H(1)H(1)}\,\rho}{2 + \rho v_{k,n}[m] + C_{H(1)H(1)}\,\rho \psi^2{}_{k,n}[1,m]}} \cdots$$
$$\psi_{k,n}[1,m] \left(\frac{1}{2} + \frac{1}{\pi} \operatorname{atan} \left\{ \sqrt{\frac{C_{H(1)H(1)}\,\rho}{2 + \rho \varphi_{k,n}[m] + C_{H(1)H(1)}\,\rho \psi^2{}_{k,n}[1,m]}}\ \psi_{k,n}[2,m] \right\} \right)$$
$$+ \sqrt{\frac{C_{H(1)H(1)}\,\rho}{2 + \rho v_{k,n}[m] + C_{H(1)H(1)}\,\rho \psi^2{}_{k,n}[2,m]}} \cdots$$
$$\psi_{k,n}[2,m] \left(\frac{1}{2} + \frac{1}{\pi} \operatorname{atan} \left\{ \sqrt{\frac{C_{H(1)H(1)}\,\rho}{2 + \rho v_{k,n}[m] + C_{H(1)H(1)}\,\rho \psi^2{}_{k,n}[2,m]}}\ \psi_{k,n}[1,m] \right\} \right) \tag{2.4.2.3.9}$$

where $\rho = E_s/N_0$ is the signal-to-noise ratio and $\psi_{k,n}[i,m]$ is the $(i,m)^{th}$ entry of the 2×4 matrix $\boldsymbol{\Psi} = \mathbf{D} \otimes \mathbf{1}_{1\times4} + \mathbf{W}$, in which $\otimes$ is the Kronecker product and $\mathbf{1}_{1\times4}$ is a 1×4 vectors of 1s, and $D = \left(D_A \quad D_B\right)^T$. $C_{H(1)H(1)} = 2\sigma^2$ in (2.4.2.3.9) we get the probability of symbol error expression of QPSK for conventional OFDM system given by eq. (16) of [53].

In case of flat fading channel, the coefficients $H(k)$ is a constant value $H(1)$ with $\sigma_R^2 = 0.5$ and C is a matrix of all ones. As a result, $v_{k,n}[m] = 0$ for all values ofs m and the coefficients represented as-

$$W_A = C^{-1}_{H(1)H(1)} \left[\Re\left[e_k^T \Lambda 1_{N-1}\right] \quad \Im\left[e_k^T \Lambda 1_{N-1}\right]\right]^T,$$
$$W_B = C^{-1}_{H(1)H(1)} \left[\Im\left[e_n^T \Lambda 1_{N-1}\right] \quad -\Re\left[e_n^T \Lambda 1_{N-1}\right]\right]^T,$$

After substituting the above value, the performance in Rayleigh flat fading channel can be written as-

$$P_s(\xi) = \frac{3}{4} - \frac{1}{2^{2N-1}} \sum_{k=1}^{2^{N-2}} \sum_{n=1}^{2^{N-2}} \sum_{m=1}^{4} \sqrt{\frac{C_{H(1)H(1)}\,\rho}{2 + C_{H(1)H(1)}\,\rho\psi^2{}_{k,n}[1,m]}} \cdots$$
$$\psi_{k,n}[1,m]\left(\frac{1}{2} + \frac{1}{\pi}\,\mathrm{atan}\left\{\sqrt{\frac{C_{H(1)H(1)}\,\rho}{2 + C_{H(1)H(1)}\,\rho\psi^2{}_{k,n}[1,m]}}\;\psi_{k,n}[2,m]\right\}\right)$$
$$+ \sqrt{\frac{C_{H(1)H(1)}\,\rho}{2 + C_{H(1)H(1)}\,\rho\psi^2{}_{k,n}[2,m]}} \cdots$$
$$\psi_{k,n}[2,m]\left(\frac{1}{2} + \frac{1}{\pi}\,\mathrm{atan}\left\{\sqrt{\frac{C_{H(1)H(1)}\,\rho}{2 + C_{H(1)H(1)}\,\rho\psi^2{}_{k,n}[2,m]}}\;\psi_{k,n}[1,m]\right\}\right) \quad (2.4.2.3.10)$$

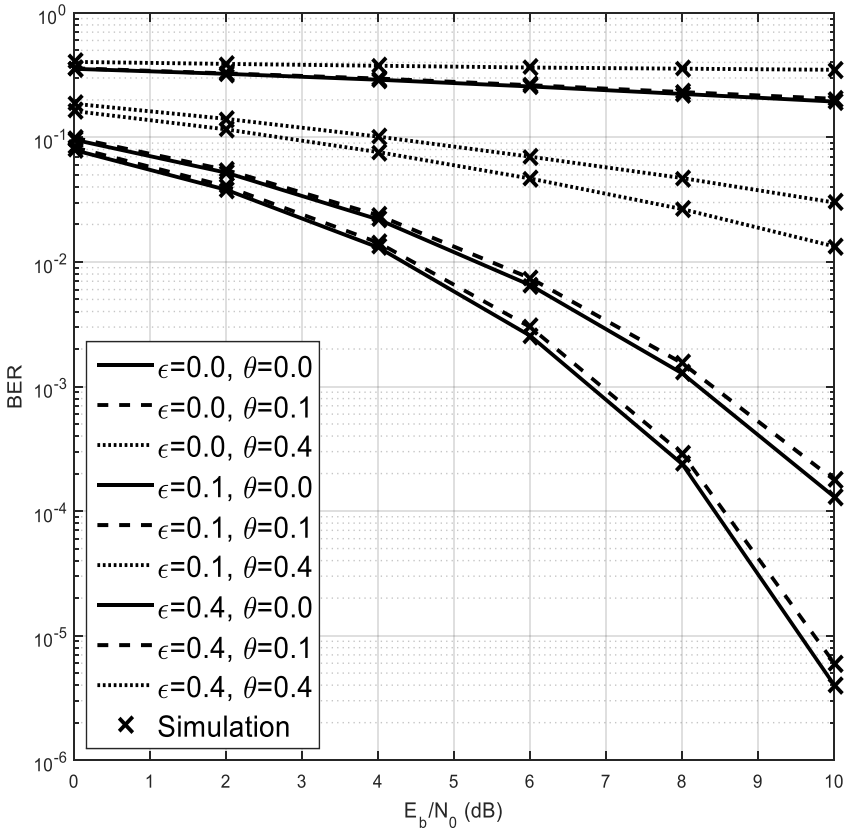

Fig. 2.4.1.1 BER expression of FFT based- OFDM system in presence of CFO and STO for BPSK in AWGN channel with $N = 16$.

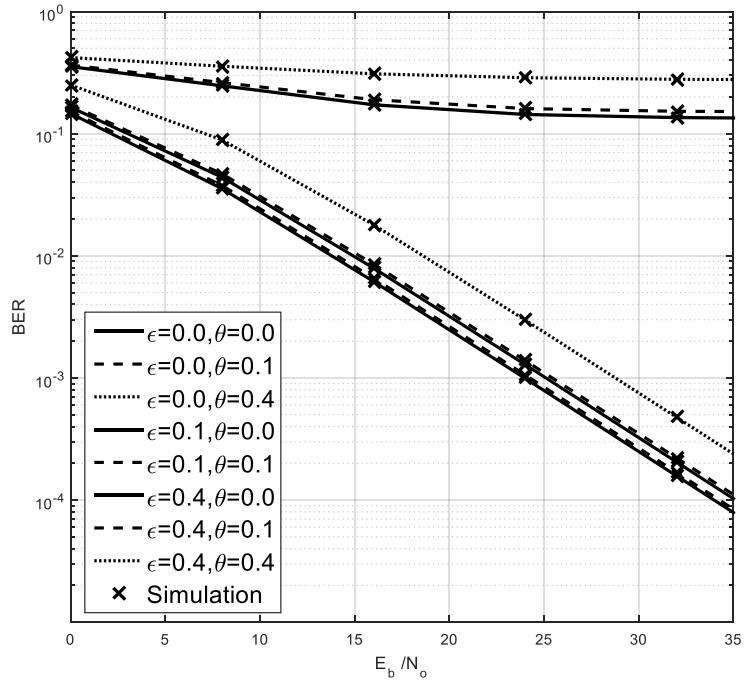

Fig. 2.4.1.2 BER expression of FFT based-OFDM system in presence of CFO and STO for BPSK in Flat fading channel with $N = 16$.

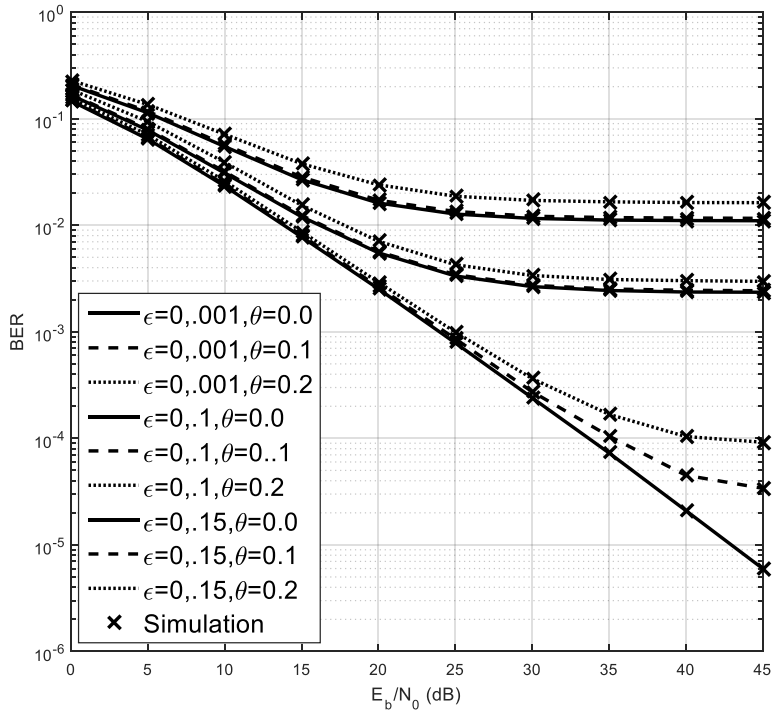

Fig. 2.4.1.3 BER expression of FFT based- OFDM system in presence of CFO and STO for BPSK in Frequency selective fading channel with $N = 16$ and $L = 2$.

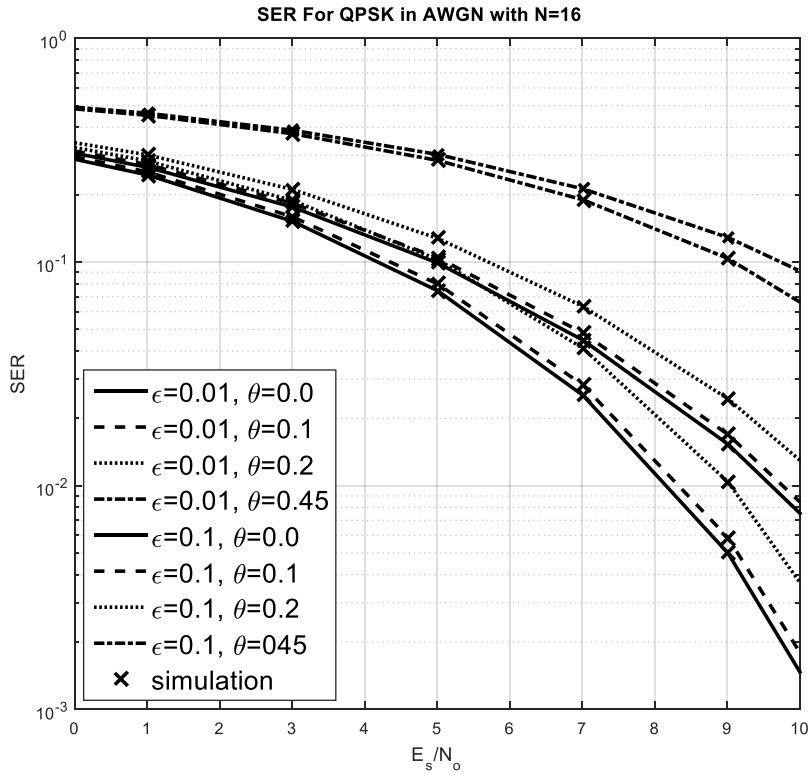

Fig. 2.4.2.1 SER expression of FFT based- OFDM system in presence of CFO and STO for QPSK in AWGN channel with $N = 16$.

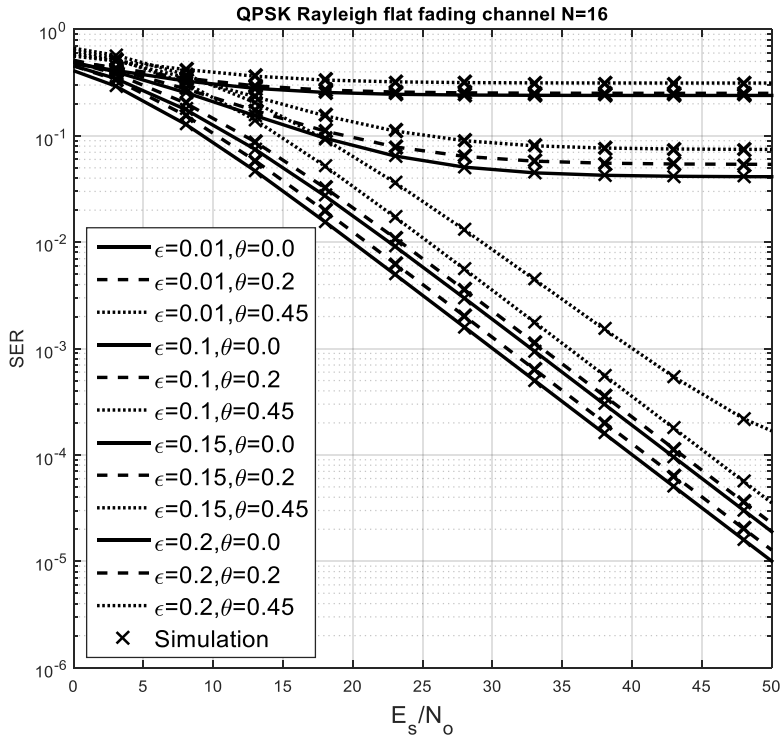

Fig. 2.4.2.2 SER expression of FFT based- OFDM system in presence of CFO and STO for QPSK in Flat fading channel with $N = 16$.

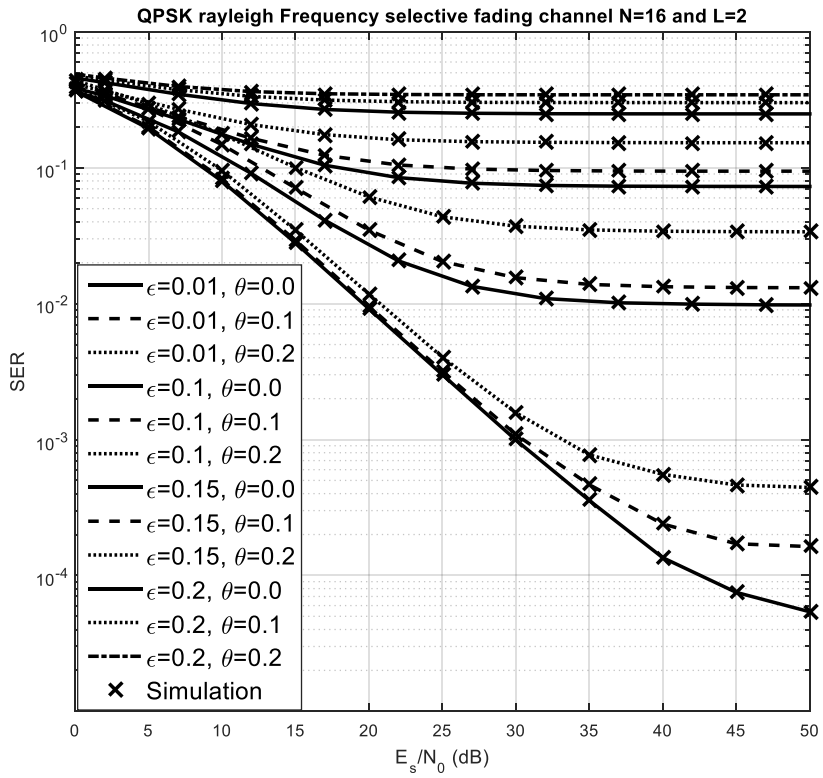

Fig.2.4.2.3 SER expression of FFT -based OFDM system in presence of CFO and STO for QPSK in frequency selective fading channel with $N = 16$ and $L = 2$

2.5. DISCUSSION OF SIMULATED RESULTS

Fig. 2.4.1.1 presents BER of an FFT -based OFDM system in presence of CFO and STO with N = 16 for BPSK modulation schemes over AWGN channel. The simulation results agree with our analytical results in (2.4.1.1.5). The BER performance of an FFT -based OFDM system with BPSK modulation scheme and N = 16 over Rayleigh flat fading channel is shown in **Fig. 2.4.1.2**. The accuracy of the newly derived BER expressions in (2.4.1.2.5) for BPSK modulation is thus verified by the simulation results. Careful inspection of the BER formulas reveals that the computational complexity increases exponentially with the number of subcarriers. **Fig. 2.4.1.3** shows the BER performance of an FFT -based OFDM system in presence of CFO and STO with $N = 16$ subcarriers and number of multipath $L = 2$ for BPSK modulation schemes over frequency selective Rayleigh fading channel, where the analytical results given with different value of CFO and STO in (2.4.1.3.17) is perfectly match with simulation result. **Fig. 2.4.2.1** presents the SER performance of an FFT -based OFDM system in presence of CFO and STO with N =16 subcarriers for QPSK modulation

scheme over the AWGN channel with different value of CFO and STO. where the analytical results given with different value of CFO and STO in (2.4.2.1.9) is perfectly match with simulation results. **Fig. 2.4.2.2** shows the analytical SER results for the frequency flat Rayleigh fading channel for QPSK modulation scheme in presence of different values of CFO and STO. where the analytical results given with different value of CFO and STO in (2.4.2.2.3) is perfectly match with simulation result. **Fig. 2.4.2.3** shows the analytical SER results for the frequency selective Rayleigh fading channel with $N = 16$ and $L = 2$ for QPSK modulation scheme in presence of CFO and STO. where the analytical results given with different values of CFO and STO in (2.4.2.3.10) is perfectly match with simulation result.

2.6. SUMMARY OF BER EXPRESSION FOR FFT -BASED OFDM

❖ ***Expressions of BER in presence of CFO given by Dharmawansa*** *et al.* [37]:

Analytically validated results of probability of symbol error rate of BPSK and QPSK over AWGN channel, flat fading channel and frequency selective fading channel with different values of CFO with $N = 8$, $\sigma_r^2 = 0.5$, $\gamma = E_b/N_o$, $Q(x)$ is the Gaussian Q-function. In this case, $E_b = 1$ *and* ${\sigma_s}^2 = N_0/2$ is assumed with N_0 as noise power spectral density.

2.6.1. In AWGN Channel

2.6.1.1 BPSK modulation:

$$P_b = \frac{1}{2^{N-1}} \sum_{k=1}^{2^{N-1}} Q\left(\sqrt{2\gamma}\,\theta_k\right) + Q\left(\sqrt{2\gamma}\,\beta_k\right) \tag{2.6.1.1.1}$$

where $S = (S_2, S_3, \ldots\ldots\ldots, S_N)^T$, $\theta_k = (S_1 + S^T e_k)$, $\beta_k = (S_1 - S^T e_k)$ and e_k is k^{th} column of $\mathrm{E_{N-1}}$ matrix dimension of (N-1) $\times 2^{\mathrm{N-2}}$ [37].

2.6.1.2 QPSK modulation:

$$P_b(\varepsilon) = 1 - \frac{1}{2^{2N-2}} \sum_{k=1}^{2^{N-2}} \sum_{n=1}^{2^{N-2}} \sum_{m=1}^{4} \left\{Q\left(-\sqrt{2\gamma}\ \Psi_{kn}[1,m]\right) \times Q\left(-\sqrt{2\gamma}\ \Psi_{kn}[1,m]\right)\right\} \tag{2.6.1.2.1}$$

where $\Psi_{kn}[\mathrm{p,q}]$ is the $(p,q)^{th}$ element of the 2×4 matrix of Ψ is defined as $\Psi = (G1\ G2\ G3\ G4)$ and $\delta(x)$ the Dirac delta function and G1, G2, G3 and G4 [37]. The other parameters used in eq.(2.6.1.2.1) are given in [37].

2.6.2. In Flat Fading channel

2.6.2.1 BPSK modulation:

$$P_b(\varepsilon) = \frac{1}{2} - \frac{1}{2^N}\sum_{k=1}^{2^{N-2}}\left\{\sqrt{\frac{2\gamma\theta_k^2\ \sigma_r^2}{1+2\gamma\theta_k^2\ \sigma_r^2}} + \sqrt{\frac{2\gamma\beta_k^2\ \sigma_r^2}{1+2\gamma\beta_k^2\ \sigma_r^2}}\right\} \tag{2.6.2.1.1}$$

The parameter which is used in eq.(2.6.2.1.1) is given in [37].

2.6.2.2 QPSK modulation:

$$P_b(\varepsilon) = \frac{1}{2} - \frac{1}{2^{N-1}}$$

$$\times \sum_{k=1}^{2^{N-2}}\sum_{n=1}^{2^{N-2}}\sum_{m=1}^{4}\left\{\begin{array}{l}\sqrt{\frac{2\gamma{\Psi_{kn}}^2[1,m]\sigma_r^2}{1+2\gamma{\Psi_{kn}}^2[1,m]\sigma_r^2}}\left(1-\frac{1}{\pi}\arctan\left(\frac{\Psi_{\mathrm{kn}}[1,m]}{\Psi_{\mathrm{kn}}[2,m]}\sqrt{1+\frac{1}{2\gamma{\Psi_{kn}}^2[1,m]\sigma_r^2}}\right)\right)\\ +\sqrt{\frac{2\gamma{\Psi_{kn}}^2[2,m]\sigma_r^2}{1+2\gamma{\Psi_{kn}}^2[2,m]\sigma_r^2}}\left(1-\frac{1}{\pi}\arctan\left(\frac{\Psi_{\mathrm{kn}}[2,m]}{\Psi_{\mathrm{kn}}[1,m]}\sqrt{1+\frac{1}{2\gamma{\Psi_{kn}}^2[2,m]\sigma_r^2}}\right)\right)\end{array}\right\} \tag{2.6.2.1.2}$$

The parameters used in eq. (2.6.2.1.2) are given in [37].

2.6.3. In Frequency Selective Fading channel

2.6.3.1 BPSK modulation:

$$P_b(\varepsilon) = \frac{1}{2} - \frac{1}{2^{N-1}}\sum_{k=1}^{2^{N-2}}\left\{\sqrt{\frac{\gamma[\Re(S_1+a_k)]^2}{1+\gamma([\Re(S_1+a_k)]^2+b_k)}} + \sqrt{\frac{\gamma[\Re(S_1-a_k)]^2}{1+\gamma([\Re(S_1-a_k)]^2+b_k)}}\right\} \tag{2.6.3.1}$$

where $a_k = \boldsymbol{S}^T C_{\boldsymbol{HH(1)}}$ and $b_k = (\boldsymbol{S}^T C_{\boldsymbol{HH}} - C_{\boldsymbol{HH(1)}})$ respectively. The other parameters used in eq. (2.6.3.1) are given in [37].

❖ ***Expressions of BER in presence of CFO given by A. K. Chaturvedi*** *et al.* [39]:

2.6.4. BPSK in Rayleigh flat fading channel

$$P_e = \frac{1}{2} - \frac{1}{2^N}\sum_{k=1}^{2^{N-2}} sgn(\theta_l)\left\{\sqrt{\frac{2\gamma\theta_l^2\ \sigma_r^2}{1+2\gamma\theta_l^2\ \sigma_r^2}} + sgn(\beta_l)\sqrt{\frac{2\gamma\beta_l^2\ \sigma_r^2}{1+2\gamma\beta_l^2\ \sigma_r^2}}\right\} \tag{2.6.4.1}$$

The parameters used in eq. (2.6.4.1) are given in [39].

2.6.5. BPSK in frequency selective fading channel:

$$P_b(\varepsilon) = \frac{1}{2} - \frac{1}{2^{N-1}} \sum_{k=1}^{2^{N-2}} \left\{ F_1 \sqrt{\frac{\gamma[\Re(S_1 + a_k)]^2}{1 + \gamma([\Re(S_1 + a_k)]^2 + b_k)}} + F_2 \sqrt{\frac{\gamma[\Re(S_1 - a_k)]^2}{1 + \gamma([\Re(S_1 - a_k)]^2 + b_k)}} \right\} \tag{2.6.5.1}$$

where $F_1 = sgn([S(1) + a_k])$ and $F_2 = sgn([S(1) - a_k])$. The parameters used in eq.(2.6.5.1) are given in [39].

❖ ***Expressions of SER in presence of CFO given by A. Hamza*** *et al.* [53]:

2.6.6. QPSK in frequency selective fading channel

$$P_s(\xi) = \frac{3}{4} - \frac{1}{2^{2N-1}} \sum_{k=1}^{2^{N-2}} \sum_{n=1}^{2^{N-2}} \sum_{m=1}^{4} \sqrt{\frac{C_{\beta(0)\beta(0)}\,\rho}{2 + \rho v_{k,n}[m] + C_{\beta(0)\beta(0)}\,\rho \psi^2{}_{k,n}[1,m]}} \cdots$$

$$\psi_{k,n}[1,m] \left(\frac{1}{2} + \frac{1}{\pi} \operatorname{atan} \left\{ \sqrt{\frac{C_{\beta(0)\beta(0)}\,\rho}{2 + \rho \varphi_{k,n}[m] + C_{\beta(0)\beta(0)}\,\rho \psi^2{}_{k,n}[1,m]}} \; \psi_{k,n}[2,m] \right\} \right)$$

$$+ \sqrt{\frac{C_{\beta(0)\beta(0)}\,\rho}{2 + \rho v_{k,n}[m] + C_{\beta(0)\beta(0)}\,\rho \psi^2{}_{k,n}[2,m]}} \cdots$$

$$\psi_{k,n}[2,m] \left(\frac{1}{2} + \frac{1}{\pi} \operatorname{atan} \left\{ \sqrt{\frac{C_{\beta(0)\beta(0)}\,\rho}{2 + \rho v_{k,n}[m] + C_{\beta(0)\beta(0)}\,\rho \psi^2{}_{k,n}[2,m]}} \; \psi_{k,n}[1,m] \right\} \right)$$

(2.6.6.1)

where $\rho = E_s/N_0$ is the signal-to-noise ratio and $\psi_{k,n}[i,m]$ is the $(i,m)^{th}$ entry of the 2×4 matrix $\boldsymbol{\Psi} = \mathbf{D} \otimes \mathbf{1}_{1\times 4} + \mathbf{W}$, in which $\otimes$ is the Kronecker product and $\mathbf{1}_{1\times 4}$ is a 1×4 vectors of 1s, and $\mathrm{D} = \begin{pmatrix} \mathrm{D_A} & \mathrm{D_B} \end{pmatrix}^{\mathrm{T}}$. The term $\mathrm{v_{k,n}[m]}$ is the m-th element of the 1×4 vector $v = (v_1\ v_2\ v_3\ v_4)$, where $v_i = \xi_i^T \Lambda C_{\beta|\beta(0)} \Lambda \xi_i$, $\xi_1 = e_k + e_k$, $\xi_2 = -e_k - e_k$, $\xi_3 = e_k - e_k$, $\xi_4 = -e_k + e_k$ *and* $C_{\beta(0)\beta(0)} = 2\sigma^2$. The other parameters used in eq.(2.6.6.1) are given in [52].

2.6.7. QPSK in Flat fading channel

$$P_s(\xi) = \frac{3}{4} - \frac{1}{2^{2N-1}} \sum_{k=1}^{2^{N-2}} \sum_{n=1}^{2^{N-2}} \sum_{m=1}^{4} \sqrt{\frac{C_{\beta(0)\beta(0)}\,\rho}{2 + C_{\beta(0)\beta(0)}\,\rho{\psi^2}_{k,n}[1,m]}} \cdots$$
$$\psi_{k,n}[1,m]\left(\frac{1}{2} + \frac{1}{\pi}\,\mathrm{atan}\left\{\sqrt{\frac{C_{\beta(0)\beta(0)}\,\rho}{2 + C_{\beta(0)\beta(0)}\,\rho{\psi^2}_{k,n}[1,m]}}\;\psi_{k,n}[2,m]\right\}\right)$$
$$+ \sqrt{\frac{C_{\beta(0)\beta(0)}\,\rho}{2 + C_{\beta(0)\beta(0)}\,\rho{\psi^2}_{k,n}[2,m]}} \cdots$$
$$\psi_{k,n}[2,m]\left(\frac{1}{2} + \frac{1}{\pi}\,\mathrm{atan}\left\{\sqrt{\frac{C_{\beta(0)\beta(0)}\,\rho}{2 + C_{\beta(0)\beta(0)}\,\rho{\psi^2}_{k,n}[2,m]}}\;\psi_{k,n}[1,m]\right\}\right) \quad (2.6.7.1)$$

The parameters used in eq.(2.6.7.1) are defined above.

❖ ***Expressions of BER in presence of CFO and STO given by A. K. Chaturvedi*** *et al.* ***and Y. Wang*** *et al.* **[44 and 45]:**

2.6.8. BPSK in AWGN Channel

$$P_b(k) = \frac{1}{2^{N-1}} \sum_{k=1}^{2^{N-1}} Q\left(\sqrt{2\gamma}\,\theta_k\right) + Q\left(\sqrt{2\gamma}\,\beta_k\right) \quad (2.6.8.1)$$

The BER is given by the average of the above expressions over all N subcarriers.

$$P_e = \frac{1}{N} \sum_{K=1}^{N} p_b(k) \quad (2.6.8.2)$$

The parameters used in eq.(2.6.8.2) are defined above.

2.6.9. BPSK in Flat fading channel

$$P_e(k) = \frac{1}{2} - \frac{1}{2^N} \sum_{k=1}^{2^{N-2}} sgn(\theta_l) \left\{ \sqrt{\frac{2\gamma\theta_l^2\,\sigma_r^2}{1 + 2\gamma\theta_l^2\,\sigma_r^2}} + sgn(\beta_l) \sqrt{\frac{2\gamma\beta_l^2\,\sigma_r^2}{1 + 2\gamma\beta_l^2\,\sigma_r^2}} \right\} \quad (2.6.9.1)$$

The Parameters used in eq. (2.6.9.1) are defined above.

2.6.10. BPSK in frequency selective fading channel

$$P_{bpsk}(\varepsilon) = \frac{1}{2} - \omega_0 \sqrt{\left(2\sigma_w^2 + \sigma_{Inf}^2\right)} \sum_{n \in N_0} n a_n K_1 \left(n\omega_0 \sqrt{\left(2\sigma_w^2 + \sigma_{Inf}^2\right)} \right)$$

(2.6.10.1)

where $K1\,(.)$ is the one order modified Bessel function of the second kind. The other parameters used in eq.(2.6.10.1) are given in [44].

❖ ***Proposed SER Expressions in presence of CFO and STO given by A. Kumar*** *et al.* **section [2.4.2]**:

2.6.11. QPSK in AWGN Channel

$$P_s(\xi) = 1 - \frac{1}{2^{2N-2}} \sum_{k=1}^{2^{N-2}} \sum_{n=1}^{2^{N-2}} \sum_{m=1}^{4} Q\{-\sqrt{2\gamma}\,\gamma_{k,n}[1,m]\ \} \times Q\{-\sqrt{2\gamma}\,\gamma_{k,n}[2,m]\ \}$$

(2.6.11.1)

The Parameters used in eq.(2.6.11.1) are given in section [2.4.2.1].

2.6.12. QPSK in Flat fading channel

$$P_s(\xi) = \frac{3}{4} - \frac{1}{2^{2N-1}} \sum_{k=1}^{2^{N-2}} \sum_{n=1}^{2^{N-2}} \sum_{m=1}^{4} \sqrt{\frac{C_{H(0)H(0)}\,\rho}{2 + C_{H(0)H(0)}\,\rho \psi^2{}_{k,n}[1,m]}} \cdots$$

$$\psi_{k,n}[1,m] \left(\frac{1}{2} + \frac{1}{\pi} \operatorname{atan} \left\{ \sqrt{\frac{C_{H(0)H(0)}\,\rho}{2 + C_{H(0)H(0)}\,\rho \psi^2{}_{k,n}[1,m]}}\ \psi_{k,n}[2,m] \right\} \right)$$

$$+ \sqrt{\frac{C_{H(0)H(0)}\,\rho}{2 + C_{H(0)H(0)}\,\rho \psi^2{}_{k,n}[2,m]}} \cdots$$

$$\psi_{k,n}[2,m] \left(\frac{1}{2} + \frac{1}{\pi} \operatorname{atan} \left\{ \sqrt{\frac{C_{H(0)H(0)}\,\rho}{2 + C_{H(0)H(0)}\,\rho \psi^2{}_{k,n}[2,m]}}\ \psi_{k,n}[1,m] \right\} \right)$$

(2.6.12.1)

The Parameters used in eq.(2.6.12.1) are given in section [2.4.2.2].

2.6.13. QPSK in frequency selective fading channel

$$P_s(\xi) = \frac{3}{4} - \frac{1}{2^{2N-1}} \sum_{k=1}^{2^{N-2}} \sum_{n=1}^{2^{N-2}} \sum_{m=1}^{4} \sqrt{\frac{C_{H(0)H(0)}\,\rho}{2 + \rho v_{k,n}[m] + C_{H(0)H(0)}\,\rho {\psi^2}_{k,n}[1,m]}} \cdots$$

$$\psi_{k,n}[1,m]\left(\frac{1}{2} + \frac{1}{\pi}\,\mathrm{atan}\left\{\sqrt{\frac{C_{H(0)H(0)}\,\rho}{2 + \rho\varphi_{k,n}[m] + C_{H(0)H(0)}\,\rho {\psi^2}_{k,n}[1,m]}}\;\psi_{k,n}[2,m]\right\}\right)$$

$$+ \sqrt{\frac{C_{H(0)H(0)}\,\rho}{2 + \rho v_{k,n}[m] + C_{H(0)H(0)}\,\rho {\psi^2}_{k,n}[2,m]}} \cdots$$

$$\psi_{k,n}[2,m]\left(\frac{1}{2} + \frac{1}{\pi}\,\mathrm{atan}\left\{\sqrt{\frac{C_{H(0)H(0)}\,\rho}{2 + \rho v_{k,n}[m] + C_{H(0)H(0)}\,\rho {\psi^2}_{k,n}[2,m]}}\;\psi_{k,n}[1,m]\right\}\right)$$

(2.6.13.1)

The Parameters used in eq.(2.6.13.1) are given in section [2.4.2.3].

****

CHAPTER-III

AN EXACT SER ANALYSIS OF FrFT-BASED OFDM

Topics:

3.1. Literature Survey on Performance Analysis of FrFT -Based OFDM System

3.2. BER Analysis for FrFT -Based OFDM In Presence of CFO

3.2.1. BPSK Modulation

3.2.1.1 AWGN Channel

3.2.1.2 Rayleigh Flat Fading Channel

3.2.1.3 Rayleigh frequency selective fading channel

3.2.2. QPSK Modulation

3.2.2.1 AWGN Channel

3.2.2.2 Rayleigh Flat Fading Channel

3.2.2.3 Rayleigh frequency selective fading channel

3.3. Discussion of Simulated Results

3.4. Summary of BER Expression For FrFT -based OFDM

- Proposed Expressions of BER/SER in presence of CFO for FrFT based-OFDM given by ***A. Kumar*** *et al.* [50, 51 and 52]:

3.4.1. AWGN Channel

3.4.1.1 BPSK modulation

3.4.1.2 QPSK modulation

3.4.2. BPSK in frequency selective fading channel

3.4.2.1 BPSK modulation

3.4.2.2 QPSK modulation

3.4.3. BPSK in flat fading channel

3.4.3.1 BPSK modulation

2.6.3.2 QPSK modulation

CHAPTER-3 AN EXACT SER ANALYSIS OF FrFT-BASED OFDM

In this chapter, literature survey on performance analysis of FrFT -based OFDM system in presence of CFO. The exact closed form bit error rate (BER) and symbol error rate (SER) expressions for FrFT -based OFDM systems with CFO are analysed. Also, an exact closed form BER/SER expression is proposed for FrFT -based OFDM system in presence of CFO given in [50]-[52] for BPSK and QPSK modulation schemes AWGN, frequency flat Rayleigh fading channel and frequency selective Rayleigh fading channel. Numerical results are given to verify the accuracy of the derivations. The chapter is concluded by giving some final remarks.

3.1. LITERATURE SURVEY ON PERFORMANCE ANALYSIS OF FrFT -BASED OFDM SYSTEM

Orthogonal frequency division multiplexing (OFDM) is a promising technology for broadband wireless communication systems due to its low complexity equalization capability in frequency selective fading channel and its adaptability/scalability to the channel condition. By definition, OFDM expects the subcarriers to be orthogonal. But, the factors such as carrier frequency mismatching, time variations due to Doppler shift or phase noise usually eliminate the orthogonality of the subcarriers. This gives rise to ICI which degrades the performance of OFDM systems significantly [32].

By following **J. Zhang** and **Z. Wang** [54], where it is shown that in presence of CFO an OFDM system based on FrFT allows a better tolerance to ICI than that based on the use of FFT. The FrFT is a generalization of the ordinary FFT that allows for more flexibility in applications. Starting from the BER expressions given in [37, 39, 53] for FFT -based OFDM, the goal was to derive analytical expressions of BER for FrFT -based OFDM and also to verify the theoretical results shown by simulation. [50]-[52].

In 2013 a paper on "Closed form relations for ICI and BER in FrFT -based OFDM system" was given by **A. Kumar** *et al.* [50]. The paper comprises of BER expressions for BPSK and QPSK in AWGN and also ICI analysis for FrFT -based OFDM system.

Later on **A. Kumar** *et al.* [51] gave the "Exact BER analysis of FrFT-based OFDM system over frequency selective Rayleigh fading channel with CFO" in 2013. This paper includes PDF and CHF for deriving the BER expression for BPSK in frequency selective Rayleigh fading channel for FrFT -based OFDM system.

Later on **A. Hamza** *et al*. [53], gave the Closed Form SER Expressions for QPSK OFDM Systems CFO in Rayleigh Fading Channel. This paper includes two dimensional PDF and CHF for deriving the SER expression. I also extend the performance of FrFT -based OFDM system in presence of CFO and derived SER expression for QPSK in case of frequency selective fading channel [52] and also compare the result of FrFT -based OFDM system with FFT based- OFDM system.

Table 3.1: Summary of performance Analysis of FrFT -based OFDM system

2013	A. kumar *et al*. [50]	Closed form relations for ICI and BER in FrFT based OFDM system
2013	A. kumar *et al*. [51]	Exact BER analysis of FrFT -based OFDM system over frequency selective Rayleigh fading channel with CFO
2014	A. Hamza, *et al*. [52]	Closed Form SER Expressions for QPSK OFDM Systems CFO in Rayleigh Fading Channel
2015	A. kumar *et al*. [53]	Exact SER Analysis of FrFT-based QPSK over Frequency Selective Rayleigh Fading Channel with CFO
2010	J. Zhang *et al*. [54]	ICI analysis for FrFT -based OFDM systems to frequency offset in time frequency selective fading channel

3.2. BER ANALYSIS FOR FrFT -BASED OFDM IN PRECENCE OF CFO

The input bit stream is encoded into complex data symbols by the encoder, which is first block of the transmitter. Data encoding can be done by using any type of digital modulation techniques viz. QPSK, QAM or FSK. After that, ***N*** such data symbols are applied to serial-to-parallel converter. These complex parallel data symbols are then fed to the IDFrFT block. After taking N-point IDFrFT.

The kernel of IDFRFT, $F_{-\alpha}(m,k)$ is defined as-

$$F_{-\alpha}(m,k) = \sqrt{\frac{sin\alpha + jcos\alpha}{N}}\, e^{\frac{-jm^2T_s^2cot\alpha}{2}} e^{\frac{-jk^2u^2cot\alpha}{2}} e^{\frac{j2\pi mk}{N}} \qquad (3.2.1)$$

were T_s and u are the sampling intervals in the time and fractional Fourier domain, respectively. The Fractional Fourier domain makes an angle $\alpha = a \times \pi/2$ with the time-domain, where, a is a real number varies from 0 to 1. Since, at $\alpha = \pi/2, i.e.\, a = 1$ FrFT converts into its counterpart FT, therefore FrFT -based OFDM also converts into FFT -based OFDM at this angle parameter.

After considering the effects of multipath fading channel and passing through multipath channel then removing the cyclic prefix, the DFrFT of received signal has been taken. The kernel of IDFRFT, $F_\alpha(q,n)$ is defined as-

$$F_\alpha(q,n) = \sqrt{\frac{sin\alpha - jcos\alpha}{N}}\, e^{\frac{jn^2T_S^2 cot\alpha}{2}} e^{\frac{jq^2u^2 cot\alpha}{2}} e^{\frac{-j2\pi nq}{N}} \quad (3.2.2)$$

After the $\boldsymbol{N}$-point DFrFT at the receiver, the signal observed on the $\boldsymbol{q^{th}}$ sub-carrier in the presence of CFO, which can be expressed as [51]-

$$Y(q) = \underbrace{\beta(q)X(q)S(q,q) + \sum_{k=0,k\neq q}^{N-1} \beta(k)X(k)S(q,k)}_{\widehat{R(q)}} + W(q), \quad q = 0,\dots,N-1, \quad (3.2.3)$$

where $X(k)$ is the symbol transmitted over the $(k+1)^{th}$ sub-carrier, $S(q,k)$ is the inter-carrier interference (ICI) coefficient, $W(q)$ is the additive white Gaussian noise (AWGN) with variance $\sigma^2 = N_o/2$ and $\beta(k)$ is the channel frequency response for the $(k+1)$-th sub-carrier. By adopting a matrix notation, let $\boldsymbol{h} = [h_1, h_2 \dots, h_L]^T$ be the $L\times1$ vector of time-domain channel coefficients, where $(\cdot)^T$ denotes the transpose operation. The vector containing the coefficients of frequency-domain channel for all the sub-carriers can be expressed as $[\beta(0), \beta(1), \dots, \beta(N-1)]^T = \boldsymbol{\mathcal{F}}_L\boldsymbol{h}$, where $\boldsymbol{\mathcal{F}}_L$ is the $N\times L$ matrix obtained by taking the first columns of $N\times N$ DFrFT matrix defined in [54].

The ICI coefficient is defined as-

$$S(q,k) = \frac{1}{N}\sum_{n=0}^{N-1} e^{-j\frac{2\pi\varepsilon n}{N}} \sum_{m=0}^{N-1} e^{-j\frac{(m^2-n^2)T_S^2 \cot\alpha}{2}} e^{j\frac{(q^2-k^2)u^2\cot\alpha}{2}} e^{j\frac{2\pi(mk-nq)}{N}} \quad (3.2.4)$$

where T_s and u are the sampling intervals in time-domain and fractional Fourier domain respectively, α is the angle parameter of the DFrFT kernel, $\varepsilon = \Delta f T_u$ is the carrier frequency offset Δf normalized to sub-carrier spacing $1/T_u$, being T_u the useful period of one OFDM symbol.

3.2.1. BPSK Modulation

3.2.1.1 AWGN Channel

For BPSK modulation $X(k) \in \{1,-1\}$ and the first subcarrier with the transmitted symbol 1 is considered. Since the constellation is purely real, only the real part of (3.2.3) will

be considered. Following [37], we obtain the characteristic function (CHF) of the real part of $Y(1)$, $\Re(Y(1))$, as-

$$\varphi_{\Re[Y(1)]}(\omega) = E\left(e^{j\omega\Re[Y(1)]}\right) \tag{3.2.1.1.1}$$

Substituting the value of $Y(1)$ from (3.2.3) in to the eq. (3.2.1.1.1)-

$$\varphi_{\Re[Y(1)]}(\omega) = \left(e^{j\omega\Re[S(1,1)]}\right).e^{j\omega W(1)}\prod_{\substack{k=2\\k\neq l}}^{N-1}\left(e^{j\omega\Re[S(1,k)]}\right) \tag{3.2.1.1.2}$$

Now, it can be simplified as-

$$\varphi_{\Re[Y(1)]}(\omega) = \left(e^{j\omega\Re[S(1,1)]-\frac{\omega^2\sigma_s^2}{2}}\right)\prod_{\substack{k=2\\k\neq l}}^{N-1} cos(\omega\Re[S(1,k)]) \tag{3.2.1.1.3}$$

This can be further simplified by using (2.4.1) as-

$$\varphi_{\Re[Y(1)]}(\omega) = \frac{1}{2^{N-1}}\sum_{k=1}^{2^{N-2}} exp\left(j\omega\theta_k - \frac{\omega^2\sigma_s^2}{2}\right) + exp\left(j\omega\beta_k - \frac{\omega^2\sigma_s^2}{2}\right) \tag{3.2.1.1.4}$$

where $\theta_k = \Re[S(1,1) + \boldsymbol{S}^T e_k]$, $\beta_k = \Re[S(1,1) - \boldsymbol{S}^T e_k]$ and $\boldsymbol{S} = (S(1,2), \ldots\ldots\ldots, S(1,N))^T$ E_{N-1} is of dimension $(N-1)\times 2^{N-2}$. It is obvious that (3.2.1.1.4) represents the CHF of a mixture of Gaussian density function.

Since the hypotheses are binary, an error occurs if $\Re[Y(1)] < 0$. Now, the bit error probability can be written as-

$$P_b(\xi) = \frac{1}{2^{N-1}}\sum_{k=1}^{2^{N-2}}\left\{Q\left(\sqrt{2\gamma}\,\theta_k\right) + Q\left(\sqrt{2\gamma}\,\beta_k\right)\right\} \tag{3.2.1.1.5}$$

where $\gamma = E_b/N_0$, $Q(x)$ is the Gaussian Q function. One should note that in our case of interest $E_b = 1$ and $\sigma^2 = N_0/2$ with N_0 being the noise power spectral density.

3.2.1.2 Rayleigh Flat Fading Channel

In the Rayleigh flat fading channel, the conditional bit error probability can be written by using (3.2.1.1.5) as-

$$P_b(\xi||\beta|) = \frac{1}{2^{N-1}}\sum_{k=1}^{2^{N-2}}\left\{Q\left(\sqrt{2\gamma}\,\theta_k|\beta|\right) + Q\left(\sqrt{2\gamma}\,\beta_k|\beta|\right)\right\} \tag{3.2.1.2.1}$$

where $|\beta|$ denotes the absolute value of β. Now, the unconditional bit error probability is calculated as in [38,eq. 8.102]-

$$P_b(\xi) = \int_0^{\infty} P_b(\xi||\beta|)P(|\beta|)\, d|\beta| \tag{3.2.1.2.2}$$

where $|\beta|$ has a Rayleigh distribution given by $P(|\beta|) = \frac{|\beta|}{\sigma_R^2} exp\left(\frac{|\beta|^2}{2\sigma_R^2}\right)$. After applying the given Craig's formula-

$$Q(x) = \frac{1}{\pi}\int_0^{\pi/2} \exp\left(-\frac{x^2}{2sin\psi}\right) d\psi, \qquad x > 0 \tag{3.2.1.2.3}$$

Individually, putting Q- function and after performing some algebraic manipulations, the bit error probability is written as-

$$P_b(\xi) = \frac{1}{2} - \frac{1}{2^N}\sum_{k=1}^{2^{N-2}} \left\{ \sqrt{\frac{2\sigma_R^2\theta_k^2\gamma}{1+2\sigma_R^2\theta_k^2\gamma}} + \sqrt{\frac{2\sigma_R^2\beta_k^2\gamma}{1+2\sigma_R^2\beta_k^2\gamma}} \right\} \tag{3.2.1.2.4}$$

Above expressions have been derived assuming the argument of Q function is positive. This is not true for higher values of CFO, leading to a mismatch between the theoretical and actual BER. The same is true for complete system model based on the CFO and STO. So, an accurate BER expression derive, by considering the argument of Q function is +ive as well as - ive.

After some mathematical manipulation an exact BER expression is written as-

$$P_b(\xi) = \frac{1}{2} - \frac{1}{2^N}\sum_{k=1}^{2^{N-2}} \left\{ sgn(\theta_k)\sqrt{\frac{2\sigma_R^2\theta_k^2\gamma}{1+2\sigma_R^2\theta_k^2\gamma}} + sgn(\beta_k)\sqrt{\frac{2\sigma_R^2\beta_k^2\gamma}{1+2\sigma_R^2\beta_k^2\gamma}} \right\} \tag{3.2.1.2.5}$$

where $sgn(.)$ denotes the signum function.

3.2.1.3 Rayleigh Frequency Selective Fading Channel

Considering the BPSK modulation scheme $X(k)\ \epsilon\ \{+1, -1\}$, symbol $X(0) = +1$ is transmitted on first subcarrier. After multiplying by the conjugate of $\beta(0)$, represented as $\bar{\beta}(0)$, and taking the real part $(\Re[.])$ only –

$$\Re\left[\bar{\beta}(0)\, Y(0)\right] = |\beta(0)|^2\Re[S(0,0)] + \sum_{k=1}^{N-1} \Re\left[\bar{\beta}(0)\beta(k)X(k)S(0,k)\right] + \bar{\beta}(0)W(0)$$

(3.2.1.3.1)

By using the identity (2.4.1), the conditional characteristic function (CHF) of $\Re\left[\bar{\beta}(0)Y(0)/\beta(0),\beta\right]$ can be written as –

$$\varphi_{\Re[\bar{\beta}(0)Y(0)/\beta(0),\beta]}(\omega) = E[\ exp(|\beta(0)|^2\Re[S(0,0)])]\ldots \times\prod_{k=1}^{N-1} exp\left(j\omega\Re\left[\bar{\beta}(0)\beta(k)X(k)S(0,k)\right]\right).exp\left(\frac{-\omega^2\sigma_\beta^2}{2}\right)$$

(3.2.1.3.2)

After further simplification the above equation is written as-

$$\varphi_{\Re[\bar{\beta}(0)Y(0)/\beta(0),\beta]}(\omega) = \frac{1}{2^{N-1}}exp(|\beta(0)|^2\Re[S(0,0)])\times exp\left(\frac{-\omega^2\sigma_\beta^2}{2}\right)\ldots \times\sum_{k=0}^{2^{N-2}-1}\left\{exp\left(j\omega\Re\left[\bar{\beta}(0)\boldsymbol{\beta}\ {S_k}^T\right]\right)+exp\left(-j\omega\Re\left[\bar{\beta}(0)\boldsymbol{\beta}\ {S_k}^T\right]\right)\right\}$$

(3.2.1.3.3)

where $\boldsymbol{\beta} = \{\beta(0),\beta(2),..,\beta(N-1)\}^T, \sigma_\beta^2 = |\beta(0)|^2\sigma^2$ and $S_k = diag[S(0,1),..,S(0,N-1)]e_k$ where e_k is the $(k+1)^{th}$ column of $N\times 2^{N-1}$ matrix E_{N-1}. Here, $diag\ (.)$ denotes the diagonal matrix. Error will occur only if $\Re\left[\bar{\beta}(0)Y(0)/\beta(0)\beta\right] < 0$.

Using the CHF defined in (3.2.1.3.3), the conditional bit error probability can be written as-

$$P_b(\xi|\beta(0),\boldsymbol{\beta}) = \frac{1}{2^{N-1}}\sum_{K=0}^{2^{N-2}-1} Q\left(\frac{|\beta(0)|^2\Re[S(0,0)]+\Re\left[\bar{\beta}(0)\boldsymbol{\beta}\ {S_k}^T\right]}{\sigma_\beta}\right)\ldots + Q\left(\frac{|\beta(0)|^2\Re[S(0,0)]-\Re\left[\bar{\beta}(0)\boldsymbol{\beta}\ {S_k}^T\right]}{\sigma_\beta}\right)$$

(3.2.1.3.4)

Unconditional BER (P_b) can be determined as –

$$P_b(\xi) = \int_{\beta(0)}\int_{\beta} P_b(\xi|\beta(0),\boldsymbol{\beta})\ P_{\boldsymbol{\beta}|\beta(0)}\left(\boldsymbol{\beta}|\beta(0)\right)d\boldsymbol{\beta}\ P_{\beta(0)}\left(\beta(0)\right)\ d\beta(0)$$

(3.2.1.3.5)

where $P_{\frac{\beta}{\beta(0)}}\left(\frac{\beta}{\beta(0)}\right)$ is conditional PDF with mean $E(\boldsymbol{\beta}/\beta(0))$ and covariance $C_{\boldsymbol{\beta}/\beta(0)}$ [(27) of 37], $E(.)$ representing the statistical expectation. Since, $P_b(\xi)$ involves N dimensional integration, therefore, it will be difficult to evaluate. Hence, converting this multidimensional integration into many single dimensional integration by averaging $P_b(\xi/\beta(0),\beta)$ over $p_{\beta/\beta(0)}(\beta/\beta(0))$ in (3.2.1.3.5) written as-

$$P_b(\xi) = \int_{\beta(0)}^{\cdot} P_b\left(\xi|\beta(0)\right) P_{\beta(0)}\left(\beta(0)\right) d\beta(0) \tag{3.2.1.3.6}$$

where $P(\xi/\beta(0))$ is defined as –

$$P_b\left(\xi|\beta(0)\right) = \frac{1}{2^{N-1}} \sum_{K=0}^{2^{N-2}-1} Q\left(\frac{\beta(0)\Re[S(0,0)] + z_k}{\sigma\sqrt{1+\frac{a_k}{2\sigma^2}}}\right) Q\left(\frac{\beta(0)\Re[S(0,0)] - z_k}{\sigma\sqrt{1+\frac{a_k}{2\sigma^2}}}\right) \tag{3.2.1.3.7}$$

Here $P(\xi/\beta(0))$ has been evaluated using mean and variance of the conditional random variable $(b_k/\beta(0))$ defined as [37] –

$$E\left(b_{\boldsymbol{k}}|\beta(0)\right) = |\beta(0)|^2 C^{-1}_{\beta(0)\beta(0)} \Re\left[\, {S_k}^T C_{\boldsymbol{\beta}\beta(0)} \,\right] = |\beta(0)|^2 z_k \tag{3.2.1.3.8a}$$

$$var(b_{\boldsymbol{k}}|\beta(0)) = \tfrac{1}{2}|\beta(0)|^2 {S_k}^T C_{\boldsymbol{\beta}|\beta(0)} \overline{S_k} = \tfrac{1}{2}|\beta(0)|^2 a_k \tag{3.2.1.3.8b}$$

where $b_k = \Re\left[\bar{\beta}(0)(S_k)^T \beta\right]$, $C_{\beta\beta(0)} = E\left[\beta\,\bar{\beta}(0)\right]$ and $C_{(\beta/\beta(0))} = \mathcal{F}_L h\, {\mathcal{F}_L}^H = C_{\beta\beta} - C^{-1}_{\beta(0)\beta(0)} C_{\beta\beta(0)}\, C^H_{\beta\beta(0)}\, C_{\beta\beta}$. Var $(.)$ and $(.)^H$ denotes the variance and Hermitian matrix respectively. Rearranging (3.2.1.3.7) by using definition of polar form of Q-function and making the change of variable as $\{|\beta(0)|^2/2\,\sigma^2\} \rightarrow \gamma/\bar{\gamma}$ and using the definition PDF of Rayleigh distribution in terms of γ, P_b can be written as-

$$P_b(\xi) = \frac{1}{\pi 2^{N-1}} \sum_{k=0}^{2^{N-2}-1} \int_0^{\pi/2} \left\{ \begin{array}{l} \int_0^{\infty} exp\left(-\frac{\gamma(\Re[S(0,0)] + z_k)^2}{\bar{\gamma}\left(1+\frac{a_k}{2\sigma^2}\right) sin^2\theta}\right) P_\gamma(\gamma) d\gamma \\ + \int_0^{\infty} exp\left(-\frac{\gamma(\Re[S(0,0)] - z_k)^2}{\bar{\gamma}\left(1+\frac{a_k}{2\sigma^2}\right) sin^2\theta}\right) P_\gamma(\gamma) d\gamma \end{array} \right\} \tag{3.2.1.3.9}$$

The $M_\gamma(s_1)$ and $M_\gamma(s_2)$ are the scaled Laplace transform of PDF $p_\gamma(\gamma)$ which can also be termed as the moment generating function of this PDF [(2.8) of 38]. Solving (3.2.1.3.9) by using the definition of moment generating function for Rayleigh fading channel and multiplying γ in numerator and denominator, $P_b(\xi)$ can be obtained as –

$$P_b(\xi) = \frac{1}{2} - \frac{1}{2^N}\sum_{k=1}^{2^{N-2}} \left\{ \begin{array}{c} \sqrt{\dfrac{\gamma C_{\beta_1\beta_1}(\Re[S(0,0)] + z_k)^2}{1+\gamma\left(C_{\beta_1\beta_1}(\Re[S(0,0)] + z_k)^2 + a_k\right)}} \\ + \sqrt{\dfrac{\gamma C_{\beta_1\beta_1}(\Re[S(0,0)] - z_k)^2}{1+\gamma\left(C_{\beta_1\beta_1}(\Re[S(0,0)] - z_k)^2 + a_k\right)}} \end{array} \right\} \tag{3.2.1.3.10}$$

Substituting $\alpha = \pi/2$ in $S(q,k)$ and ($C_{\beta_1\beta_1} = 2\sigma^2$) in (3.2.1.3.10), it will convert into BER expression of BPSK for conventional OFDM system. This is in conformity of the fact that FrFT -based OFDM will be a generalization of conventional OFDM system. But, above result is not suitable for all the values of CFOs because, at the higher value of CFO the argument of Q-function is found negative [37]. By changing the order of integration, (3.2.1.3.7) can be solved for negative argument of Q- function. Hence, for all CFOs, P_b can be obtained as-

$$P_b(\xi) = \frac{1}{2} - \frac{1}{2^N}\sum_{k=1}^{2^{N-2}} \left\{ \begin{array}{c} A_1\sqrt{\dfrac{\gamma 2\sigma^2(\Re[S(0,0)] + z_k)^2}{1+\gamma(2\sigma^2(\Re[S(0,0)] + z_k)^2 + a_k)}} \\ +A_2\sqrt{\dfrac{\gamma 2\sigma^2(\Re[S(0,0)] - z_k)^2}{1+\gamma(2\sigma^2(\Re[S(0,0)] - z_k)^2 + a_k)}} \end{array} \right\} \tag{3.2.1.3.11}$$

where $A_1 = sgn(\Re\,[S(0,0) + z_k])$ and $A_2 = sgn(\Re\,[S(0,0) - z_k])$.

3.2.2. QPSK Modulation

3.2.2.1 AWGN Channel

As usual we consider the first subcarrier with the transmitted symbol $X(1) = 1 + j$ with $X(k) = \{\pm 1 \pm j\}$ and the received signal is defined as-

$$Y(1) = X(1)S(1,1) + \sum_{k=1}^{N-1} S(1,k)X(k) \tag{3.2.2.1.1}$$

The probability of a correct decision is the probability that $Y(1) + W(1)$ lies inside $D1$ (the first quadrant of the complex plane) and it is given as-

$$p\big(Y(1)+W(1)\in D_1\big|X(1)=1+j,Y(k)\big)=Q\left(\frac{-\Re(Y(k))}{\sigma}\right)Q\left(\frac{-\Im(Y(k))}{\sigma}\right)$$

(3.2.2.1.2)

where $\Im(z)$ is the imaginary part of z. The average correct symbol decision probability is obtained by averaging (3.2.2.1.2) over Y for which the required pdf of $Y(k)$ is derived below. Since the variable $Y(k)$ is two dimensional and $X(1)=1+j$, its two dimensional CHF can be written as -

$$\varphi(\omega_I,\omega_Q)=exp\big(j\{\omega_I\Re[S(1,k)]+\omega_Q\Im[S(1,k)]\}\big)\,..$$
$$\times\prod_{k=1}^{N-1}\Big\{cos\big(\omega_I\Re[S(1,k)]+\omega_Q\Im[S(1,k)]\big)\times cos\big(\omega_I\Im[S(1,k)]-\omega_Q\Re[S(1,k)]\big)\Big\}$$

(3.2.2.1.3)

Now, more compact version of (3.2.2.1.3) can be written using the vector notations as-

$$\varphi(\omega_I,\omega_Q)=exp(j\sigma^T\{S_A^1+S_B^1\})\times\prod_{k=1}^{N-1}\{cos(\sigma^T(S_A)^l)\times cos(\sigma^T(S_B)^l)\}$$

(3.2.2.1.4)

where $\sigma=\begin{pmatrix}\omega_I & \omega_Q\end{pmatrix}^T$, $(S_A)^l=(\Re[S(1,k)]+\Im[S(1,k)])^T$ and $(S_B)^l=(\Re[S(1,k)]-\Im[S(1,k)])^T$ for all $k=1,2,\dots,N$. Then, using (2.4.1) to express (3.2.2.1.4) as-

$$\varphi(\omega_I,\omega_Q)=exp(j\sigma^T\{S_A^1+S_B^1\})\times\frac{1}{2^{2(N-2)}}\sum_{n=1}^{2^{N-2}}\sum_{k=1}^{2^{N-2}}\{cos(\sigma^T S_A e_k)\times cos(\sigma^T S_B e_n)\}$$

(3.2.2.1.5)

where $S_A=\{(S_A)^2\ (S_A)^3\dots(S_A)^N\}$, $S_B=\{(S_B)^2\ (S_B)^3\dots(S_B)^N\}$, e_k and $\boldsymbol{e}_n$ are column vectors taken from more general matrix E_{N-1}.

By using Euler's relationship with some rearrangements of terms, (3.2.2.1.5) can be written as-

$$\varphi(\omega_I,\omega_Q)=exp(j\sigma^T\{S_A^1+S_B^1\})\times\frac{1}{2^{2(N-2)}}\sum_{n=1}^{2^{N-2}}\sum_{k=1}^{2^{N-2}}\left\{\begin{matrix}e^{-j\sigma^T S_A e_k}+e^{j\sigma^T S_A e_k}\\+e^{-j\sigma^T S_B e_n}+e^{j\sigma^T S_B e_n}\end{matrix}\right\}$$

(3.2.2.1.6)

It can be further written in simple form as-

$$\varphi(\omega_I,\omega_Q)=\frac{1}{2^{2(N-2)}}\sum_{n=1}^{2^{N-2}}\sum_{k=1}^{2^{N-2}}\left\{e^{j\sigma^T G_1}+e^{j\sigma^T G_2}+e^{j\sigma^T G_3}+e^{j\sigma^T G_4}\right\}$$

(3.2.2.1.7)

where $G1 = (S_A)^1 - (S_B)^1 + S_A e_k + S_B e_n$, $G2 = (S_A)^1 - (S_B)^1 + sS_A e_k - S_B e_n$

$G3 = (S_A)^1 - (S_B)^1 - S_A e_k + S_B e_n$ and $G4 = (S_A)^1 - (S_B)^1 - S_A e_k - S_B e_n$

The Fourier transform of (3.2.2.1.7) will give two dimensional PDF written as-

$$P\big(\Re(u), \Im(u)\big) = \frac{1}{2^{2(N-2)}} \sum_{n=1}^{2^{N-2}} \sum_{k=1}^{2^{N-2}} \sum_{m=1}^{4} \{\delta(\Re[Y] - \psi_{\mathrm{kn}}[1,m])\delta(\Re[Y] - \psi_{\mathrm{kn}}[2,m])\}$$

(3.2.2.1.8)

where $\psi_{kn}[p,q]$ is the $(p,q)^{th}$ element of the 2×4 matrix Ψ defined as $\Psi = (G1 \;\; G2 \;\; G3 \;\; G4)$ and $\delta(x)$ is the Dirac delta function. Averaging (3.2.2.1.8) with respect to the pdf given in (3.2.2.1.2) yields the SER written as-

$$P_b(\xi) = 1 - \frac{1}{2^{2(N-1)}} \sum_{n=1}^{2^{N-2}} \sum_{k=1}^{2^{N-2}} \sum_{m=1}^{4} \{Q\big(-\sqrt{2\gamma}\,\psi_{\mathrm{kn}}[1,m]\big)Q\big(-\sqrt{2\gamma}\,\psi_{\mathrm{kn}}[2,m]\big)\}$$

(3.2.2.1.9)

In the absence of ICI (i.e. ε= 0), Ψ can be expressed as $\psi = \begin{pmatrix} 1 & 1 & 1 & 1 \\ 1 & 1 & 1 & 1 \end{pmatrix}$. since, $S(k) = 0$ for all k $\neq$1 and $S(1) = 1$.

3.2.2.2 Rayleigh Flat Fading Channel

The conditional symbol error rate can be expressed as-

$$P_b(\xi||\beta|) = 1 - \frac{1}{2^{2(N-1)}} \sum_{n=1}^{2^{N-2}} \sum_{k=1}^{2^{N-2}} \sum_{m=1}^{4} \{Q\big(-\sqrt{2\gamma}\,\psi_{\mathrm{kn}}[1,m]\,|\beta|\big)Q\big(-\sqrt{2\gamma}\,\psi_{\mathrm{kn}}[2,m]\big)|\beta|\}$$

(3.2.2.2.1)

where $|\beta|$ is Rayleigh distributed random variable. Now, for finding the unconditional bit error rate, the evaluation of integral will be encountered. After averaging (3.2.2.2.1), it can be solved using [38,eq. 4.8], [38,eq. 5.102] and [38,eq. 5.6] to give the SER.

$$P_b(\xi) = \frac{3}{4} - \frac{1}{2^{(N-1)}} \sum_{n=1}^{2^{N-2}} \sum_{k=1}^{2^{N-2}} \sum_{m=1}^{4} \sqrt{\frac{2\sigma_r^2\psi_{kn}^2[1,m]\,\gamma}{1 + 2\sigma_r^2\psi_{kn}^2[1,m]\,\gamma}} \;\cdot\cdot$$
$$\times \left(1 - \frac{1}{\pi} arctan\left\{\frac{\psi_{\mathrm{kn}}[1,m]}{\psi_{\mathrm{kn}}[2,m]} \sqrt{1 + \frac{1}{2\sigma_r^2\psi_{kn}^2[1,m]\,\gamma}}\right\}\right)$$
$$+ \sqrt{\frac{2\sigma_r^2\psi_{kn}^2[2,m]\,\gamma}{1 + 2\sigma_r^2\psi_{kn}^2[2,m]\,\gamma}} \left(1 - \frac{1}{\pi} arctan\left\{\frac{\psi_{\mathrm{kn}}[2,m]}{\psi_{\mathrm{kn}}[1,m]} \sqrt{1 + \frac{1}{2\sigma_r^2\psi_{kn}^2[2,m]\,\gamma}}\right\}\right)$$

(3.2.2.2.2)

However, the analytical SER expression given in the (3.2.2.2.2) is not correct for all values of CFO because the expressions have been derived assuming the argument of Q function positive. This is not true for higher values of CFO, leading to a mismatch between the theoretical and actual SER. So for, an accurate SER expression derive by considering the argument of Q function is + ive as well as – ive.

After some mathematical manipulation an exact SER expression written as-

$$P_b(\xi) = \frac{3}{4} - \frac{1}{2^{(N-1)}} \sum_{n=1}^{2^{N-2}} \sum_{k=1}^{2^{N-2}} \sum_{m=1}^{4} sgn\left(\frac{\psi_{\mathrm{kn}}[1,m]}{\psi_{\mathrm{kn}}[2,m]}\right) \sqrt{\frac{2\sigma_r^2\psi_{kn}^2[1,m]\,\gamma}{1+2\sigma_r^2\psi_{kn}^2[1,m]\,\gamma}} \cdot\cdot$$
$$\times\left(1-\frac{1}{\pi}arctan\left\{\frac{\psi_{\mathrm{kn}}[1,m]}{\psi_{\mathrm{kn}}[2,m]}\sqrt{1+\frac{1}{2\sigma_r^2\psi_{kn}^2[1,m]\,\gamma}}\right\}\right) + sgn\left(\frac{\psi_{\mathrm{kn}}[2,m]}{\psi_{\mathrm{kn}}[2,m]}\right)\ldots$$
$$\sqrt{\frac{2\sigma_r^2\psi_{kn}^2[2,m]\,\gamma}{1+2\sigma_r^2\psi_{kn}^2[2,m]\,\gamma}}\left(1-\frac{1}{\pi}arctan\left\{\frac{\psi_{\mathrm{kn}}[2,m]}{\psi_{\mathrm{kn}}[1,m]}\sqrt{1+\frac{1}{2\sigma_r^2\psi_{kn}^2[2,m]\,\gamma}}\right\}\right) \quad (3.2.2.2.3)$$

3.2.2.3 Rayleigh Frequency selective Fading Channel

Considering QPSK modulation, where symbols are drawn from the set $\{\pm 1 \pm j\}$, as in [37] we assume that symbol $X(0) = 1 + j$ is transmitted on the first subcarrier. The equalized signal on the first sub-carrier is-

$$\bar{\beta}(0)\,Y(0) = |\beta(0)|^2 X(0)S(0,0) + \sum_{k=1}^{N-1} \bar{\beta}(0)\beta(k)X(k)S(0,k) + \bar{\beta}(0)W(0) \quad (3.2.2.3.1)$$

where $\bar{\beta}(0)$ is the complex conjugate of $\beta(0)$. The probability of making a correct decision is given by the probability that $\bar{\beta}(0)Y(0) = \bar{\beta}(0)R(0) + \bar{\beta}(0)W(0)$ lies inside the first quadrant D_1 of the complex plan. Following the same approach of [53], the probability of making a correct decision conditioned to transmission of symbol $1 + j$ on the first subcarrier is given by-

$$P_c\left(\bar{\beta}(0)Y(0) \in D_1\,|X(0) = 1 + \mathrm{j}\,, \bar{\beta}(0)R(0)\right) = \mathrm{Q}\left(-\frac{\Re[\bar{\beta}(0)R(0)]}{\sigma_\beta}\right)\mathrm{Q}\left(-\frac{\Im[\bar{\beta}(0)R(0)]}{\sigma_\beta}\right)$$

(3.2.2.3.2)

where $\Re[\mathrm{c}]$ and $\Im[\mathrm{c}]$ denotes the real and the imaginary part of complex number c respectively, and $\sigma_\beta = |\beta(0)|\,\sigma$. The conditional probability of correct decision is obtained by averaging (3.2.2.3.2) over the probability density function (PDF) of $\bar{\beta}(0)R(0)$ which is obtained from the

CHF as reported in what follows. Since $\bar{\beta}(0)R(0)$ is a complex random variable its CHF is two-dimensional (2-D) and, as shown in [53], it is given by

$$\varphi(\omega_I,\omega_Q)=exp\left(j|\beta(0)|^2\left(\omega_I(\Re[S(0,0)]-\Im[S(0,0)])+\omega_Q\left(\Im[S(0,0)]+\Re[S(0,0)]\right)\right)\right)$$
$$\times\prod_{k=1}^{N-1}\cos\left(\omega_I\Re\left[\bar{\beta}(0)\beta(k)S(0,k)\right]+\omega_Q\Im\left[\bar{\beta}(0)\beta(k)S(0,k)\right]\right)$$
$$\times\cos\left(\omega_I\Im\left[\bar{\beta}(0)\beta(k)S(0,k)\right]-\omega_Q\Re\left[\bar{\beta}(0)\beta(k)S(0,k)\right]\right) \quad (3.2.2.3.3)$$

where $\boldsymbol{\beta}=\left(\beta(1),\dots,\beta(N-1)\right)^T$. Following the mathematical derivation reported in [53], the 2-D PDF resulting from the inverse Fourier transform of (3.2.2.3.3) can be written as-

$$p\left(\Re\left[\bar{\beta}(0)R(0)\right],\Im\left[\bar{\beta}(0)R(0)\right]\right)=\frac{1}{2^{2N-2}}\ ..$$
$$\sum_{k=1}^{2^{N-2}}\sum_{n=1}^{2^{N-2}}\sum_{m=1}^{4}\delta\left[\Re\left(\bar{\beta}(0)R(0)\right)-\left(|\beta(0)|^2\,D_A+\gamma_{k,n}[1,m]\right)\right]$$
$$\times\delta\left[\Im\left(\bar{\beta}(0)R(0)\right)-\left(|\beta(0)|^2D_B+\gamma_{k,n}[2,m]\right)\right] \quad (3.2.2.3.4)$$

where $\delta[.]$ is the Dirac delta function, $D_A=\Re[S(0,0)]-\Im[S(0,0)]$, $D_B=\Re\left[[S(0,0)]\right]+\Im\left[[S(0,0)]\right]$ and $\gamma_{k,n}[p,q]$ is the (p,q) entry of the 2×4 matrix of $\boldsymbol{\Gamma}$ defined as $\boldsymbol{\Gamma}=\left((\boldsymbol{\Gamma}_A+\boldsymbol{\Gamma}_B)\ (-\boldsymbol{\Gamma}_A-\boldsymbol{\Gamma}_B)\ (\boldsymbol{\Gamma}_A-\boldsymbol{\Gamma}_B)\ (-\boldsymbol{\Gamma}_A+\boldsymbol{\Gamma}_B)\right)$ with matrices

$$\boldsymbol{\Gamma}_A=\left[\Re\left[\bar{\beta}(0)\mathbf{e}_k^T\boldsymbol{\Lambda}\boldsymbol{\beta}\right]\quad\Im\left[\bar{\beta}(0)\mathbf{e}_n^T\boldsymbol{\Lambda}\boldsymbol{\beta}\right]\right]^T,$$
$$\boldsymbol{\Gamma}_B=\left[\Im\left[\bar{\beta}(0)\mathbf{e}_k^T\boldsymbol{\Lambda}\boldsymbol{\beta}\right]\quad-\Re\left[\bar{\beta}(0)\mathbf{e}_n^T\boldsymbol{\Lambda}\boldsymbol{\beta}\right]\right]^T,$$

where $\boldsymbol{\Lambda}=\mathrm{diag}\left(S(0,1),S(0,2),\dots,S(0,N-1)\right)$ and $\mathbf{e}_k$ is an $N\times1$ vector corresponding to the binary codeword of the number $2^{N-1}-k$, where zeros are replaced with -1s. The analytical expression of the probability of symbol error given $(\beta(0),\boldsymbol{\beta})$ can be obtained by subtracting (3.2.2.3.2) to 1 and averaging over (3.2.2.3.4) as-

$$P_s(\xi|\beta(0),\boldsymbol{\beta})=1-\frac{1}{2^{2N-2}}\sum_{k=1}^{2^{N-2}}\sum_{n=1}^{2^{N-2}}\sum_{m=1}^{4}Q\left\{\frac{-\left(|\beta(0)|^2\,S_A+\gamma_{k,n}[1,m]\right)}{\sigma_\beta}\right\}$$
$$\times Q\left\{\frac{-\left(|\beta(0)|^2\,S_B+\gamma_{k,n}[2,m]\right)}{\sigma_\beta}\right\} \quad (3.2.2.3.5)$$

The unconditional probability of symbol error can be calculated from the integral

$$P_s(\xi) = \int_{\beta(0)}^{\cdot} P_s\big(\xi|\beta(0)\big)p_{\beta(0)}\big(\beta(0)\big)d\beta(0) \tag{3.2.2.3.6}$$

where $p_{\beta(0)}(\beta(0))$ is the probability density function of the Rayleigh distribution and

$$P_s\big(\xi|\beta(0)\big) = 1 - \frac{1}{2^{2N-2}} \sum_{k=1}^{2^{N-2}} \sum_{n=1}^{2^{N-2}} \sum_{m=1}^{4} Q\left\{\frac{-\big(|\beta(0)|\, S_A + \vartheta_{k,n}[1,m]\big)}{\sigma\sqrt{1+\frac{v_{k,n}[m]}{2\sigma^2}}}\right\}\cdot\cdot$$

$$\times Q\left\{\frac{-\big(|\beta(0)|\, S_B + \vartheta_{k,n}[2,m]\big)}{\sigma\sqrt{1+\frac{v_{k,n}[m]}{2\sigma^2}}}\right\} \tag{3.2.2.3.7}$$

By following the same approach reported in [53], the conditional probability of symbol error $P_s\big(\xi|\beta(0)\big)$ in (3.2.2.3.7) has been evaluated using the mean $|\beta(0)|^2\vartheta_{k,n}[i,m]$ and the variance $|\beta(0)|^2 v_{k,n}[m]/2$ of the conditional Gaussian random variable $\gamma_{k,n}[i,m]|\beta(0)$.

The term $\vartheta_{k,n}[i,m]$ is the entry (i,m) of the 2×4 matrix $\mathbf{W} = \big((\mathbf{W}_A + \mathbf{W}_B)\ (-\mathbf{W}_A - \mathbf{W}_B)\ (\mathbf{W}_A - \mathbf{W}_B)\ (-\mathbf{W}_A + \mathbf{W}_B)\big)$ with

$$\mathbf{W}_A = C^{-1}_{\beta(0)\beta(0)}\left[\Re\big[\mathbf{e}_k^T\boldsymbol{\Lambda}\boldsymbol{C}_{\boldsymbol{\beta}\beta(0)}\big] \quad \Im\big[\mathbf{e}_k^T\boldsymbol{\Lambda}\boldsymbol{C}_{\boldsymbol{\beta}\beta(0)}\big]\right]^T$$

$$\mathbf{W}_B = C^{-1}_{\beta(0)\beta(0)}\left[\Im\big[\mathbf{e}_n^T\boldsymbol{\Lambda}\boldsymbol{C}_{\boldsymbol{\beta}\beta(0)}\big] \quad -\Re\big[\mathbf{e}_n^T\boldsymbol{\Lambda}\boldsymbol{C}_{\boldsymbol{\beta}\beta(0)}\big]\right]^T$$

where $\boldsymbol{C}_{\boldsymbol{\beta}|\beta(0)}$ is the channel autocovariance matrix given in [37]. The term $v_{k,n}[m]$ is the m-th element of the 1×4 vector $\mathbf{v} = (v_1\ v_2\ v_3\ v_4)$, where $v_i = \boldsymbol{\xi}_i^T\boldsymbol{\Lambda}\boldsymbol{C}_{\boldsymbol{\beta}|\beta(0)}\boldsymbol{\Lambda}\boldsymbol{\xi}_i$, $\boldsymbol{\xi}_1 = \mathbf{e}_k + \mathbf{e}_k$, $\boldsymbol{\xi}_2 = -\mathbf{e}_k - \mathbf{e}_k$, $\boldsymbol{\xi}_3 = \mathbf{e}_k - \mathbf{e}_k$, $\boldsymbol{\xi}_4 = -\mathbf{e}_k + \mathbf{e}_k$. The probability of symbol error for QPSK resulting from computation of (3.2.2.3.6) is –

$$P_s(\xi) = \frac{3}{4} - \frac{1}{2^{2N-1}} \sum_{k=1}^{2^{N-2}} \sum_{n=1}^{2^{N-2}} \sum_{m=1}^{4} \sqrt{\frac{C_{\beta(0)\beta(0)}\,\rho}{2 + \rho v_{k,n}[m] + C_{\beta(0)\beta(0)}\,\rho \psi^2{}_{k,n}[1,m]}} \cdots$$
$$\psi_{k,n}[1,m] \left(\frac{1}{2} + \frac{1}{\pi} \operatorname{atan} \left\{ \sqrt{\frac{C_{\beta(0)\beta(0)}\,\rho}{2 + \rho \varphi_{k,n}[m] + C_{\beta(0)\beta(0)}\,\rho \psi^2{}_{k,n}[1,m]}}\ \psi_{k,n}[2,m] \right\} \right)$$
$$+ \sqrt{\frac{C_{\beta(0)\beta(0)}\,\rho}{2 + \rho v_{k,n}[m] + C_{\beta(0)\beta(0)}\,\rho \psi^2{}_{k,n}[2,m]}} \cdots$$
$$\psi_{k,n}[2,m] \left(\frac{1}{2} + \frac{1}{\pi} \operatorname{atan} \left\{ \sqrt{\frac{C_{\beta(0)\beta(0)}\,\rho}{2 + \rho v_{k,n}[m] + C_{\beta(0)\beta(0)}\,\rho \psi^2{}_{k,n}[2,m]}}\ \psi_{k,n}[1,m] \right\} \right) \quad (3.2.2.3.8)$$

where $\rho = E_s/N_0$ is the signal-to-noise ratio and $\psi_{k,n}[i,m]$ is the $(i,m)^{th}$ entry of the 2×4 matrix $\mathbf{\Psi} = \mathbf{D} \otimes \mathbf{1}_{1\times4} + \mathbf{W}$, in which $\otimes$ is the Kronecker product and $\mathbf{1}_{1\times4}$ is a 1×4 vectors of 1s, and $\mathrm{D} = \begin{pmatrix} \mathrm{D_A} & \mathrm{D_B} \end{pmatrix}^{\mathrm{T}}$. Substituting $\alpha = \pi/2$ in $\mathrm{S(q,k)}$ and $C_{\beta(0)\beta(0)} = 2\sigma^2$ in (3.2.2.3.8) we get the probability of symbol error expression of QPSK for conventional OFDM system given by eq. (16) of [53]. This is in conformity of the fact that FrFT based OFDM is a generalization of conventional OFDM system.

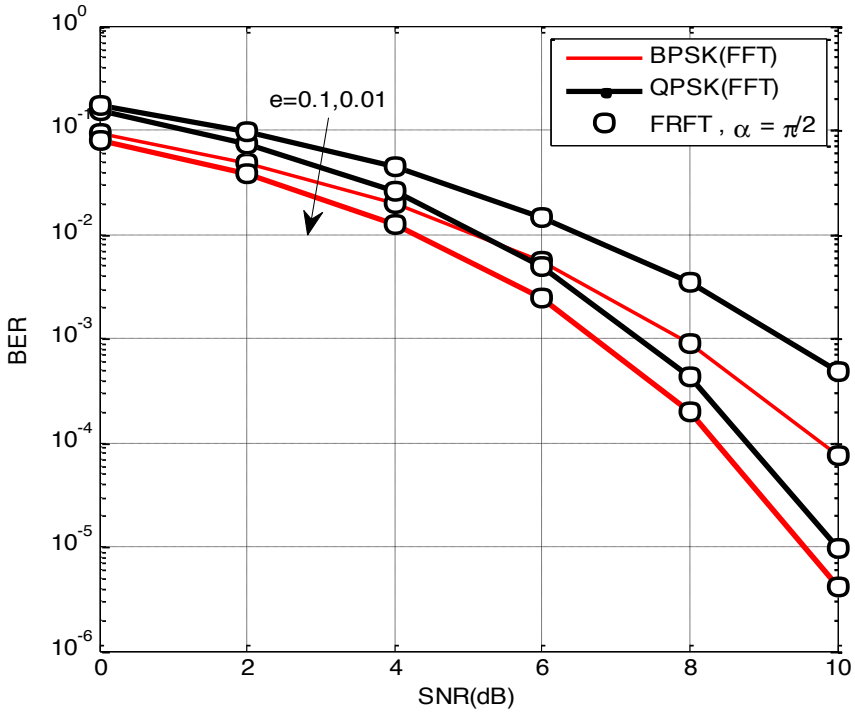

Fig. 3.2.1.1.1 BER/SER comparison between FFT and FrFT -based OFDM system in presence of CFO BPSK/QPSK in AWGN channel with N = 8

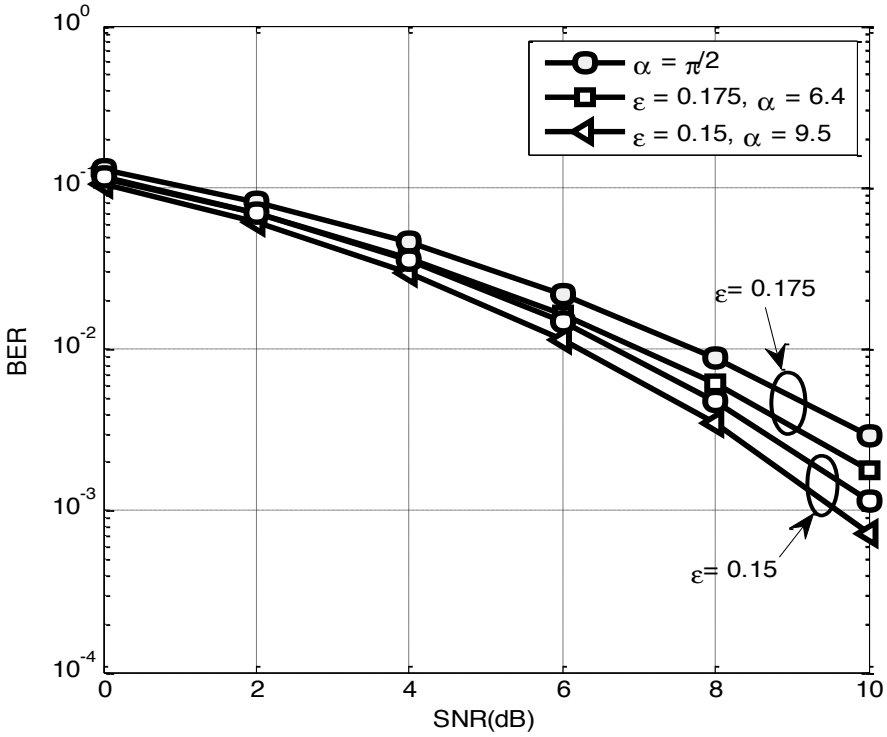

Fig. 3.2.1.1.2 BER expression of FrFT based-OFDM system in presence of CFO BPSK channel in AWGN with N = 8.

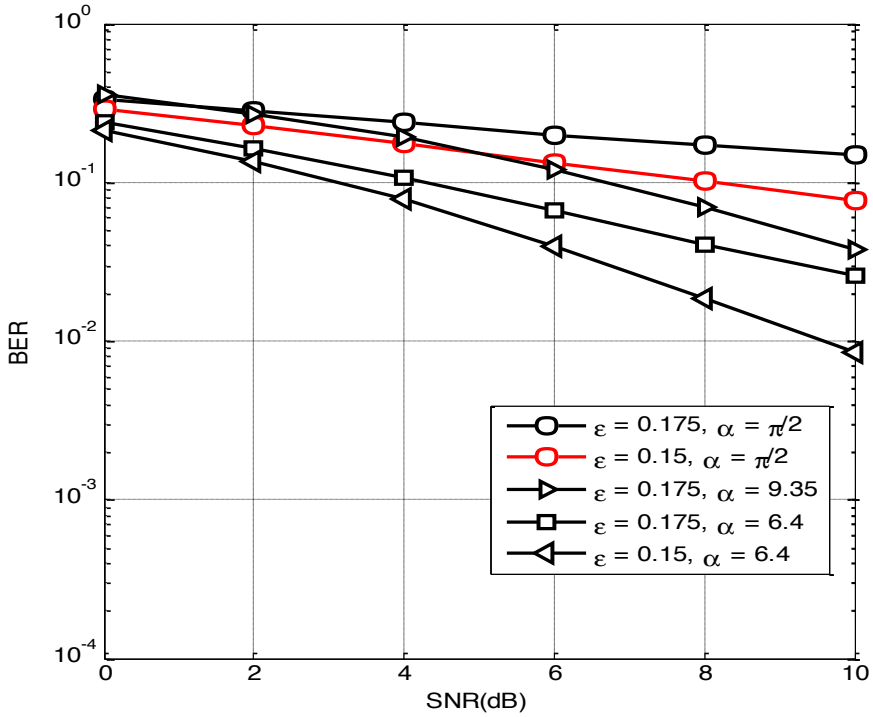

Fig. 3.2.2.1.1 BER expression of FrFT based-OFDM system in presence of CFO QPSK in AWGN channel with N = 8.

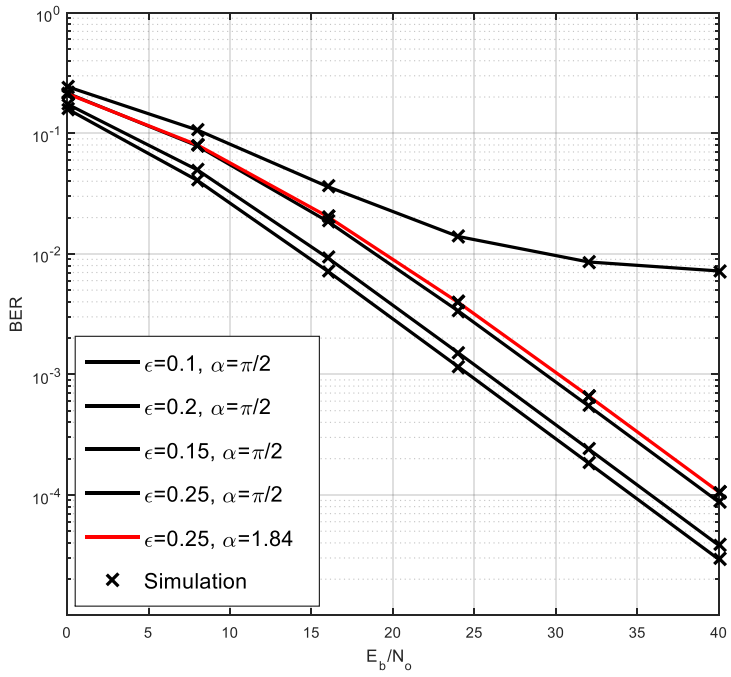

Fig. 3.2.1.2.1 BER expression of FrFT based- OFDM system in presence of CFO BPSK in Flat fading channel with $N = 8$

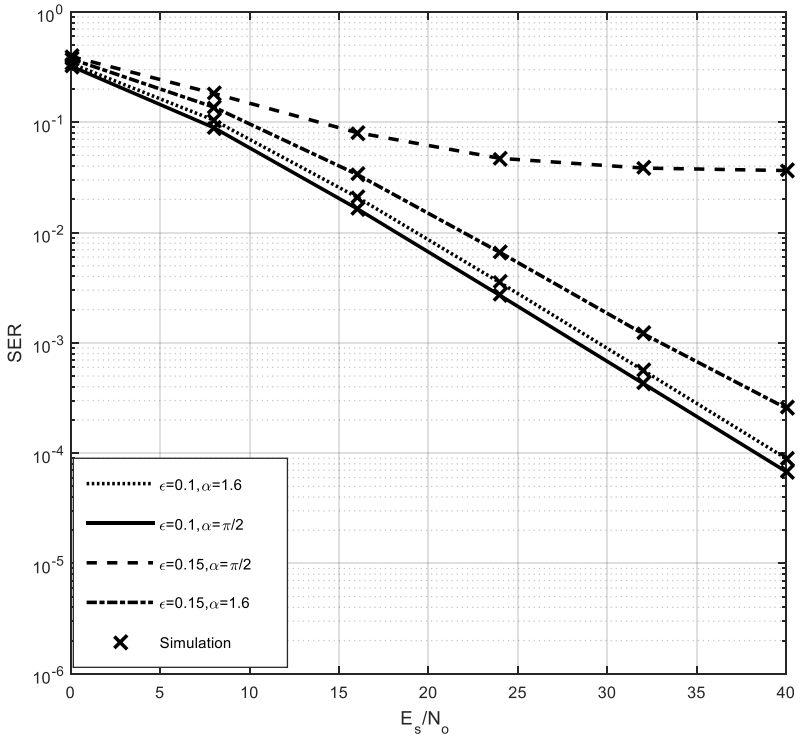

Fig. 3.2.2.2.1 BER expression of FrFT based- OFDM system in presence of CFO QPSK in Flat fading channel with $N = 8$.

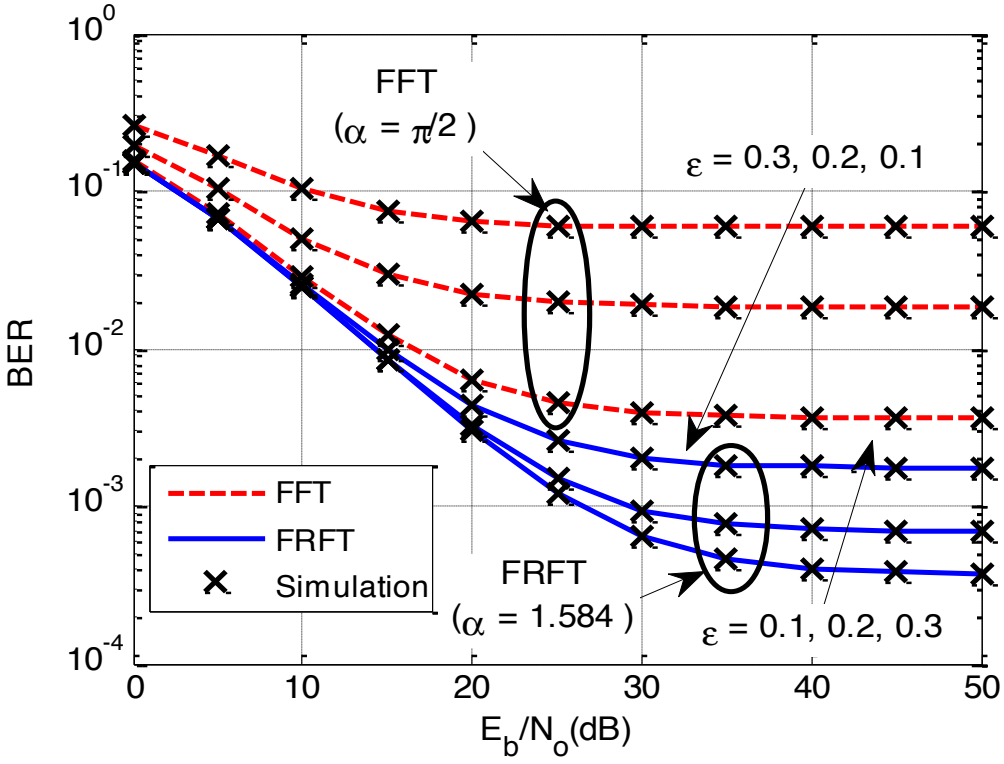

Fig. 3.2.1.3.1 BER for BPSK in FrFT-OFDM over frequency selective Rayleigh fading channel with $N = 8$ sub-carriers and $L = 2$ taps.

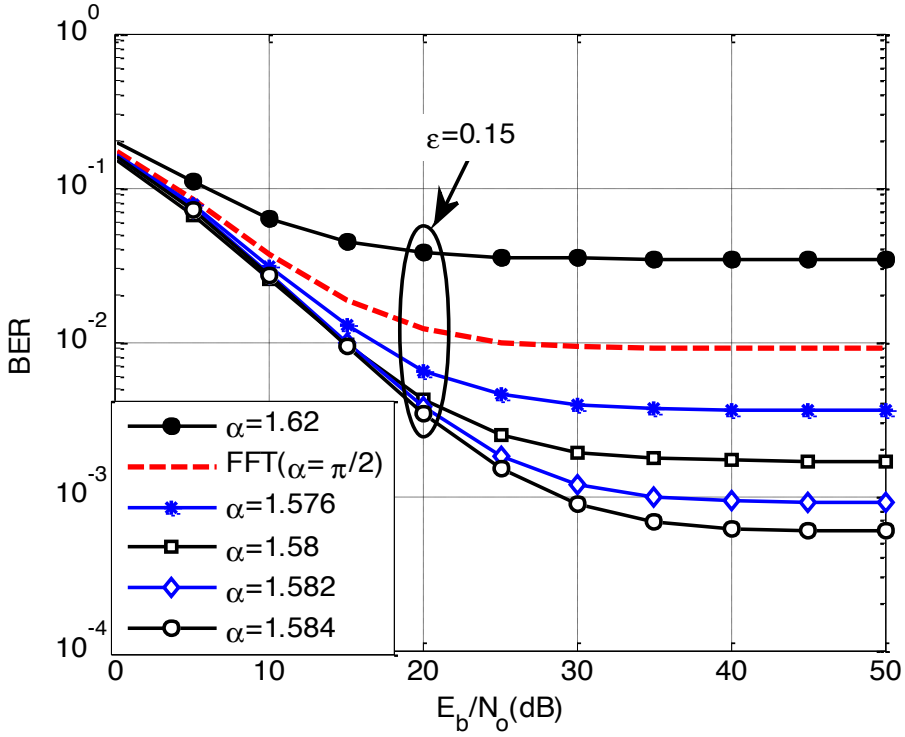

Fig. 3.2.1.3.2 BER for BPSK in FrFT-OFDM over frequency selective Rayleigh fading channel with $N = 8$ sub-carriers and $L = 2$ taps for different values of α.

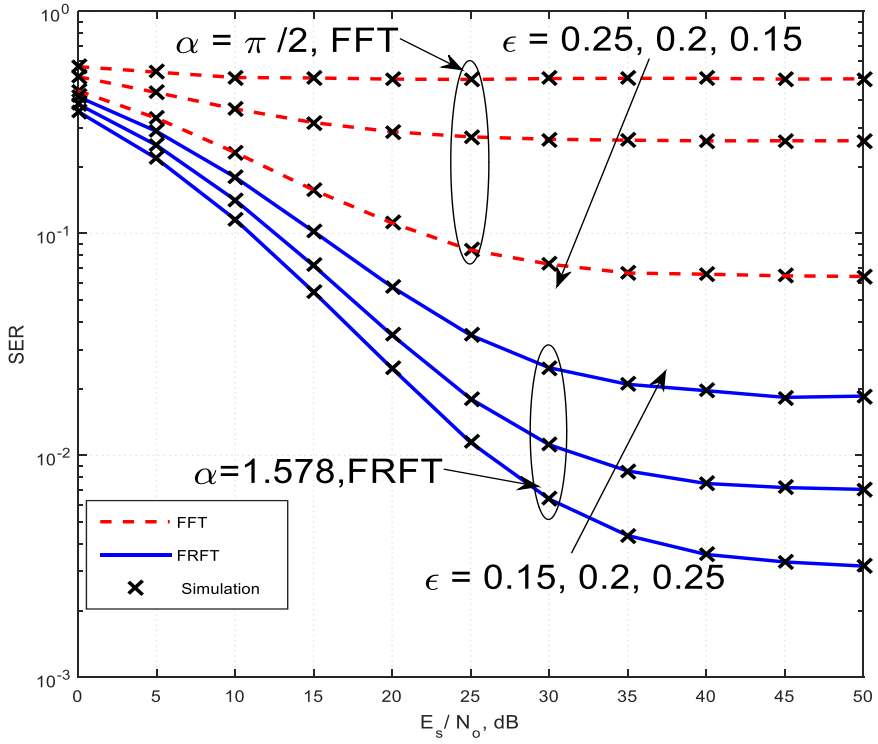

Fig. 3.2.2.3.1 SER for QPSK in FrFT-OFDM over frequency selective Rayleigh fading channel with $N = 16$ sub-carriers and $L = 2$ taps.

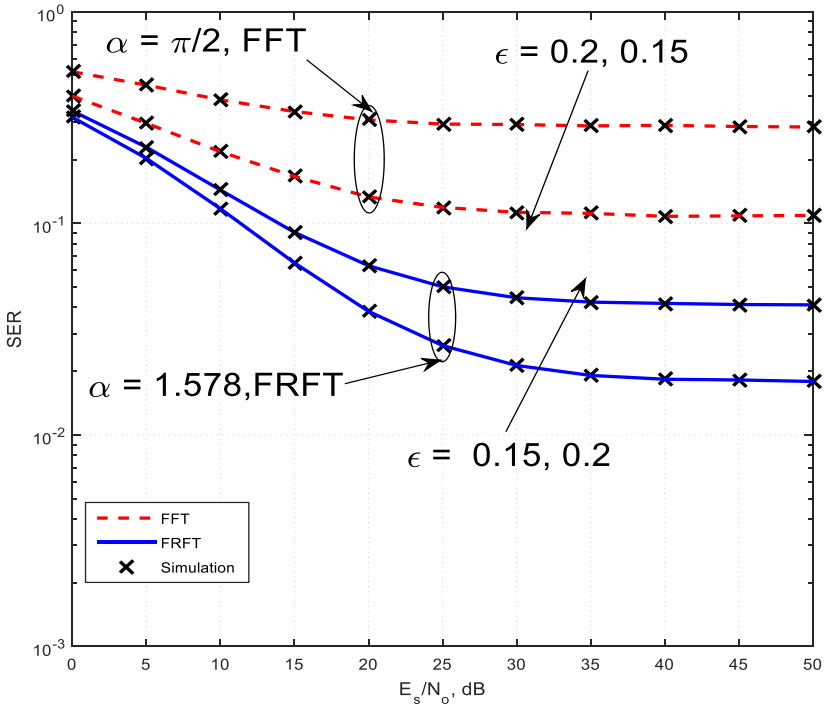

Fig. 3.2.2.3.2 SER for QPSK in FrFT-OFDM over frequency selective Rayleigh fading channel with $N = 16$ sub-carrier and $L = 5$ taps.

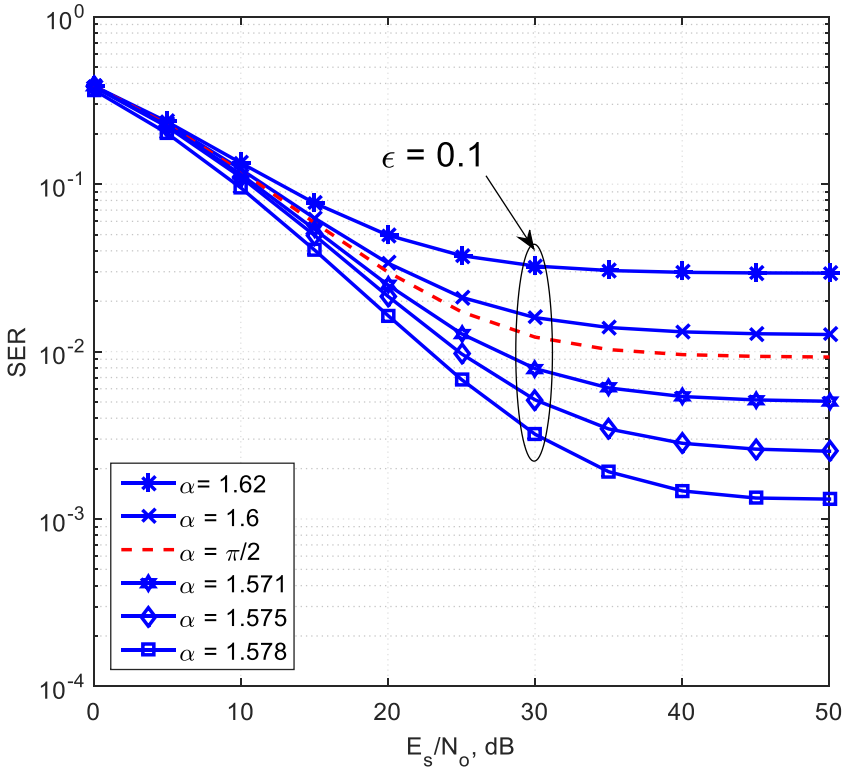

Fig. 3.2.2.3.3 SER for QPSK in FrFT-OFDM over frequency selective Rayleigh fading channel with $N = 8$ sub-carriers and $L = 2$ taps for different values of α.

3.3. DISCUSSION OF SIMULATED RESULTS

Fig. 3.2.1.1.1 BER/SER Comparison between FFT and FrFT -based OFDM system in presence of CFO BPSK/QPSK in AWGN channel with $N = 8$. The results show that at $\alpha = \frac{\pi}{2}$, FrFT -based OFDM system performs similar to one based on FFT. **Fig. 3.2.1.1.2** shows the analytical BER results for AGWN channel with $N = 8$ for BPSK modulation scheme in presence of CFO for FrFT -based OFDM system. The analytical results given with different values of CFO in (3.2.1.1.5) is perfectly match with simulation result. **Fig. 3.2.2.1.1** shows the analytical BER results for AGWN channel with $N = 8$ for QPSK modulation scheme in presence of CFO for FrFT -based OFDM system. where the analytical results given with different values of CFO in (3.2.2.1.9) is perfectly match with simulation result. **Fig. 3.2.1.2.1** shows the analytical BER results for Flat fading channel with $N = 8$ for BPSK modulation scheme in presence of CFO for FrFT -based OFDM system. where the analytical results given with different values of CFO in (3.2.1.2.5) is perfectly match with simulation result. **Fig. 3.2.2.2.1** shows the analytical BER results for Flat fading channel with $N = 8$ for QPSK

modulation scheme in presence of CFO for FrFT -based OFDM system. where the analytical results given with different values of CFO in (3.2.2.2.3) is perfectly match with simulation result. **Fig. 3.2.1.3.1** shows the analytical BER results for frequency selective Rayleigh fading channel with $N = 8$ sub-carriers and $L = 2$ taps, for BPSK modulation scheme in presence of CFO for FrFT -based OFDM system. where the analytical results given with different values of CFO in (3.2.1.3.11) is perfectly match with simulation result. **Fig. 3.2.1.3.2** shows the analytical BER results for frequency selective Rayleigh fading channel with $N = 8$ sub-carriers and $L = 2$ taps, for BPSK modulation scheme in presence of CFO for FrFT -based OFDM system. where the analytical results given with different values of FrFT angle parameter α with CFO=0.15 is perfectly match with simulation result. **Fig. 3.2.2.3.1** shows the analytical SER results for frequency selective Rayleigh fading channel with $N = 16$ sub-carriers and $L = 2$ taps, for QPSK modulation scheme in presence of CFO for FrFT -based OFDM system. where the analytical results given with different values of CFO in (3.2.2.3.8) is perfectly match with simulation result. **Fig. 3.2.2.3.2** shows the analytical SER results for frequency selective Rayleigh fading channel with $N = 16$ sub-carriers and $L = 5$ taps, for QPSK modulation scheme in presence of CFO for FrFT -based OFDM system. where the analytical results given with different values of CFO is perfectly match with simulation result. **Fig. 3.2.2.3.3** shows the analytical SER results for frequency selective Rayleigh fading channel with $N = 8$ sub-carriers and $L = 2$ taps, for QPSK modulation scheme in presence of CFO for FrFT -based OFDM system. where the analytical results given with different values of α and single value of CFO=0.1 is perfectly match with the simulation result. From this we can say that some values of α. Performance of FrFT -based OFDM system is better than FFT -based OFDM system. This study confirms that FrFT -based OFDM system prevails because its BER can be controlled by varying FrFT order under the effect of CFO. This study confirms that FrFT -based OFDM system prevails because its BER can be controlled by varying FrFT order under the effect of CFO.

3.4. SUMMARY OF BER EXPRESSION FOR FrFT-BASED OFDM

In this chapter, BER expression derived for FrFT -based OFDM system in presence of CFO for BPSK and QPSK modulation schemes in AWGN, Flat and Rayleigh Frequency selective fading channel. The performance of BPSK and QPSK modulation schemes are considered with the new mathematical formulation introduced here for frequency flat, AWGN channels and frequency selective channel. At $\alpha = \pi/2$ FrFT -based OFDM system is

equivalent to one based on FFT, and some values of α, performance of FrFT -based OFDM system is better than FFT -based OFDM system. This study confirms that FrFT -based OFDM system prevails because its BER can be controlled by varying FrFT order under the effect of CFO.

However, it is obvious that the analytical expressions are easy to evaluate when the number of subcarriers are sufficiently low (i.e. N = 8, 16, 32). For fairly high number of subcarriers, the exponential computational complexity associated with the analytical results suggests the use of simulation based approach to find the approximate BER/SER values. This is a trade-off between computational efficiency and analytical exactness of our approach.

- ***Proposed Expressions of BER/SER in presence of CFO for FrFT based- OFDM given by A. Kumar*** *et al.* **[50, 51, 53]:**

3.4.1. In AWGN Channel

3.4.1.1 BPSK modulation:

$$P_b(k) = \frac{1}{2^{N-1}} \sum_{k=1}^{2^{N-1}} Q\left(\sqrt{2\gamma}\,\beta_k\right) + Q\left(\sqrt{2\gamma}\,\delta_k\right) \tag{3.4.1.1.1}$$

The parameters used in eq.(3.4.1.1.1) are given in [50].

3.4.1.2 QPSK modulation:

$$P_b(\varepsilon) = 1 - \frac{1}{2^{2N-2}} \sum_{k=1}^{2^{N-2}} \sum_{n=1}^{2^{N-2}} \sum_{m=1}^{4} \left\{Q\left(-\sqrt{2\gamma}\ \Psi_{kn}[1,m]\right) \times Q\left(-\sqrt{2\gamma}\ \Psi_{kn}[1,m]\right)\right\} \tag{3.4.1.2.1}$$

The parameters used in eq.(3.4.1.2.1) is define [50].

3.4.2. In frequency selective fading channel

3.4.2.1 BPSK modulation:

$$P_b(\varepsilon) = \frac{1}{2} - \frac{1}{2^N} \sum_{k=1}^{2^{N-2}} \left\{ A_1 \sqrt{\frac{\gamma 2\sigma^2 [\Re(S(0,0) + z_k)]^2}{1 + \gamma([\Re(S(0,0) + z_k)]^2 + a_k)}} + F_2 \sqrt{\frac{\gamma [\Re(S(0,0) - z_k)]^2}{1 + \gamma([\Re(S(0,0) - z_k)]^2 + b_k)}} \right\} \tag{3.4.2.1.1}$$

where $A_1 = sgn([S(1) + a_k])$ and $A_2 = sgn([S(1) - a_k])$. The other parameters used in eq.(3.4.2.1.1) are given in [51].

3.4.2.2 QPSK modulation:

$$P_s(\xi) = \frac{3}{4} - \frac{1}{2^{2N-1}} \sum_{k=1}^{2^{N-2}} \sum_{n=1}^{2^{N-2}} \sum_{m=1}^{4} \sqrt{\frac{C_{\beta(0)\beta(0)}\,\rho}{2 + \rho v_{k,n}[m] + C_{\beta(0)\beta(0)}\,\rho {\psi^2}_{k,n}[1,m]}} \cdots$$
$$\psi_{k,n}[1,m]\left(\frac{1}{2} + \frac{1}{\pi}\,\mathrm{atan}\left\{\sqrt{\frac{C_{\beta(0)\beta(0)}\,\rho}{2 + \rho\varphi_{k,n}[m] + C_{\beta(0)\beta(0)}\,\rho {\psi^2}_{k,n}[1,m]}}\;\psi_{k,n}[2,m]\right\}\right)$$
$$+ \sqrt{\frac{C_{\beta(0)\beta(0)}\,\rho}{2 + \rho v_{k,n}[m] + C_{\beta(0)\beta(0)}\,\rho {\psi^2}_{k,n}[2,m]}} \cdots$$
$$\psi_{k,n}[2,m]\left(\frac{1}{2} + \frac{1}{\pi}\,\mathrm{atan}\left\{\sqrt{\frac{C_{\beta(0)\beta(0)}\,\rho}{2 + \rho v_{k,n}[m] + C_{\beta(0)\beta(0)}\,\rho {\psi^2}_{k,n}[2,m]}}\;\psi_{k,n}[1,m]\right\}\right) \quad (3.4.2.2.1)$$

where $\rho = E_s/N_0$ is the signal-to-noise ratio and $\psi_{k,n}[i,m]$ is the $(i,m)^{th}$ entry of the 2×4 matrix $\mathbf{\Psi} = \mathbf{D}\otimes\mathbf{1}_{1\times4} + \mathbf{W}$, in which $\otimes$ is the Kronecker product and $\mathbf{1}_{1\times4}$ is a 1×4 vectors of 1s, and $\mathrm{D} = \begin{pmatrix}\mathrm{D_A} & \mathrm{D_B}\end{pmatrix}^{\mathrm{T}}$. The term $\mathrm{v_{k,n}[m]}$ is the m-th element of the 1×4 vector $\mathrm{v} = (\mathrm{v_1}\ \mathrm{v_2}\ \mathrm{v_3}\ \mathrm{v_4})$, where $\mathrm{v_i} = \xi_i^{\mathrm{T}}\Lambda\mathrm{C}_{\beta|\beta(0)}\Lambda\xi_i$, $\xi_1 = \mathrm{e_k}+\mathrm{e_k}$, $\xi_2 = -\mathrm{e_k}-\mathrm{e_k}$, $\xi_3 = \mathrm{e_k}-\mathrm{e_k}$, $\xi_4 = -\mathrm{e_k}+\mathrm{e_k}$. Substituting $\alpha = \pi/2$ in $\mathrm{S(q,k)}$ and $\mathrm{C}_{\beta(0)\beta(0)} = 2\sigma^2$ in (3.5.2.2.1) we get the probability of symbol error expression of QPSK for conventional OFDM system given in [37]. This is in conformity of the fact that FrFT based OFDM is a generalization of conventional OFDM system.

****

CHAPTER-IV

HARDWARE IMPLEMENTATION

Topics:

4.1. Introduction

4.2. Fixed Point Design

4.2.1. CORDIC Theory and Survey

4.2.2. CORDIC Algorithms

4.2.2.1. CORDIC Trigonometric Algorithms

4.2.2.1.1 Sine and Cosine

4.2.2.1.2 Inverse Sine and Cosine

4.2.2.2. CORDIC Algorithm for Hyperbolic Functions

4.3. Simulink HDL Coder Tools

4.3.1. Target-independent HDL Code Generation also optimizing HDL code

4.3.2. Synthesis and Analysis of HDL code

CHAPTER-4 HARDWARE IMPLEMENTATION

This chapter contains three sections: first discusses about the fixed point design and Historical development of cordic theory. After that, by using the "HDL coder" the HDL code is generated and also optimize the code through the HDL workflow Advisor. Finally, FPGA in the Loop co-simulation is run with the Xilinx ZYNQ SoC FPGA by using the HDL Verifier Toolbox, for Verification of HDL code by putting in FPFA in LOOP.

4.1. INTRODUCTION

The current trend toward hardware intensive signal processing has uncovered a relative lack of understanding of hardware signal processing architectures. Many hardware efficient algorithms exist, among these algorithms there is a set of shift-add algorithms collectively known as Coordinate Rotation Digital Computer (CORDIC) for computing a wide range of functions including certain trigonometric, hyperbolic, linear and logarithmic functions and explain commonly used functions that may be accomplished using a CORDIC architecture and how the algorithms work. In this chapter focused on the hardware implementation of FrFT based- OFDM system in FPGAs by following the HDL coder and HDL verifier tool.

4.2. FIXED POINT DESIGN

4.2.1 Cordic Survey and Theory

The digital signal processing landscape has long been dominated by microprocessors with enhancements such as single cycle multiply-accumulate instructions and special addressing modes. While these processors are low cost and offer extreme flexibility, they are often not fast enough for truly demanding DSP tasks. The advent of reconfigurable logic computers permits the higher speeds of dedicated hardware solutions at costs that are competitive with the traditional software approach. Unfortunately, algorithms optimized for these microprocessor based systems do not usually map well into hardware. While hardware-efficient solutions often exist, the dominance of the software systems has kept those solutions out of the spotlight. Among these hardware efficient algorithms there is a class of iterative solutions for trigonometric and other transcendental functions that use only shifts and adds to perform operations. The trigonometric functions are based on vector rotations, while other functions such as square root are implemented using an incremental expression of the desired function. The trigonometric algorithm is called CORDIC. The incremental functions are

performed with a very simple extension to the hardware architecture. The CORDIC algorithms generally produce one additional bit of accuracy for each iteration.

The trigonometric CORDIC algorithms were originally developed as a digital solution for real-time navigation problems. The original work is credited to **Jack Volder** [48 and 49]. Extensions to the CORDIC theory based on work by **John Wahher** [55] and others provide solutions to a broader class of functions. The CORDIC algorithm has found its way into diverse applications including the 8087 math coprocessor, radar signal processors [56] and robotics. CORDIC rotation has also been proposed for computing Discrete Fourier [48], Discrete Cosine [48] and Chirp-Z [49] transforms.

All of the trigonometric functions can be computed or derived from functions using vector rotations. Vector rotation can also be used for polar to rectangular and rectangular to polar conversions, for vector magnitude, and as a building block in certain transforms such as the DFT. The CORDIC algorithm provides an iterative method of performing vector rotations by arbitrary angles using only shifts and adds. The algorithm, credited to **Volder** [48], is derived from the general rotation transform-

$$x' = x\cos\alpha - y\sin\alpha \qquad (4.2.1.1)$$

$$y' = y\cos\alpha + x\sin\alpha \qquad (4.2.1.2)$$

Which rotates a vector in a Cartesian plane by the angle α. These can be rearranged so that-

$$x' = \cos\alpha\,[x - y\tan\alpha] \qquad (4.2.1.3)$$

$$y' = \cos\alpha\,[y + x\tan\alpha] \qquad (4.2.1.4)$$

However, if the rotation angles are restricted so that $\tan(\alpha) = \pm 2^{-i}$, the multiplication by the tangent term is reduced to simple shift operation. Arbitrary angles of rotation are obtainable by performing a series of successively smaller elementary rotations. If the decision at each iteration i is which direction to rotate rather than whether or not to rotate, then the $\cos(\delta_i)$ term becomes a constant. Then the iterative rotation can now be expressed as-

$$x_{i+1} = K_i\,[x_i - y_i.d_i\,2^{-i}] \qquad (4.2.1.5)$$

$$y_{i+1} = K_i\,[y_i + x_i.d_i\,2^{-i}] \qquad (4.2.1.6)$$

where $K_i = \cos(\tan^{-1}2^{-i}) = 1/\sqrt{1+2^{-2i}}$ and $d_i = \pm 1$. Removing the scale constant from the iterative equations yields a shift-add algorithm for vector rotation. The product of the $K_i's$ can be applied elsewhere in the system or treated as part of a system processing gain. That product approaches 0.6073 as the number of iterations goes to infinity. Therefore, the

rotation algorithm has a gain A_n of approximately 1.647. The exact gain depends on the number of iterations and obeys the relation

$$A_n = \prod_n \sqrt{1 + 2^{-2i}} \tag{4.2.1.7}$$

The angle of a composite rotation is uniquely defined by the sequence of directions of the elementary rotations. That sequence can be represented by a decision vector. The set of all possible decision vectors is an angular measurement system based on binary arctangents. Conversions between this angular system and any other can be accomplished using a look-up. A better conversion method uses an additional adder-subtract or that accumulates the elementary rotation angles at each iteration. The elementary angles can be expressed in any convenient angular unit. Those angular values are supplied by a small lookup table (one entry per iteration) or are hardwired, depending on the implementation. The angle accumulator adds a third difference equation to the CORDIC algorithm-

$$Z_{i+1} = Z_i - d_i \tan^{-1}(2^{-i}) \tag{4.2.1.8}$$

Obviously, in cases where the angle is useful in the arctangent base, this extra element is not needed, the CORDIC rotator is normally operated in one of two modes. The first, called rotation by **Volker** [48] rotates the input vector by a specified angle (given as an argument). The second mode, called vectoring which rotates the input vector to the x-axis while recording the angle required making that rotation. In rotation mode, the angle accumulator is initialized with the desired rotation angle. The rotation decision at each iteration is made to diminish the magnitude of the residual angle in the angle accumulator. The decision at each iteration is therefore based on the sign of the residual angle after each step. Naturally, if the input angle is already expressed in the binary arctangent base, the angle accumulator may be eliminated. For rotation mode, the CORDIC equations are-

$$x_{i+1} = x_i - y_i . d_i \, 2^{-i} \tag{4.2.1.9}$$

$$y_{i+1} = y_i + x_i . d_i \, 2^{-i} \tag{4.2.1.10}$$

$$Z_{i+1} = Z_i - d_i \tan^{-1}(2^{-i}) \tag{4.2.1.11}$$

where $d_i = -1$ if $Z_i < 0, +1$ Otherwise. Which provides the following result-

$$x_n = A_n[x_0 \cos Z_0 - y_0 \sin Z_0] \tag{4.2.1.12}$$

$$y_n = A_n[y_0 \cos Z_0 + x_0 \sin Z_0] \tag{4.2.1.13}$$

$$Z_n = 0 \tag{4.2.1.14}$$

$$A_n = \prod_n \sqrt{1 + 2^{-2i}} \tag{4.2.1.15}$$

In the vectoring mode, the CORDIC rotator rotates the input vector through whatever angle is necessary to align the result vector with the x-axis. The result of the vectoring operation is a rotation angle and the scaled magnitude of the original vector. The vectoring function works by seeking to minimize the y component of the residual vector at each rotation. The sign of the residual y component is used to determine which direction to rotate next. If the angle accumulator is initialized with zero, it will contain the traversed angle at the end of the iterations. In vectoring mode, the CORDIC equations are-

$$x_{i+1} = x_i - y_i . d_i \, 2^{-i} \tag{4.2.1.16}$$

$$y_{i+1} = y_i + x_i . d_i \, 2^{-i} \tag{4.2.1.17}$$

$$Z_{i+1} = Z_i - d_i \, \tan^{-1}(2^{-i}) \tag{4.2.1.18}$$

where $d_i = +1$ if $x_i < 0, -1$ Otherwise and $x_n = A_n \sqrt{x_0^2 + y_0^2}$, $y_n = 0$, $Z_n = Z_0 + \tan^{-1}(y_0/x_0)$ and $A_n = \prod_n \sqrt{1 + 2^{-2i}}$

The CORDIC rotation and vectoring algorithms as stated are limited to rotation angles between $-\frac{\pi}{2}$ and $\frac{\pi}{2}$. This limitation is due to the use of 2° for the tangent in the first iteration. For composite rotation angles larger than$\frac{\pi}{2}$, an additional rotation is required. **Volder** *et al.* [4] describes an initial rotation $\frac{\pi}{2}$. This gives the correction iteration-

$$x' = d.y \tag{4.2.1.19}$$

$$y' = d.x \tag{4.2.1.20}$$

$$Z' = Z + d.\frac{\pi}{2} \tag{4.2.1.21}$$

where $d = +1$ if $y < 0, -1$ otherwise. There is no growth for this initial rotation. Alternatively, an initial rotation of either π or 0 can be made, a voiding the reassignment of the x and y components to the rotator elements. Again, there is no growth due to the initial rotation-

$$x' = d.x \tag{4.2.1.22}$$

$$y' = d.y \tag{4.2.1.23}$$

$Z' = Z$ If $d = +1$ or $Z - \pi$ if $d = -1, d = -1$ If $x < 0, +1$ otherwise

Both reduction forms assume a module 2π representation of the input angle. The style of first reduction is more consistent with the succeeding rotations, while the second reduction may be more convenient when wiring is restricted, as is often the case with FPGAs.

The CORDIC rotator described is usable to compute several trigonometric functions directly and others indirectly. Choice of initial values and modes permits direct computation of sine, cosine, arctangent, vector magnitude and transformations between polar and Cartesian coordinates.

4.2.2 Cordic Algorithms

4.2.2.1 Trigonometric Cordic Algorithms

4.2.2.1.1 Sine and Cosine

The rotational mode CORDIC operation can simultaneously compute the sine and cosine of the input angle. Setting the y component of the input vector to zero reduces the rotation mode result -

$$x_n = A_n[x_0 \cos Z_0] \quad (4.2.2.1.1.1)$$

$$y_n = A_n[x_0 \ \sin Z_0] \quad (4.2.2.1.1.2)$$

By setting x_0 equal to $1/A_n$, the rotation produces the unscaled sine and cosine of the angle argument Z_0. The sine and cosine values modulate a magnitude value using the look up table requires a pair of multipliers to obtain the modulation. The CORDIC technique performs the multiply as part of the rotation operation, and therefore eliminates the need for a pair of explicit multipliers. The output of the CORDIC rotator is scaled by the rotator gain. If the gain is not acceptable, a single multiply by the reciprocal of the gain constant placed before the CORDIC rotator will yield unscaled results. It is worth noting that the hardware complexity of the CORDIC rotator is approximately equivalent to that of a single multiplier with the same word size.

A logical extension to the sine and cosine is a polar to Cartesian coordinate transformer. The transformation from polar to Cartesian space is defined as-

$$x = r\cos\theta \quad (4.2.2.1.1.3)$$

$$y = r\sin\theta \quad (4.2.2.1.1.4)$$

As pointed out above, the multiplication by the magnitude comes for free using the CORDIC rotator. The transformation is accomplished by selecting the rotation mode with x_0 = polar magnitude, Z_0= polar phase and $y_0 = 0$. The vector result represents the polar input

transformed to Cartesian space. The transform has a gain equal to the rotator gain, which needs to be accounted for somewhere in the system. If the gain is unacceptable, the polar magnitude may be multiplied by the reciprocal of the rotator gain before it is presented to the CORDIC rotator.

4.2.2.1.2 Inverse Sine and Cosine

In most cases, if a function can be generated by a CORDIC, its inverse can also be computed. Unless the inverse is calculable by changing the mode of the rotator, its computation normally involves comparing the output to a target value. The CORDIC inverse is illustrated by the Arcsine and Arccosine function. The Arcsine and Arccosine can be computed by starting with a unit vector on the positive x axis, then rotating it so that its y component is equal to the input argument. The arcsine is then the angle subtended to cause the y component of the rotated vector to match the argument. The decision function in this case is the result of a comparison between the input value and the y component of the rotated vector at each iteration-

$$x_{i+1} = x_i - y_i . d_i \, 2^{-i} \qquad (4.2.2.1.2.1)$$

$$y_{i+1} = y_i + x_i . d_i \, 2^{-i} \qquad (4.2.2.1.2.2)$$

$$Z_{i+1} = Z_i - d_i \, \tan^{-1}(2^{-i}) \qquad (4.2.2.1.2.3)$$

where $d_i = +1$ if $y_i < c, -1$ Otherwise and c = input argument

Rotation produces the following formula-

$$x_n = \sqrt{(A_n . x_0)^2 - c^2} \qquad (4.2.2.1.2.4)$$

$$y_n = c \qquad (4.2.2.1.2.5)$$

$$Z_n = Z_0 + \arcsin\left(c/(A_n . x_0)\right) \qquad (4.2.2.1.2.6)$$

$$A_n = \prod_n \sqrt{1 + 2^{-2i}} \qquad (4.2.2.1.2.7)$$

The arcsine function as stated above returns correct angles for inputs -1 < $(c/(A_n . x_0))$ < 1, although the accuracy suffers as the input approaches +1 (the error increases rapidly for Inputs larger than about 0.98). This loss of accuracy is due to the gain of the rotator. For angles near the y-axis, the rotator gain causes the rotated vector to be shorter than the reference (input), so the decisions are made improperly. The gain problems can be corrected using a "double iteration algorithm [49] at the cost of an increase in complexity. The Arccosine computation is similar, except the difference between the x component and the

input is used as the decision function. Without modification, the arccosine algorithm works only for inputs less than $1/A_n$, making the double iteration algorithm a necessity. The Arccosine could also be computed by using the arcsine function and subtracting $\pi/2$ from the result, followed by an angular reduction if the result is in the fourth quadrant.

4.2.2.2 Cordic Algorithm for Hyperbolic Functions

The close relationship between the trigonometric and hyperbolic functions suggests the same architecture can be used to compute the hyperbolic functions. While, there is early mention of using the CORDIC structure for hyperbolic coordinate transforms [48]. The CORDIC equations for hyperbolic rotations are derived using the same manipulations as those used to derive the rotation in the circular coordinate system. For rotation mode these are-

$$x_{i+1} = x_i - y_i . d_i \, 2^{-i} \tag{4.2.2.2.1}$$

$$y_{i+1} = y_i + x_i . d_i \, 2^{-i} \tag{4.2.2.2.2}$$

$$Z_{i+1} = Z_i - d_i \, \tan^{-1}(2^{-i}) \tag{4.2.2.2.3}$$

where $d_i = -1$ if $Z_i < 0, +1$ Otherwise. This provides the following result-

$$x_n = A_n[x_0 \cosh Z_0 - y_0 \sinh Z_0] \tag{4.2.2.2.4}$$

$$y_n = A_n[y_0 \cosh Z_0 + x_0 \sinh Z_0] \tag{4.2.2.2.5}$$

$$Z_n = 0 \tag{4.2.2.2.6}$$

$$A_n = \prod_n \sqrt{1 + 2^{-2i}} = 0.80 \tag{4.2.2.2.7}$$

In vector mode $d_i = +1$ if $y_i < 0, -1$ Otherwise, then the rotation produces-

$$x_n = A_n \sqrt{x_0^2 - y_0^2} \tag{4.2.2.2.8}$$

$$y_n = 0 \tag{4.2.2.2.9}$$

$$Z_n = Z_0 + \tanh^{-1}\left(\frac{y_0}{x_0}\right) \tag{4.2.2.2.10}$$

$$A_n = \prod_n \sqrt{1 - 2^{-2i}} \tag{4.2.2.2.11}$$

The elemental rotations in the hyperbolic coordinate system do not converge. However, it can be shown [48] that convergence is achieved if certain iterations ($I = 4, 13, 40, k, 3k + l$) are repeated.

The other trigonometry functions can be derived from the CORDIC functions-

$$tan\alpha = \frac{sin\alpha}{cos\alpha},\ tanh\alpha = \frac{sinh\alpha}{cosh\alpha},\ exp\alpha = sinh\alpha + cosh\alpha,\ ln\alpha = 2\tanh^{-1}\left(\frac{y}{x}\right)$$

where $x = \alpha + 1$ and $y = \alpha - 1$.

Embedded MATLAB Function Block also employs fixed-point arithmetic via fixed point function (fi) function that is in Fixed-Point Toolbox. By using this tool, we can select the value of "word length", "fractional length" and the "signed or unsinged" for the fi function.

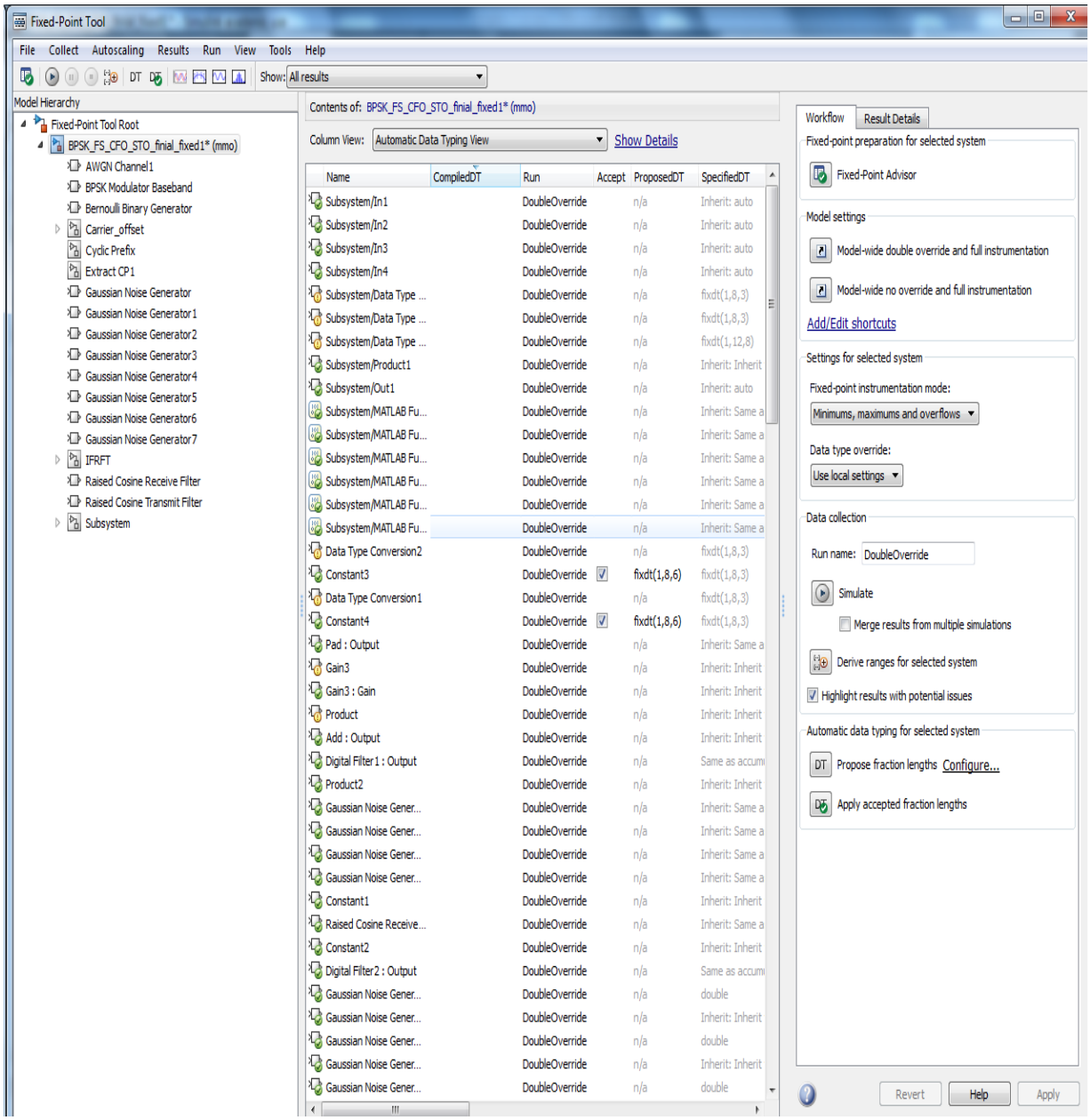

Fig. 4.2.1 Fixed-Point Tool For Proposing Fractional Length For Given Word Length

Using MATLAB "Fixed point tool" we can generate fixed point code from floating point with the help of fixed point advisor, Fixed-Point Advisor uses either the design or simulation minimum and maximum from the floating-point data to propose the initial fixed-point scaling. Using the Fixed-Point Tool's scaling function, we analyse, refine, and optimize scaling for relevant blocks in the model that we initially scaled using Fixed-Point Advisor. We use the data type override feature to collect the dynamic range of signals in double precision. The Fixed-Point Tool uses this information to propose a more suitable fixed-point scaling for each block, based on the number of available bits. Individual blocks can be locked down to prevent them from being modified by the tool. automatic scaling with individually scaled blocks and accept or reject the proposed scaling for each signal. FPGA implementation use fixed-point representations

4.3. HDL Coder Tool

Hardware implementation of FrFT based- OFDM system in this transmitter and receiver implementation is presented and simulated. The design is developed using Simulink and the RTL code is generated by the Mathworks HDL coder. We wondered how HDL Coder compares with "high-level synthesis" tools currently on the market. Indeed, much like high-level synthesis tools, HDL Coder is converting un-timed algorithms (captured in MATLAB) to specific, timed microarchitectures in HDL. High-level synthesis tools do that and quite a bit more including user-controlled architectural exploration, flexible memory generation, and interface synthesis. However, HDL Coder offers control over the most commonly used data path optimizations like pipelining, resource sharing, and loop unrolling. HDL Coder also offers both manual and automatic floating- to fixed-point conversion. That capability alone will expedite many design flows, as getting bit-widths optimized for your desired dynamic range is a bit of a tricky art all in itself.

4.3.1 Target- Independent HDL Code Generation and Optimization

Simulink HDL Coder is high level design tool which generates synthesizable HDL codes, such as VHDL and Verilog, from HDL code from Matlab function, Simulink models and State flow finite state machines. Simulink HDL coder also provides interfaces to combine manually written HDL codes. It supports both FPGA and ASIC implementations. It is able to generate the corresponding testbench. Working together with Mathworks HDL verifier, it is also capable to verify the design and do FPGA-in-the-loop simulation. Assisted by its workflow adviser, users can easily generate the HDL codes by simple configuration.

Furthermore, HDL coder provides options on loop optimization and streaming optimization. Multichannel designs are also supported. According to the type of the high level model, the workflow of the HDL coder has two types: Matlab workflow and Simulink workflow.

A user uses Simulink HDL Coder via the following steps-

1) First creates a Simulink design or the mat lab function to simulate a desired application
2) If the simulation requirements are met, then runs the Simulink HDL Coder compatibility checker for the designs' suitability for HDL code generation
3) The co-simulates the design within Simulink using Zed board with zynq software support package with following setting

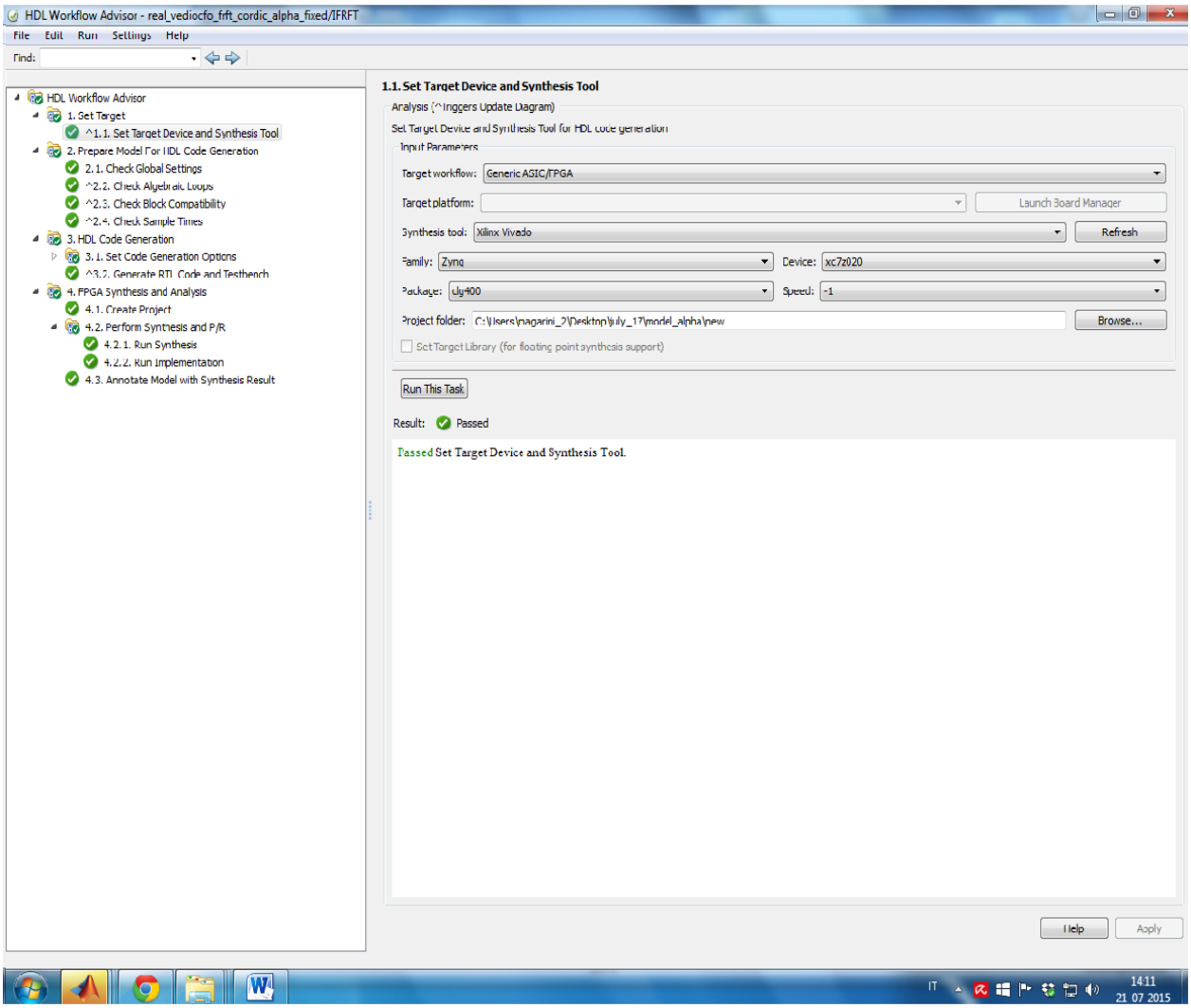

Fig. 4.3.1.1 Workflow Advisor For configure the The Zed Board

4) If Simulink design is compatible to generate HDL code, then runs Simulink HDL coder to generate HDL files for the design as well as a testbench in either Verilog or VHDL which are bit-true and cycle accurate
5) Now, by using testbench and HDL simulation tools to test the generated design
6) If the user is satisfied with the design, then export HDL codes to synthesis and layout tools for real hardware implementation. Simulink HDL coder also generates required scripts for the synthesis tools.

Code Generation file give more flexibility for generating the overall or some part of the design by specifying some of the properties of certain blocks in the beginning, saving them in persistent form and reusing them if desired in the future designs. A code generation control file is simply Matlab (.m) file and currently supports selection and action statements. A user selects a group of blocks within a model, block type and location need to be defined, with selection commands. By choosing different implementation methods for the blocks which might include optimization for speed and/or area and specifying the stages for generation of Output pipeline stages. A code generation control file is attached to the design and executed when code generation process is invoked. If no specifications are provided, a default code generation file is created.

Simulink HDL coder provides a detailed code generation report which eases for the traceability of hundred lines of codes generated automatically. Simulink HDL coder provides two types of linkage between the model and generated HDL code. Code-to-model and Model-to-code are hyperlinks, let user to view the blocks or subsystems from which the code was generated and generated code for any block in the model respectively.

Simulink HDL Coder also provides Embedded MATLAB Function Block which automatically generates HDL code from a MATLAB (.m) file. Embedded MATLAB Function Block also employs fixed-point arithmetic via fi function that is in Fixed-Point Toolbox.

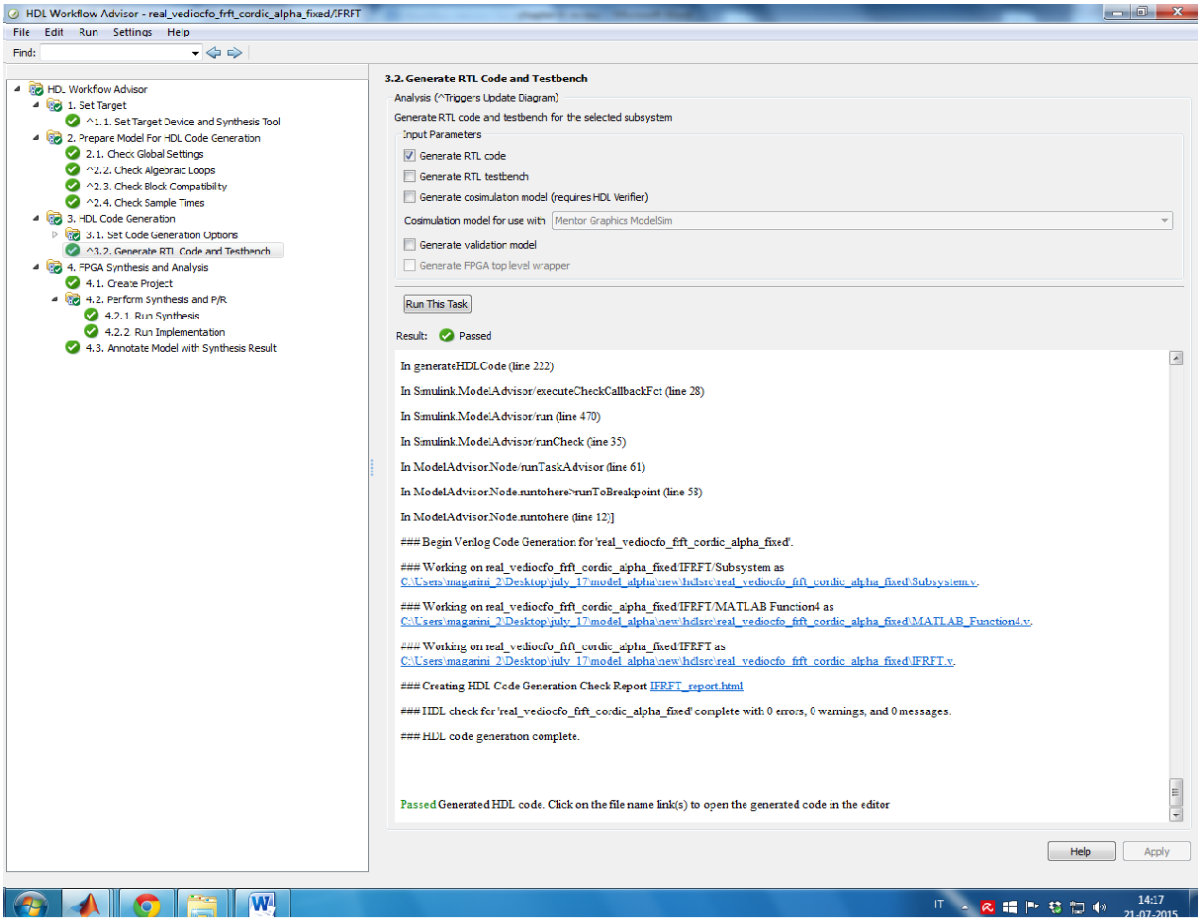

Fig. 4.3.1.2 HDL Code Generation Using Zed Board

4.3.2 Synthesis and Analysis of HDL code

The Synthesis and Simulation Design tool provides an overview of designing Field Programmable Gate Array (FPGA) devices using a Hardware Description Language (HDL). After the generation and optimization of HDL coder our next goal is to synthesis the HDL code through the zed board with Vivado® Design Suite, The Vivado® Design Suite environment enables a rapid product development for software, hardware and systems engineers because after the synthesis we can find the resources requirement for this design. During the synthesis, several steps perform. In this I will discuss the result of each step for both FrFT and IFrFT kernel.

❖ **Report RTL Partitions IFrFT Block :**

Start RTL Hierarchical Component Statistics

```
Hierarchical RTL Component report
Module IFRFT-

+---Multipliers:
                        21x43 Multipliers: = 1
                        15x35 Multipliers: = 15
                        15x33 Multipliers: = 15
+---Muxes:
           2 Input     21 Bit        Muxes: = 34
           2 Input     18 Bit        Muxes: = 27
           2 Input     17 Bit        Muxes: = 2
           2 Input     16 Bit        Muxes: = 40
           3 Input     16 Bit        Muxes: = 2
           2 Input     15 Bit        Muxes: = 6
           2 Input     14 Bit        Muxes: = 2
           2 Input     13 Bit        Muxes: = 1
           2 Input     12 Bit        Muxes: = 1
           2 Input     11 Bit        Muxes: = 2
           2 Input     10 Bit        Muxes: = 1
           2 Input      9 Bit        Muxes: = 1
           2 Input      8 Bit        Muxes: = 1
           2 Input      7 Bit        Muxes: = 1
           2 Input      6 Bit        Muxes: = 1
           2 Input      5 Bit        Muxes: = 1
           2 Input      4 Bit        Muxes: = 1
           2 Input      3 Bit        Muxes: = 1
           2 Input      2 Bit        Muxes: = 5
           3 Input      1 Bit        Muxes: = 1
           2 Input      1 Bit        Muxes: = 1
```

Report Check Net list:

```
+------+------------------+-------+---------+-------+------------------+
|      |Item              |Errors |Warnings |Status |Description       |
+------+------------------+-------+---------+-------+------------------+
|1     |multi_driven_nets |      0|        0|Passed |Multi driven nets |
+------+------------------+-------+---------+-------+------------------+
```

Start Writing Synthesis Report

```
Report BlackBoxes:
+-+--------------+----------+
| |BlackBox name |Instances |
+-+--------------+----------+
+-+--------------+----------+

Report Cell Usage:
+------+--------+------+
|      |Cell    |Count |
+------+--------+------+
|1     |CARRY4  |  2756|
|2     |DSP48E1 |    18|
|3     |LUT1    |  1950|
|4     |LUT2    |  3701|
|5     |LUT3    |  4662|
|6     |LUT4    |  3055|
|7     |LUT5    |  2408|
|8     |LUT6    |  1646|
```

```
+------+--------+------+
Report Instance Areas:
+------+--------------------+-----------------+------+
|      |Instance            |Module           |Cells |
+------+--------------------+-----------------+------+
|1     |top                 |                 | 20196|
|2     |  u_MATLAB_Function4 |MATLAB_Function4 | 20028|
+------+--------------------+-----------------+------+
-------------------------------------------------------------------------
------
Finished Writing Synthesis Report: Time (s): cpu = 00:00:57; elapsed =
00:01:00. Memory (MB): peak = 860.461; gain = 729.453.
```

❖ **Report RTL Partitions FrFT Block :**

Start RTL Hierarchical Component Statistics

```
Hierarchical RTL Component report
Module FrFT-
+---Multipliers:
                       21x43 Multipliers: = 1
                       15x32 Multipliers: = 30
+---Muxes:
           2 Input     21 Bit        Muxes: = 34
           2 Input     18 Bit        Muxes: = 27
           2 Input     17 Bit        Muxes: = 2
           3 Input     16 Bit        Muxes: = 2
           2 Input     16 Bit        Muxes: = 40
           2 Input     15 Bit        Muxes: = 6
           2 Input     14 Bit        Muxes: = 2
           2 Input     13 Bit        Muxes: = 1
           2 Input     12 Bit        Muxes: = 1
           2 Input     11 Bit        Muxes: = 2
           2 Input     10 Bit        Muxes: = 1
           2 Input      9 Bit        Muxes: = 1
           2 Input      8 Bit        Muxes: = 1
           2 Input      7 Bit        Muxes: = 1
           2 Input      6 Bit        Muxes: = 1
           2 Input      5 Bit        Muxes: = 1
           2 Input      4 Bit        Muxes: = 1
           2 Input      3 Bit        Muxes: = 1
           2 Input      2 Bit        Muxes: = 5
           3 Input      1 Bit        Muxes: = 1
           2 Input      1 Bit        Muxes: = 1

Report Check Net list:
+------+------------------+-------+---------+-------+------------------+
|      |Item              |Errors |Warnings |Status |Description       |
+------+------------------+-------+---------+-------+------------------+
|1     |multi driven_nets |      0|        0|Passed |Multi driven nets |
+------+------------------+-------+---------+-------+------------------+

Start Renaming Generated Instances
Report BlackBoxes:
+-+--------------+----------+
| |BlackBox name |Instances |
+-+--------------+----------+
```

```
Report Cell Usage:
+------+--------+------+
|      |Cell    |Count |
+------+--------+------+
|1     |CARRY4  |  2664|
|2     |DSP48E1 |    34|
|3     |LUT1    |  1666|
|4     |LUT2    |  3602|
|5     |LUT3    |  4422|
|6     |LUT4    |  3015|
|7     |LUT5    |  2376|
|8     |LUT6    |  1676|
+------+--------+------+

Report Instance Areas:
+------+---------------------+-----------------+------+
|      |Instance             |Module           |Cells |
+------+---------------------+-----------------+------+
|1     |top                  |                 | 19455|
|2     | u_MATLAB_Function3 |MATLAB_Function3 | 11037 |
+------+---------------------+-----------------+------+

Finished Writing Synthesis Report: Time (s): cpu = 00:00:55; elapsed =
00:00:58. Memory (MB): peak = 859.145; gain = 727.422
-------------------------------------------------------------------------------
```

4.3.3 Model Validation

After the synthesis the last step is model validation

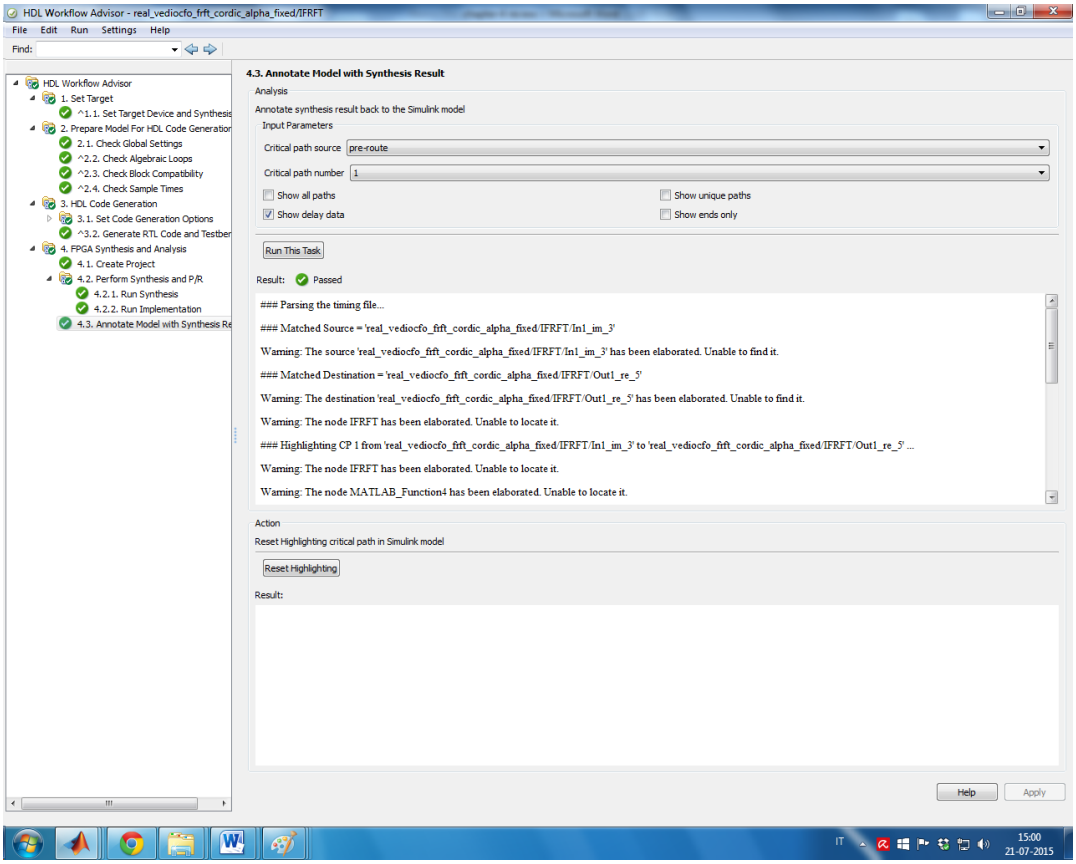

Fig. 4.3.2.1 Annotate Model With Synthesis

4.3.4 Advantages and Disadvantages of HDL coder Design

4.3.4.1 Advantages Of Simulink HDL Coder Design Tool

- Simulink HDL coder users to realize hardware directly from Simulink designs
- Simulink HDL coder provides Code Generation Control Files options that a user can specify the properties of certain blocks including different implementation methods and pipeline stages, save and reuse these control files
- Simulink HDL coder provides a detailed code generation report from code-to-model and model-to-code and lets user to add text annotations in different ways
- Simulink HDL coder user insert distributed pipeline using Embedded MATLAB Function Blocks. Inserting pipeline lets user to gain higher clock rates using pipeline registers with the price of increasing latency

4.3.4.2 Disadvantages Of Simulink HDL Coder Design Tool

- Not all the Simulink built-in blocks are supported. Code Generation Control Files are under development, therefore provides access to some certain blocks with certain capabilities
- Embedded MATLAB Function Block has its own limitations and do not support all the operations such as nested functions and use of multiple values in the left side of an expression. HDL compatibility checker that provided is only capable of processing a basic compatibility checks on this block.

Summary of the the Fixed-point tool and the HDL coder tool box:

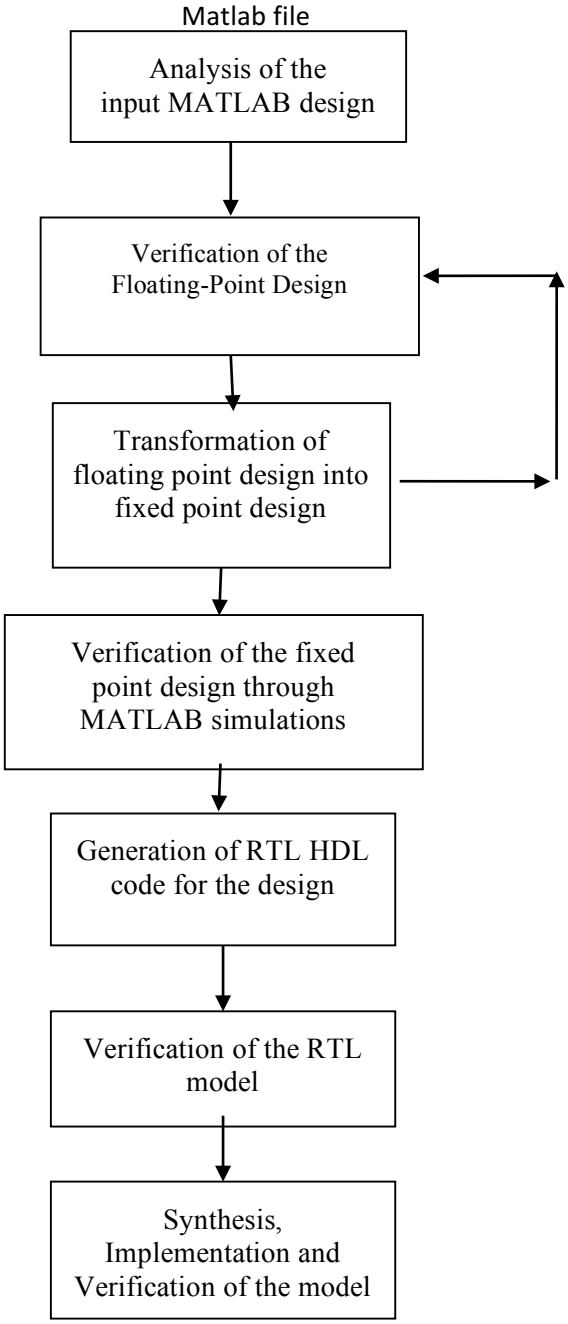

4.4. HDL Verifier tool

In this part, discussed about the HDL verifier tool after completion of the HDL coder tool. Mathworks announced "HDL Verifier Tool" which provides FPGA-based hardware-in-the-loop capabilities. This allows execution of the algorithm and evaluating to be done at hardware speeds, allowing a much more exhaustive set of stimulus and test data to be applied. From the MATLAB or Simulink and go directly to synthesizable, simulatable HDL,

and then to an FPGA-based hardware-in-the-loop prototype platform. HDL Coder can re-generate HDL, and you're back in the evaluation part of the loop quickly. This should dramatically accelerate the iteration loop for algorithmic designs or subsystems - particularly those that are data path-oriented (such as signal processing.) Auto-generation of HDL generally makes synthesis and timing closure.

Mathworks has partnered with Xilinx, has actually automated the flow, and supports a number of FPGA development boards for the hardware-in-the-loop function. All of this partnering means that you can use the most popular FPGAs and development boards, along with the most popular simulation engines, and enjoy the new capabilities of HDL Coder and HDL Verifier.

For hard-core custom chip designs, teams may still often end up doing hand-coded optimization of their HDL code. However, for most prototyping and FPGA work, HDL Coder should provide an express lane from algorithm to implementation, and it should allow us to try a lot more variations and iterations on our design before settling in on our favorite. It should also make the path from algorithm to verified hardware much more deterministic.

4.4.1 FPGA-in-the-loop verification using Xilinx (Zed board)

Hardware-in-the-Loop (HIL) has seen extensive use to test algorithms in embedded systems. More recently, HIL has become increasingly popular in the design of complex ICs and embedded system for all kinds of electronics. As FPGAs increase in capacity and performance, they more closely resemble custom ICs in terms of their capabilities, and HIL has become a necessary verification strategy for modern FPGAs. Let's consider a typical usage scenario. We start in the software simulation domain, verifying the design at a high level of abstraction. This allows us to benefit from the acceleration of much of the design yielding dramatically faster simulation iterations. As each new block is verified at the RTL level in the context of our full-chip design, its synthesized/gate-level equivalent can be moved over into the physical FPGA. Using this technology – combining conventional simulation with physical hardware and an appropriate debugging environment – it is possible to very quickly detect, isolate, identify, and resolve bugs, irrespective of where they originated in the FPGA design flow.

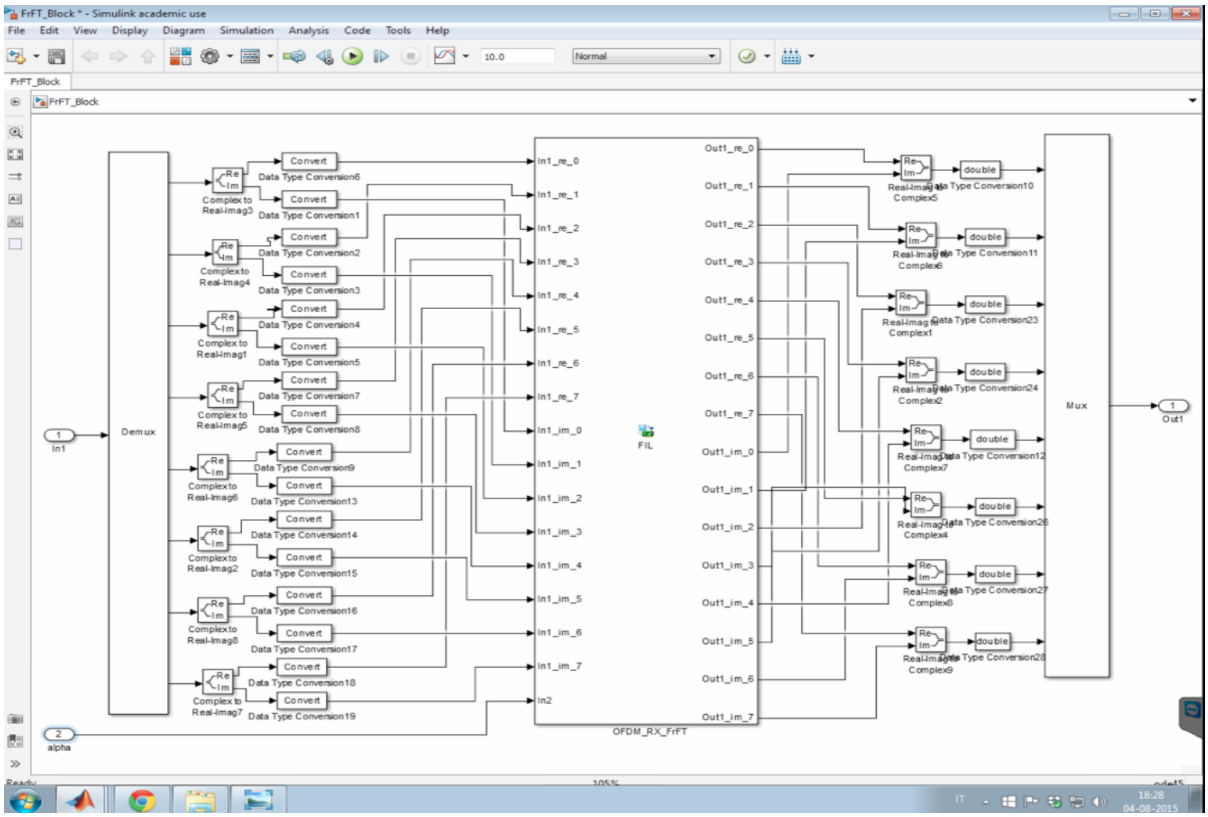

Fig. 4.4.1.1 FPGA-In-LOOP IFrFT kernel

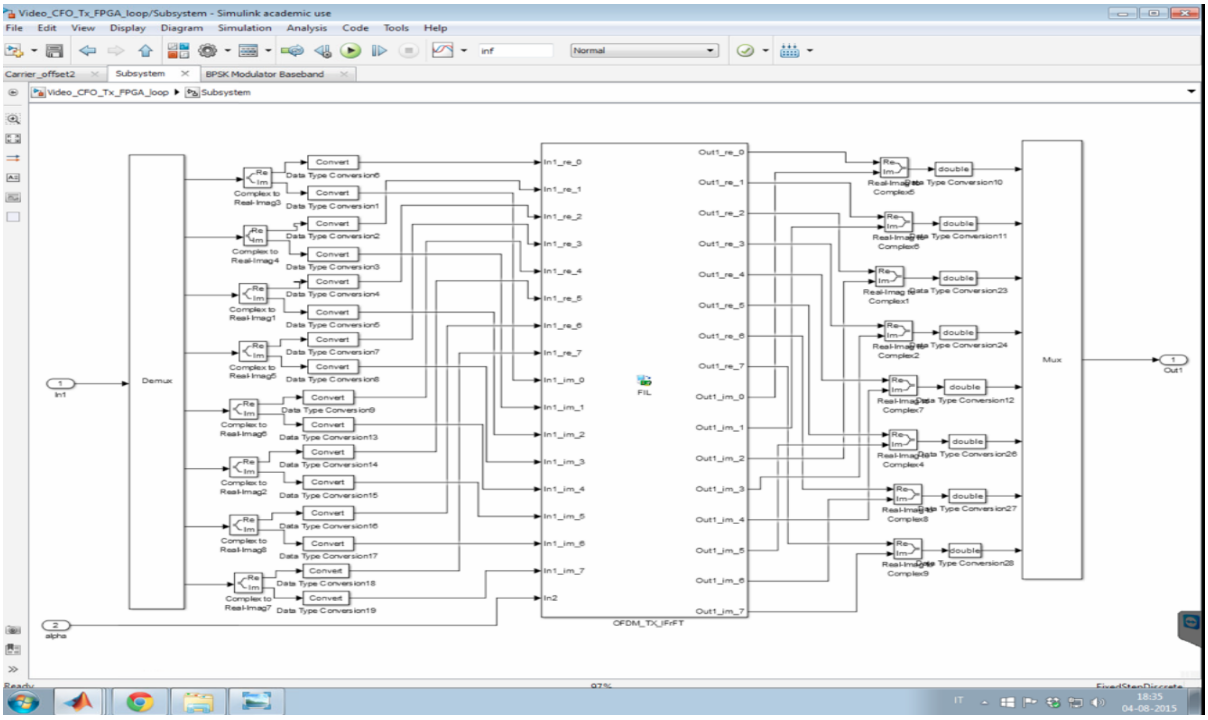

Fig. 4.4.1.2 FPGA-In-LOOP FrFT kernel

4.5. Real-time transmission of a video signal

An example of a real time Simulink model implementing an FrFT based- OFDM system for the transmission of a video signal over a frequency selective Rayleigh fading channel in presence of CFO is considered. The video signal is captured from webcam and FPGA-in-loop is used to accelerate the processing at the transmitter and receiver. In this case the students can directly observe the improved quality of the reconstructed video signal at the output of the receiver in case of FrFT based- OFDM system in comparison to an FFT based ones. The model of the implemented system is shown in Fig. 4.5.2. The demonstration of the simulation speed improvement is the main goal of this lab.

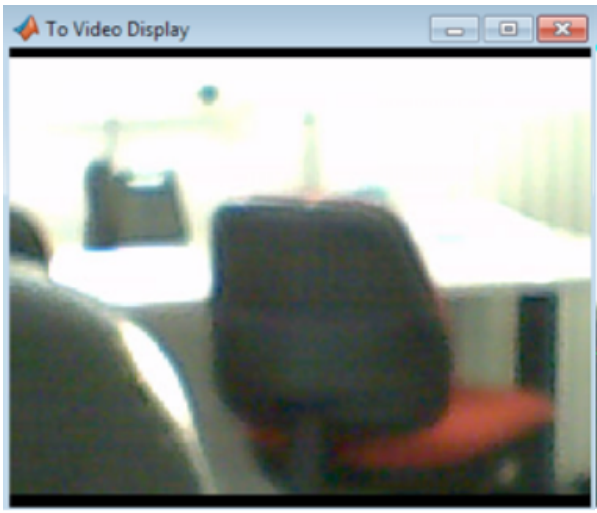

Capture Video From Webcam

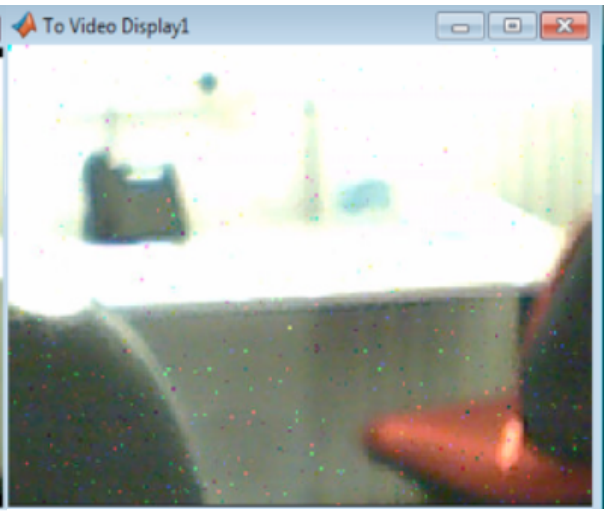

Receive Video at $\alpha = \pi/2$ (FFT based - OFDM) for SNR=40 dB at $\varepsilon = 0.1$. BER=. 00235.

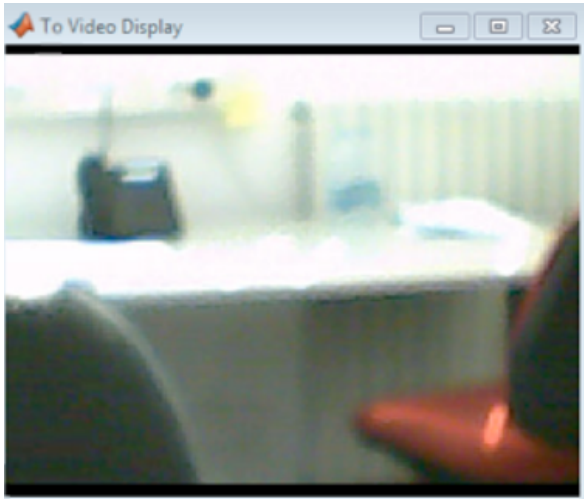

Receive Video at $\alpha = 1.584$ (FFT based - OFDM) for SNR=40 dB at $\varepsilon = 0.1$. BER=. 000318.

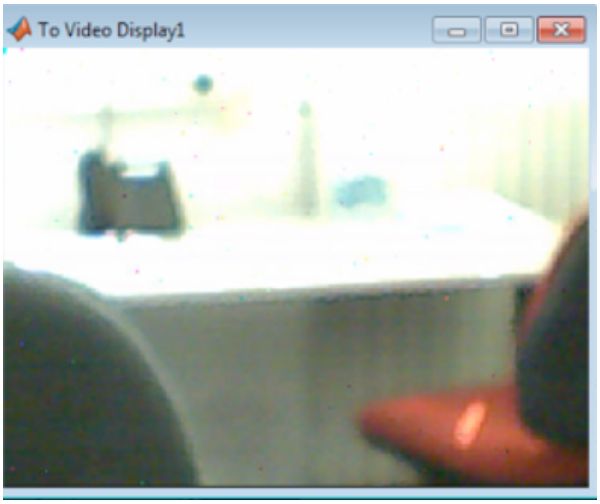

Receive Video at $\alpha = 1.578$ (FFT based - OFDM) for SNR=40 dB at $\varepsilon = 0.1$. BER=. 000618.

Fig. 4.5.1 Example of captured and reproduced video signals in case of an FrFT based- system and an FFT based- system.

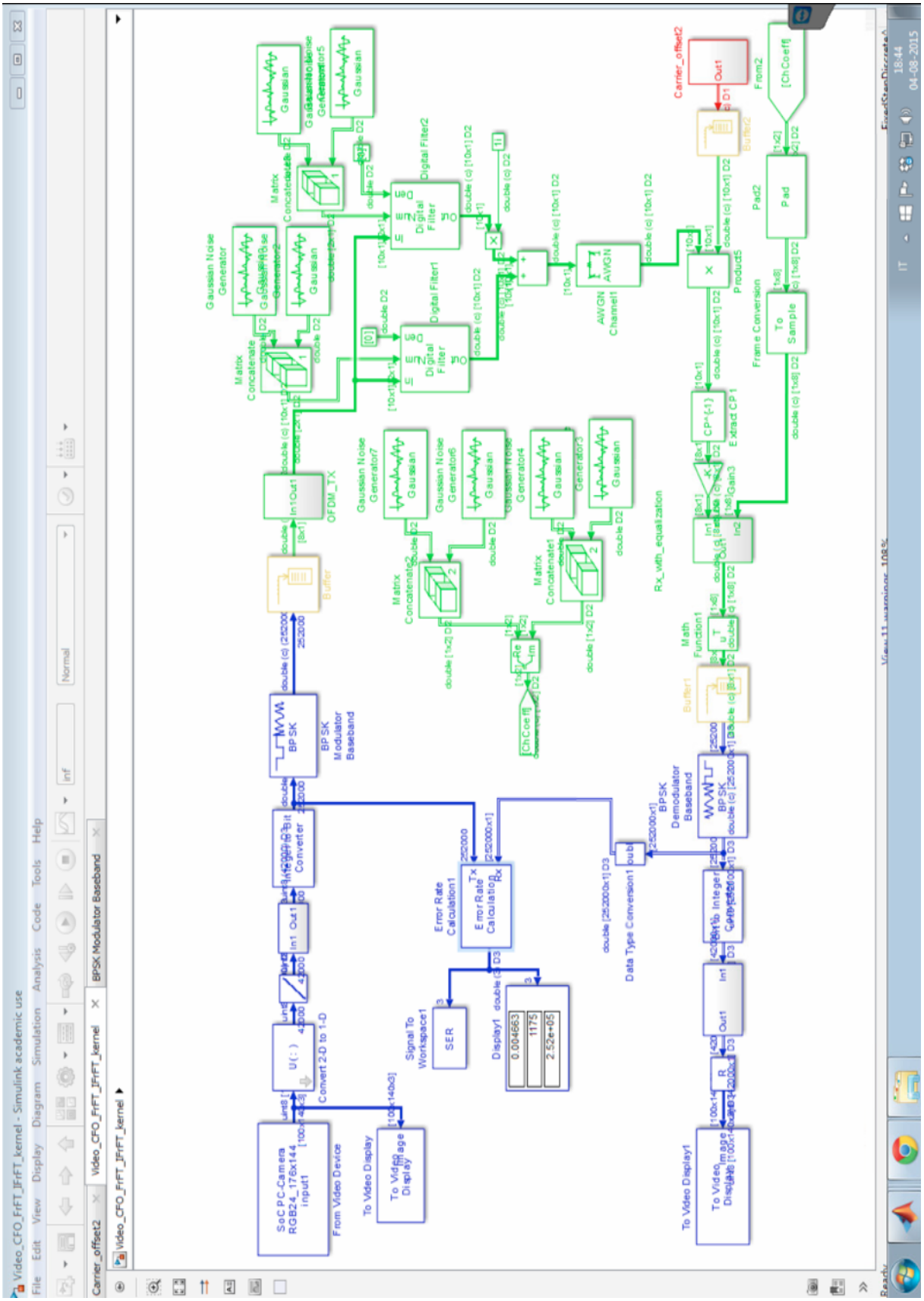

Fig. 4.5.2 Model for real-time video capture simulation

CHAPTER-V

CONCLUSION & FUTURE SCOPE

Topics:

5.1. Conclusion

5.2. Future Scope

CHAPTER-5 CONCLUSION & FUTURE SCOPE

This chapter is organised as: In first section, the Thesis report is concluded regarding the Performance Analysis and Hardware Implementation of FrFT/FFT -based OFDM System in presence of CFO and STO. In second section, the further scope of this work is decided through the problem formulation after making a literature survey thoroughly based on "*Performance Analysis and Hardware Implementation of FrFT/FFT -based OFDM System in presence of CFO and STO*". And efficient hardware implementation of FrFT because implementation complexity is a major problem of FrFT. The use FrFT is also in Generalized Frequency Division Multiplexing (GFDM) in 5th Generation Non-Orthogonal Waveforms for Asynchronous Signalling (5GNOW) based on GFDM. After discussing the further scope of this work, future plan can easily be formulated.

5.1. CONCLUSION

OFDM is a special case of wideband multicarrier modulation in which multiple symbols are transmitted in parallel using different sub-carriers with overlapping frequency bands that are mutually orthogonal. An equivalent wideband frequency bandwidth is separated into a number of narrowband signals. The time dispersion caused by multipath delay is reduced because the symbol duration of a narrowband signal will be larger than that of a wideband transmission scheme. The overlapping multicarrier techniques can implement the same number of channels as conventional FDM system but with a reduced amount of bandwidth. In conventional FDM, adjacent channels are separated using guard band.

In OFDM, each subcarrier has integer number of cycles within a given time interval T, and the number of cycles by which each adjacent subcarrier differs is exactly one. This implementation adds orthogonality to the subcarriers. Because of these inherent properties (orthogonal subcarriers) it saves the bandwidth during the transmission. In OFDM system the bandwidth is divided into N slots and then data rate is increased by N-times.

In 3rd generation WCDMA and OFDM was used. Just because of these OFDM (multicarrier system) a large number of high data rate applications became possible like-

- DAB
- HDTV
- Wireless LAN networks

- IEEE 802.16 Broadband Wireless Access System
- Multimedia applications e.g. video games etc.

The subcarriers are data modulated using phase shift keying or quadrature amplitude modulation. The amplitude spectrum of each modulated subcarrier using either PSK or QAM, narrowband channels where N is the number of sub-carriers. However, if the delay spread is longer than the symbol duration, multipath will affect performance. A guard time is introduced to eliminate ISI caused by delay spread. As a rule, the guard time is usually two to four times larger than the expected delay spread. To reduce ICI, OFDM symbols are cyclically extended into the guard interval. An OFDM symbol will have an integer number of cycles in the FFT interval as long as the delay is less than the guard time.

It is well known that synchronization is a major issue of OFDM systems based on the use of FFT. It has already been established that an OFDM system based on the use of the FrFT, a generalization of the Fourier transform with α. where 'α' is FrFT angle parameter at $\alpha = \pi/2$ FrFT become FFT, are less affected by synchronization errors in comparison to OFDM systems based on the use of FFT.

The impact of synchronization issues can also be higher in future wireless cellular system, where the use of non-proportional subcarrier spacing will be required to accommodate the necessary bandwidth. As a consequence, orthogonality is destroyed and ICI among the sub-carriers and ISI will arise.

Our main objective was Performance Analysis and Hardware Implementation of FrFT/FFT -based OFDM System in presence of CFO and STO. First of all, a careful literature survey was done based on the ***FFT -based OFDM in presence of CFO and STO system***.

❖ FFT-OFDM system

During the literature survey the paper [44 and 45] has been followed where the proposed work based on the BER evaluation of FFT based- OFDM system in presence of CFO and STO, have been summarised till 2015 with considerations the BPSK modulation techniques in AWGN as well as fading environment(multi path channel). So, in [44, 45] the following results have been discussed and all results existing in this article [44, 45] are verified correctly by us. The results are following-

❖ BER expression for BPSK modulation in following environments-

- AWGN channel
- Flat fading channel
- Frequency selective fading channel

By following the above system mode in this thesis work, proposed SER expressions for QPSK modulation technique in presence of CFO and STO.

- **QPSK modulation in following environments -**
  - AWGN channel
  - Flat fading channel
  - Frequency selective fading channel

➢ **FrFT -based OFDM system**

After taking literature review on FFT -based OFDM system, we moved towards the thoroughly literature review on the FrFT -based OFDM system. During the literature review the latest research paper based on "performance evaluation of FrFT -based OFDM system" [54] in 2010 was taken in which it is found that only ICI expression has been derived in FrFT -based OFDM system. In the literature BER expression [50, 51] are given first time, and also continued to analyze performance of FrFT -based OFDM system in presence of CFO and derived SER expression for QPSK in case of frequency selective fading channel [52]. Now, BER/SER expression is derived for the FrFT -based OFDM system with different modulation schemes with different channel environments.

These results are following-

- **BER expression for BPSK modulation scheme in following environments-**
  - AWGN channel
  - Flat Fading channel
  - Frequency Selective Fading channel

- **QPSK modulation in following environments -**
  - AWGN channel
  - Flat fading channel
  - Frequency selective fading channel

Till now, above results are derived successfully and simulated also. It is also verified that FrFT -based OFDM system performs similar to FFT -based OFDM at $\alpha = \pi/2$ and performs better than it for other values of α. The FrFT -based OFDM system (with different values of 'α') provides better BER and ICI than DFT based OFDM system.

Based on these results, some paper were published and summited listed below-

1. S. Kumari, S. Kr. Rai, A. Kumar, H. D. Joshi, A. Kr. Singh, R. Saxena: "***Closed form relations for ICI and BER in FRFT-OFDM system***", in Proc. Int. Advance Comp., pp. 708-712, 2013.
2. S. Kumari, S. Kr. Rai, A. Kumar, H. D. Joshi, A. Kr. Singh, and R. Saxena: "***Exact BER analysis of FRFT-OFDM system over frequency selective Rayleigh fading channel with CFO***", Elect. Lett., vol. 49, no.13, pp. 1299-1301, Sept. 2013.
3. A. Kumar, M. Magarini, H. D. Joshi, and R. Saxena: "**Exact SER Analysis of FrFT-based QPSK OFDM system over Frequency Selective Rayleigh Fading Channel with CFO**", submitted to Electron. Lett., May 2015.
4. I extended work done in [44] for ***FFT-based QPSK OFDM in the presence of both carrier frequency offset (CFO) and symbol timing offset (STO)***, We intend to submit results to in "IEEE Transactions on wireless communications.

Through above discussions our proposed work is concluded. By, studying thoroughly our proposed work, the further scope of this work can be decided easily. Now, in next section the future plan or further scope of this work will be discussed.

5.2. FUTURE SCOPE

Further, in FFT -based OFDM and FrFT -based OFDM system the future work can be planned separately based on the literature review.

- **FFT –based OFDM system**

  After studying [44, 45], further work on "performance evaluation of FFT –based OFDM system in presence of CFO and STO" can be planned as-

  - **BER expression of QAM modulation scheme-**
    - AWGN channel
    - Flat fading channel
    - Frequency selective fading channel.

In wireless communication, QAM modulation techniques is being used. So, BER evaluation of QAM modulation technique is very important.

➢ **FrFT -based OFDM system**

After studying [54], further work can be proposed based on "*performance Analysis of FrFT -based OFDM system in presence of CFO and STO".* These work can be:-

- ❖ **BER expression for BPSK modulation scheme in following environments-**
  - AWGN channel
  - Flat Fading channel
  - Frequency Selective Fading channel
- ❖ **BER expression of QPSK modulation scheme-**
  - AWGN channel
  - Flat Fading channel
  - Frequency fading channel
- ❖ **BER expression of QAM modulation scheme-**
  - AWGN channel
  - Flat Fading channel
  - Frequency Fading channel

These above results have not been given yet. So, anyone can take step from here for further "*performance Analysis of OFDM system.*" Apart from these many scopes are there based on the performance evaluation. If anyone is interested in ***Error Control Coding*** subject then the performance can be improved to a better extent by using different coding system. So, a better scope is there by using coding system.

❖ **One important aspect with this work "*Hardware Implementation of FrFT*"**

Future wireless systems will be based on configurable MCM techniques. Software defined radio approach seems the most promising solution to implement reconfigurable MCM where many DSP operations.

It is well known that synchronization is a major issue of OFDM systems based on the use of FFT. It has already been established that an OFDM system based on the use of the FrFT, a generalization of the Fourier transform with α. where α is FrFT angle parameter at $\alpha = \pi/2$ FrFT become FFT, are less affected by synchronization errors in comparison to OFDM systems based on the use of FFT.

The impact of synchronization issues can also be higher in future wireless cellular system, where the use of non-proportional subcarrier spacing will be required to accommodate the

necessary bandwidth. As a consequence, orthogonality is destroyed and ICI among the sub-carriers and ISI will arise.

A solution recently investigated to address this problem consists in abandoning strict orthogonality among subcarriers, partially or altogether, and controls the impairments instead. To this aim, the concept of flexible non-orthogonal multicarrier waveforms has come into existence. In such a context several multicarrier schemes are currently being evaluated as candidate air interface of next generation wireless communication systems. Among these, filter bank multi-carrier (FBMC), generalized frequency division multiplexing (GFDM), unified frequency multi-carrier (UFMC), filtered-OFDM are brought up and being actively studied to meet the diverse demands of different scenarios.

In the future we can do efficient implementation of an FrFT -based OFDM system in order to verify the improved tolerance to ICI and ISI. We will consider the adaptation to FrFT of all major synchronization algorithms developed for FFT -based OFDM systems. We will also analyze performance with different modulation techniques over different channel environments including multiple-input multiple-output (MIMO) channels.

There are many more problems and scope of innovation in future mobile systems to improve the performance of systems based on the use of non-orthogonal multicarrier waveforms. The main hypothesis of this proposal is that the underlying design principles-synchronism and orthogonality of the physical layer of mobile radio systems constitute a major obstacle for the envisioned service architecture. Hence, there is a clear motivation for an innovative and in part disruptive re-design of the physical layer from scratch. In this project we will explore the inherent trade-offs between possible relaxation in orthogonality and synchronism and their corresponding impact on performance versus the required signal processing capabilities. The project proposal will focus on implementation aspects of emerging MCM technologies suitable for future wireless multicarrier systems.

One of the main future scope of this work is the development of a flexible software defined air interface based on MCM and the increase of the simulation speed by FPGA in the loop. This will allow for the definition of the fundamental building blocks and the related parameters including spectrum, bandwidth, multiple access schemes, waveform, and so on. The implementation of the considered MCM technique will be tested by using FPGA in the loop co-simulation in the case where the transmitted signal will be acquired form a generic USB webcam.

Future Lab Activity:

Lab Activity 1: Efficient Implementation of the GFDM

Abstract: In 5GNOW several multicarrier schemes are currently being evaluated candidates for physical layer of next generation of mobile communication system, namely Generalized Frequency Division Multiplexing (GFDM), Universal Filtered Multicarrier (UFMC), Filter Band Multicarrier (FBMC) and Bi-orthogonal Frequency Division Multiplexing (BFDM). Among these, GFDM has been proposed as air interface of 5G networks. GFDM is based on the modulation of independent blocks, where each block consists of a number of sub-carriers and sub-symbols with a single CP, so that the spectral efficiency improves as compared to OFDM. In this lab activity focus on Hardware implementation of GFDM using MATLAB with Zed-board. First prepare the Simulink model of GFDM after that using "Fixed Point Tool" along with fixed point advisor generate the efficient fixed point model and then by using the "HDL coder" generate the HDL code and also for optimizing the code through the HDL workflow Advisor and finally FPGA in the Loop co-simulation with the Xilinx ZYNQ SoC FPGA by using the HDL Verifier Toolbox.

Lab Activity 2: GFDM Base Transceiver Implementation In presence of CFO and STO

Abstract: Generalized Frequency Division Multiplexing (GFDM) base transceiver in presence of CFO and STO design as proof-of-concept for a new waveform with low implementation complexity. The implementation is based on the MATLAB along with Zed-board hardware platform. GFDM is investigated within 5GNOW as a candidate 5G waveform. In this lab activity focus on Hardware implementation of complete receiver with equalization and synchronization of both CFO and STO using MATLAB with Zed-board. First prepare the complete Simulink model in presence of CFO and STO along with synchronization algorithms using FrFT. After that using "Fixed Point Tool" along with fixed point advisor generate the efficient fixed point model and then by using the "HDL coder" generate the HDL code and also for optimizing the code through the HDL workflow Advisor and finally FPGA in the Loop co-simulation with the Xilinx ZYNQ SoC FPGA by using the HDL Verifier Toolbox.

Lab Activity 3: Implementation of FBMC and UFMC

Abstract: In this activities focused on basic transceiver functionalities of Universal Filtered Multi-Carrier (UFMC), Universal Filtered OFDM (UF-OFDM) and Filter Band Multicarrier (FBMC). UFMC is investigated within 5GNOW as a candidate 5G waveform. Hardware

implementation of FBMC and UFMC using MATLAB along with Zed-board. In this lab activity focus on Hardware implementation of GFBMC and UFMC using MATLAB with Zed-board. First prepare the Simulink model then after that using "Fixed Point Tool" along with fixed point advisor generate the efficient fixed point model and then by using the "HDL coder" generate the HDL code and also for optimizing the code through the HDL workflow Advisor and finally FPGA in the Loop co-simulation with the Xilinx ZYNQ SoC FPGA by using the HDL Verifier Toolbox.

Lab Activity 4: Real-time transmission of a video signal through FrFT- based 5GNOW system in presence of CFO and STO

Abstract: An example of a real time Simulink model implementing an FrFT-based 5GNOW system for the transmission of a video signal over a frequency selective Rayleigh fading channel in presence of CFO and STO is considered. The video signal is captured from webcam and FPGA-in-loop is used to accelerate the processing at the transmitter and receiver. In this lab activity we can directly observe the improved quality of the reconstructed video signal at the output of the receiver in case of FrFT-based 5GNOW system.

****

REFERENCES

[1] Y. Wu and W. Y. Zou, "Orthogonal frequency division multiplexing: a multi-carrier modulation scheme," *IEEE Trans. Consum. Electron*., vol. 41, no. 3, pp. 392-399, Aug. 1995.

[2] S. Hara and R. Prasad, "*Multi-Carrier Techniques for 4G Mobile Communications",* 1st Edition, Artech House, Boston, 2003.

[3] L. Hanzo, M. Munster, B. J. Chol, and T. Keller, "*OFDM and MC- CDMA for Broadband Multi-user Communications, WLANs and Broadcasting,"* John Wiley & Sons, 2003.

[4] Peled, A. and Ruiz, A.; "Frequency doma in data transmission using reduced comput-ational complexity algorithms", Acoustics, Speech, and Signal Processing, IEEE International Conference on ICASSP '80, vol. 5, pp.964 –967, Apr. 1980.

[5] T. Keller and L. Hanzo, "Adaptive multicarrier modulation: A convenient framework for time-frequency processing in wireless communications," *Proc. IEEE*, vol. 88, no. 5, pp. 611–640, May 2000.

[6] L.J. Cimini, "Analysis and simulation of a digital mobile channel using orthogonal frequency division multiplexing," *IEEE Trans. Commun*. , vol. COM-33, pp. 665-675 July 1985.

[7] Kalet, "The multitone channel*," IEEE Trans. Commun.* vol. 37, pp.119-124. Feb.1989.

[8] ETSI EN 300 744 v1.4.1 (2001-01), "Digital video broadcasting (DVB-T); framing structure, channel coding and modulation for digital terrestrial television," 2001.

[9] M. L. Dolez, E.T. Heald, and D.L. Martin, "Binary data transmission techniques for linear systems," *Proc. I.R.E;* vol. 45, pp. 656-661, May 1957.

[10] http://standards.ieee.org/getieee802/802.11.html

[11] P. A. Bello, "Selective fading limitations of the KATHRYN modem and some system design considerations," *IEEE Trans. Commun. Technol*., vol. COM-13, pp. 320–333, Sept. 1965.

[12] M. S. Zimmerman and A. L. Kirsch, ''The AN/GSC-10 (KATHRYN) variable rate data modem for HF radio,'' *IEEE Trans. Commun. Technol., v*ol. COM-15, pp.197–205, April 1967.

[13] P. A. Bello, "Selective fading limitations of the KATHRYN modem and some system design considerations," *IEEE Trans. Commun. Technol*., vol. COM-13, pp. 320–333, Sept. 1965.

[14] M. S. Zimmerman and A. L. Kirsch, ''The AN/GSC-10 (KATHRYN) variable rate data modem for HF radio,'' *IEEE Trans. Commun. Technol., v*ol. COM-15, pp.197–205, April 1967.

[15] R.W. Chang and R. A. Gibby, "A theoretical study of performance of an orthogonal multiplexing data transmission scheme," *IEEE Trans. Commun. Tech*., vol. COM-16, pp. 529–540, Aug. 1968.

[16] Orthogonal Frequency Division Multiplexing,'' U.S. Patent No. 3,488,445, Filed Nov. 14, 1966, Issued Jan. 6, 1970.

[17] S. B. Weinstein and P. M. Ebert, ‘‘Data Transmission by Frequency-Division Multiplexing Using the Discrete Fourier Transform,’’ *IEEE Trans. Commun. Tech.,v*ol. COM-19, pp. 628–634, October 1971.

[18] B. R. Saltzberg, “Performance of an efficient parallel data transmission system,” IEEE Trans. Commun. Tech., vol. COM-15, pp.805–813, Dec. 1967.

[19] H. F. Marmuth, ‘‘On the Transmission of Information by Orthogonal Time Functions,’’ *AIEE Trans; (communication and Electronics), v*ol. 79, pp. 248–255, July 1960.

[20] S. B. Weinstein and P. M. Ebert, ‘‘Data Transmission by Frequency-Division Multiplexing Using the Discrete Fourier Transform,’’ *IEEE Trans. Commun. Tech.,v*ol. COM-19, pp. 628–634, October 1971.

[21] J. S. Chow, J. C. Tu, and J. M. Cioffi, ‘‘A Discrete multitone transceiver System for HDSL applications,’’ *IEEE J. Select. Areas Commun*., vol. 9, no. 6, pp 895–908, August 1991.

[22] P. S. Chow, J. C. Tu and J. M. Cioffi, “Performance evaluation of a multichannel transceiver system for ADSL and VHDSL services,” *IEEE J. Selected Area*, vol., SAC-9, no.6, pp. 909-919, Aug. 1991.

[23] R.V. Paiement, “Evaluation of single carrier and multicarrier modulation techniques for digital ATV terrestrial broadcasting,” *CRC Report, no. CRC-RP-004*, Ottawa, Dec. 1994.

[24] B. Hirosaki, “An analysis of automatic equalizers for orthogonally multiplexed QAM systems,” *IEEE Trans. Commun.*, vol. COM-28, pp. 73–83, Jan. 1980

[25] Peled, A. and Ruiz, A.; “Frequency doma in data transmission using reduced Computationnal complexity algorithms”, Acoustics, Speech, and Signal Processing, IEEE International Conference on ICASSP '80, vol. 5, pp.964 –967, Apr. 1980

[26] W. E. Keasler and D. L. Bitzer, “High speed modem suitable for operating with a switched network,” U. S. Patent No. 4,206,320, June 1980.

[27] E. F. Casas and Cyril Lung, “OFDM for data communication over mobile radio FM channels-Part I: Analysis and experimental results,” *IEEE Trans. Commun.*, vol.39, no.5, pp. 783–793, May 1991.

[28] E. F. Casas and Cyril Lung, “OFDM for data communication over mobile radio FM channels-Part II: Performance improvement,” *IEEE Trans. Commun*., vol.40, no.4, pp. 680–683, Apr 1992.

[29] M. Okada, S. Hara, and N. Morinaga, “A Study on Bit Error Rate Performance for Multicarrier Modulation Radio Transmission Systems,’’ *IEICE Technical Report, RCS91-44,* pp. 19–24, 1991.

[30] M. Okada, S. Hara, and N. Morinaga, ‘‘Bit error rate performance of orthogonal multicarrier modulation radio transmission systems,’’ *IEICE Trans. on Comm.*, vol. E76-B, no. 2, pp. 113–119, Feb 1993.

[31] S. Hara, M. Mouri, M. Okada and N. Morinaga, ‘‘Transmission performance analysis of multi-carrier modulation in frequency selective fast rayleigh fading channel,’’ *Wireless Personal Commun.*, vol. 2, no. 4, pp. 335–356, 1995/1996.

[32] T. Pollet, M. Van Bladel, and M. Moeneclaey, “BER sensitivity of OFDM to carrier frequency offset and Wiener phase noise,” *IEEE Trans. Commun*., vol. 43, no. 2, pp. 191–193, Feb. 1995

[33] P. Tan and N. C. Beaulieu, “Reduced ICI in OFDM systems using the `better than` raised-cosine pulse,” *IEEE Commun. Lett.*, vol. 8, no. 3, pp. 135- 137, Mar. 2004.

[34] N. C. Beaulieu and P. Tan, “On the effects of receiver windowing on OFDM performance in the presence of carrier frequency offset,” *IEEE Trans Wireless Commun*. vol. 6, no.1, pp. 202-209, Jan 2007.

[35] K. Sathananthan and C. Tellambura, “Probability of Error Calculation of OFDM Systems with Frequency Offset,” *IEEE Trans. on Commun*. vol. 49, no. 11, pp. 1884-1888, Nov 2001.

[36] L. Rugini and P. Banelli, “BER of OFDM systems impaired by carrier frequency offset in multipath fading channels,” *IEEE Trans. on Wireless Commun*., vol 4, no. 5, pp.2279-2288, Sep 2005.

[37] P. Dharmawansa, N. Rajatheva, and H. Minn, “An exact error probability analysis of OFDM systems with frequency offset,” *IEEE Trans. Commun*., vol. 57, no. 1, pp. 26-31, Jan. 2009.

[38] M. K. Simon and M. S. Alouini , *Digital Communication over Fading Channels,* 2nd ed. New York: Wiley, 2005.

[39] R. Uma Mahesh and A. K. Chaturvedi, “Closed form ber expressions for BPSK OFDM systems with frequency offset”, *IEEE Trans. on Commun*. vol. 14, no. 8, pp. 731-733, Aug 2010.

[40] Jing Zhang , Zulian Wang , “ICI analysis for FRFT-OFDM systems to frequency offset in time frequency selective fading channels,” *IEEE Commun. Lett.,* vol. 14, pp. 888-890, October 2010.

[41] R. Saxena and H. D. Joshi, “Performance Improvement in OFDM system with MBH Combinational pulse shapes,” Digital Signal Processing, Elsevier Publication, vol. 23, pp. 314-321, Jan 2013.

[42] R. Saxena and H. D. Joshi, “ICI Reduction in OFDM system using IMBH combinational pulse shape,” Wireless Personal Communications, Springer Publication, DOI 10.1007/s11277-012-0978-7.

[43] S. C. Pei and J. J. Ding, “Closed-form discrete fractional and affine Fourier transform,” IEEE Trans. Signal Process., vol. 48, pp. 1338-1353, May 2000.

[44] Y. Wang, Z. Zhang, and Y. Chen, “BER analysis of BPSK OFDM systems with residual frequency and timing offsets over frequency selective Rayleigh fading channels,” *J. Comput. Inform. Syst*., vol. 8, no. 24, pp. 10349-10357, Dec. 15, 2012.

[45] U. Mahesh and A. K. Chatuvedi, "Closed form BER expressions for BPSK OFDM systems with fractional timing offset and carrier frequency offset," in *Proc. Nat. Conf. Commun.,* Kharagpur, India, 2012, pp. 1–4.

[46] R. Saxena, and H. D. Joshi, "FRFT based timing estimation method for an OFDM system," *Pertanika J. Sci. & Technol*, pp. 15-24, 2014.

[47] AsG. Wunder, *et al.*, "5GNOW: non-orthogonal, asynchronous waveforms for future mobile applications," *IEEE Commun.*, vol. 52, no. 2, pp. 97-105, Feb. 2014.

[48] Deprettere,E., Dewilde, P., and Udo, R., "Pipelined CORDIC Architecture for Fast VLSI Filtering and Array Processing," *Proc. ICASSP'S4*, 1984, pp. 41.A.6.1-41.A.6.4.

[49] Hu, Y.H., and Naganathan, S., "ANovel Implementation of Chirp Z-Transformation Using a CORDIC Processor," *IEEE Transactionson ASSP*, Vol. 38, pp. 352-354,199O.

[50] S. Kumari, S. Kr. Rai, A. Kumar, H. D. Joshi, A. Kr. Singh, R. Saxena: "Closed form relations for ICI and BER in FRFT-OFDM system", in Proc. Int. Advance Comp., pp. 708-712, 2013.

[51] S. Kumari, S. Kr. Rai, A. Kumar, H. D. Joshi, A. Kr. Singh, and R. Saxena: "Exact BER analysis of FRFT-OFDM system over frequency selective Rayleigh fading channel with CFO", *Elect. Lett.,* vol. 49, no.13, pp. 1299-1301, Sept. 2013.

[52] A. Kumar, M. Magarini, H. D. Joshi, and R. Saxena: "Exact SER Analysis of FrFT-based QPSK OFDM system over Frequency Selective Rayleigh Fading Channel with CFO", submitted to *Electron. Lett.,* May 2015

[53] A. Hamza and J. Mark. "Closed form SER expressions for QPSK OFDM systems with frequency offset in Rayleigh fading channels," *IEEE Commun. Lett*., vol. 18, no. 10, pp. 1687–1690, Oct. 2014.

[54] J. Zhang and Z. Wang, "ICI analysis for FRFT-OFDM systems to frequency offset in time frequency selective fading channels", *IEEE Commun. Lett.,* vol. 14, pp. 888-890, Oct. 2010.

[55] S. and Piuri, V., "A Unified View of CORDIC Processor Design", Application Specific Processors, Edited by Earl E. Swartzlander, Jr., Ch. 5, pp. 121-160,Kluwer Academic Press, November 1996.

[56] Duprat, J. and Muller, J.M., "*The CORDIC Algorithm: New Results for Fast VLSI Implementation*," IEEE Transactionson Computers, Vol. 42, pp. 168-178, 1993.